Chem Soc Rev

Unveiling Practical Considerations for Reliable and Standardized SERS Measurements: Lessons from a Comprehensive Review of Oblique Angle Deposition-Fabricated Silver Nanorod Array Substrates

Journal:	*Chemical Society Reviews*
Manuscript ID	CS-REV-07-2023-000540.R1
Article Type:	Review Article
Date Submitted by the Author:	22-Oct-2023
Complete List of Authors:	Zhao, Yiping; University of Georgia, Department of Physics and Astronomy Kumar, Amit; University of Georgia, Department of Physics and Astronomy Yang, Yanjun ; University of Georgia,

Unveiling Practical Considerations for Reliable and Standardized SERS Measurements: Lessons from a Comprehensive Review of Oblique Angle Deposition-Fabricated Silver Nanorod Array Substrates

Yiping Zhao [a] *, Amit Kumar [a], and Yanjun Yang [b] *

[a] Department of Physics and Astronomy

[b] School of Electrical and Computer Engineering, College of Engineering

The University of Georgia, Athens, GA 30602, USA

* Corresponding Author: E-mail: zhaoy@uga.edu; YanjunYang@uga.edu

Abstract

Recently, there has been an exponential growth in the number of publications focusing on surface-enhanced Raman scattering (SERS), primarily driven by advancements in nanotechnology and the increasing demand for chemical and biological detection. While many of these publications have focused on the development of new substrates and detection-based applications, there is a notable lack of attention given to various practical issues related to SERS measurements and detections. This review aims to address this gap by utilizing silver nanorod (AgNR) SERS substrates fabricated through the oblique angle deposition method as an illustrative example. The review highlights and addresses a range of practical issues associated with SERS measurements and detections. These include optimization of SERS substrates in terms of morphology and structural design, considerations for measurement configurations such as polarization and incident angle of the excitation laser, exploration of enhancement mechanisms encompassing both intrinsic properties induced by the structure and materials, as well as extrinsic factors arising from wetting/dewetting phenomena and analyte size. The manufacturing and storage aspects of SERS substrates, including scalable fabrication techniques, contamination control, cleaning procedures, and appropriate storage methods, are also discussed. Furthermore, the review delves into device design considerations, such as well arrays, flow cells, and fiber probes, and explores various sample preparation methods such as drop-cast and immersion. Measurement issues, including the

effect of excitation laser wavelength and power, as well as the influence of buffer, are thoroughly examined. Additionally, the review discusses spectral analysis techniques encompassing baseline removal, chemometric analysis, and machine learning approaches. The wide range of AgNR-based applications of SERS, across various fields, is also explored. Throughout the comprehensive review, key lessons learned from the collective findings are outlined and analyzed, particularly in the context of detailed SERS measurements and standardization. The review also provides insights into future challenges and perspectives in the field of SERS. It is our hope that this comprehensive review will serve as a valuable reference for researchers seeking to embark on in-depth studies and applications involving their own SERS substrates.

1. Introduction

Surface-enhanced Raman scattering (SERS) is a powerful spectroscopic technique that has been extensively used for chemical and biological sensing. When target analyte molecules are in close proximity to specially designed nanostructured metallic surfaces (or other plasmonic nanostructures), the Raman signal of the target molecules can be significantly enhanced due to local electromagnetic field enhancement and possible chemical enhancement resulting from charge transfer.[1, 2] Due to its high enhancement factor (usually in the order of 10^6 to 10^8), SERS can detect molecules at very low concentrations and can even achieve single molecule detection.[3, 4] The intrinsic vibrational modes of analyte molecules enable the SERS spectrum to be treated as a molecular fingerprint, thus exhibiting high selectivity (or specificity) and enabling the identification of specific molecules within complex metrices. These characteristics form the basis for SERS being considered as a label-free detection method. Furthermore, SERS allows for the measurement of analytes in real-time and in situ, making it ideal for monitoring dynamic biological processes. These advantages have led to the widespread application of SERS in the detection and identification of a broad range of chemical and biological analytes, covering various domains within the chemical and biological sensor community, including medical diagnostics, drug discovery, food safety, environmental monitoring, and more.[2]

In recent years, the number of publications related to SERS has grown almost exponentially (see **Figure 1**), particularly after 2000, due to advancements in nanotechnology and high demands for sensor applications. Historically, from the 1970s to the 1990s, researchers struggled to produce highly enhanced and reproducible SERS substrates.[5, 6] However, in the turn of the millennium, more reliable and reproducible SERS substrates began to emerge.[7-9] Despite this progress, many

SERS-based publications still focus on developing new substrates, even though the number of papers on SERS-based detections has increased significantly. These publications generally follow a standard format.

For new SERS substrate-related publications, the fabrication or synthesis process is typically reported, along with the SERS performance, which is often compared to known substrates. A numerical calculation based on electromagnetic theory and the substrate's structure is presented to demonstrate possible hotspots and explain the underlying mechanism. Additionally, various other aspects are often included, such as substrate optimization, specific applications, or other related topics. Detection-based publications primarily focus on different SERS detection strategies, while some also address reproducibility and spectral variations.

However, after many years of working in the SERS field, it becomes evident that comprehending SERS measurements and substrates is not a trivial task. Notably, even for the same analyte, the spectral shapes can differ when different SERS substrates (or even the same SERS substrate) are used.[10] Numerous factors contribute to this variance, including the substrate, sample preparation conditions, measurement conditions (such as excitation wavelength, laser power, laser beam size, Raman instrument), and more. However, the exact reasons behind these variations remain unknown.

This seemingly trivial issue holds importance for two main reasons: establishing a standard SERS database and utilizing it for machine learning models. In both cases, known SERS spectra serve as standard references for classifying and quantifying specific targets. Subtle changes in the standard spectra can lead to significantly different outcomes. In other words, the SERS community currently lacks a standardized approach that covers SERS substrate fabrication, sample preparation, SERS measurement, and spectral pretreatment. While there is extensive literature on commonly used substrates like Ag or Au nanoparticles (NPs), the procedures mentioned above can vary greatly between publications, making the SERS spectra from even the same analyte incomparable, except for the characteristic SERS peaks (which is generally the case in the literature).

Based on our previous experience, to standardize a SERS measurement, one must address or understand the following issues: (1) comprehending the mechanism of a SERS substrate, especially those with complex plasmonic structures, is not easy; (2) numerous tricks exist to achieve repeatable and reproducible SERS measurements; (3) the sample preparation strategy plays a significant role in understanding the SERS substrate performance, and subsequent spectral

characterization & analysis; (4) caution must be exercised when dealing with analytes in complex metrices; (5) for practical applications, large-scale and reproducible fabrication/synthesis methods are essential; (6) different applications require the adaptation of the substrate into various devices; (7) advanced measurements are necessary for special applications; and (8) proper spectral pretreatment is crucial to avoid introducing artifacts, misinterpretation, false prediction during the data analysis process.

Thus far, the SERS community lacks a comprehensive and systematic review that addresses the aforementioned issues. However, such a review is crucial, as it can shed light on how to establish a standardized approach to SERS measurements.

Here, we would like to address the aforementioned issues using silver nanorod arrays (AgNRs) SERS substrates fabricated by oblique angle deposition (OAD).[11-13] Since 2005, this substrate has been utilized in numerous sensor applications,[12-14] including biomedical applications such as detecting bacteria, viruses, biomarkers, and more. It has also found application in fields like food safety, where it can sense illegal food additives, bacteria, carcinogenic substances, and environmental monitoring of antibiotic pollution, heavy metal ion pollution, and so on. Additionally, the use of AgNRs fabricated through OAD for forensic science purposes, such as drug detection, and national defense applications like explosive detection and nerve gas detection, have been explored. Details can be found in **Table 1** of **Section 8**.

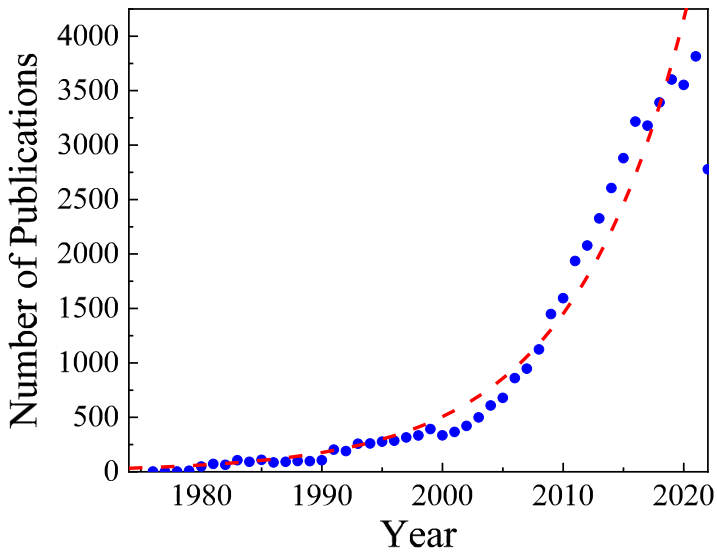

Fig. 1 A survey of SERS publication since 1970's. The dashed curve is a guide for eye and shows the exponential growth trend.

The use of OAD to prepare SERS substrates can be traced back to 1985 when Meier et al. at Oak Ridge National Laboratory (ORNL) published the first paper utilizing angled evaporation to prepare elongated Ag nanoparticles (NPs) on structured fused silica substrates. [15, 16] In this study and a subsequent one, the evaporation angle was varied from 0° to 78°, and the Ag evaporation thickness was changed up to 150 nm. [15, 16] Following this, in 1986, Martinez et al. at Université P. et M. Curie studied the polarization-dependent SERS performance of obliquely evaporated Ag film.[17, 18] They focused on the vapor incident angle ranging from 65° to 85°, with a fixed deposition thickness (20 sec under a vapor pressure of 10^{-4} Torr). Later in 1992, Wachter er al. produced high aspect ratio (5:1) Ag nano-needle arrays and demonstrate the SERS capability.[19] These studies yielded interesting SERS results but failed to produce SERS signals of sufficient magnitude for detection applications.

It was not until 2005 that Zhao and coworkers at the University of Georgia conducted a series of detailed investigations on how the morphology and substrate design of AgNRs affect their SERS performance.[11, 20] They demonstrated that a thin layer of Ag thin film (approximately 50-100 nm) combined with long AgNR arrays (length of about 1000 nm, diameter of approximately 100 nm, nanorod density of about 13/μm^2, and nanorod tilting angle of around 73^o (vapor incident angle θ of approximately 86^o)) can produce a SERS enhancement factor of approximately 10^9. The enhancement mechanisms of such an AgNR substrate as well as the excitation incident configurations have been thoroughly investigated.[11] Subsequently, various device designs utilizing AgNR substrates have been explored, and several applications have been investigated by our team and others. [12, 13, 20]

This paper provides a comprehensive and systematic review of AgNR SERS substrates, and lessons learnt from AgNR developments. It is structured into nine interconnected sections. **Section 2** discusses the growth of AgNRs and explores how different growth parameters, such as growth conditions and structural design, impact the SERS performance. Since AgNRs are anisotropic, the optical configuration of the detection significantly influences the final SERS signals. **Section 3** demonstrates how the SERS performance of an AgNR substrate is influenced by the polarization and incident angle of the excitation laser. Building upon these insights and the optical properties of AgNR substrates, **Section 4** focuses on understanding the SERS mechanism of this type of substrate. It is established that the most significant contribution to SERS from an AgNR substrate occurs when analyte molecules adsorb on the side surfaces of the AgNRs. Additionally, a simple

phenomenological model is developed to explain some observed phenomena from **Sections 2** & **3**. In **Section 5**, the quality of AgNR substrates is discussed, covering topics such as defects, contamination, cleaning, and storage. **Section 6** addresses various issues encountered in SERS measurements, including sample preparation methods, phenomena like the coffee-ring effect and capillary-induced bundling, and factors such as the power and wavelength of the excitation laser. **Section 7** presents the manufacturing process of AgNR and explores potential SERS devices fabricated by AgNR substrates, including flexible AgNR substrates, multi-well arrays, fiber probes, flow cells, electrochemical cells, ultra-thin layer chromatography, and integrated portable Raman systems. **Section 8** compiles the chemical and biological applications of AgNR substrates and addresses important issues that emerged in applications. **Section 9** outlines lessons learnt from the comprehensive reviews on AgNR substrates and potential challenges. Finally, **Section 10** summarizes the main pros and cons of AgNR substrates and points out possible future challenges.

2. The Growth and Design of AgNR Substrates

Oblique angle deposition (OAD) is a physical vapor deposition technique in which the evaporation beam forms a large angle θ (> 70°) with respect to the surface normal of the substrate during deposition. Typically, substrates during OAD are maintained at room temperature or lower temperatures. Due to the self-shadowing effect and limited surface diffusion, nanocolumnar structures can be formed.[21] **Figure 2a** shows the deposition configuration of OAD, and **Figure 2b** illustrates a general structure of a typical AgNR SERS substrate. During evaporation, the thickness of the deposited Ag is monitored using a quartz crystal microbalance positioned at normal incidence to the vapor source. As a result of the shadowing growth mechanism, OAD deposition leads to arrays of Ag nanorods tilting toward the source material (**Figure 2b**). The Ag nanorod tilting angle, denoted as β, represents the angle between the Ag nanorod tilting direction and the surface normal of the substrate, as shown in **Figure 2b**. A typical SEM image of the resulting AgNR substrate (θ = 86°) is presented in **Figure 2c**.

Additionally, during the OAD process, the substrate's azimuthal angle can be rotated, resulting in a deposition technique called glancing angle deposition (GLAD).[21] This enables easy control over the diameter, shape, spacing, and density of the nanostructures by adjusting deposition conditions such as deposition angles, azimuthal rotation, growth time, growth rate, and substrate temperature.

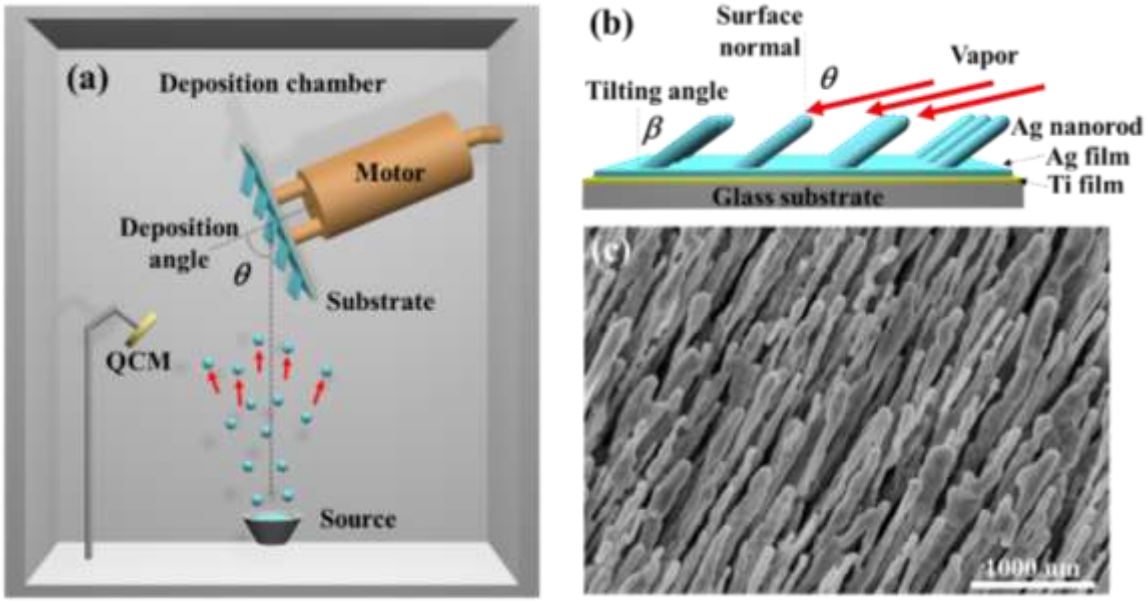

Fig. 2 (a) The schematic diagram of Ag nanorod array fabricated by oblique angle deposition; (b) the definition of deposition angle θ and Ag nanorod tilting angle β; and (c) a representative SEM image of the AgNR substrates (= 86°).

The SERS performance of the AgNR substrates is strongly influenced by several critical parameters, including the morphology of the AgNR, deposition conditions, and the design of the underlayer thin film. As mentioned in the Introduction section, historically, Ag NP substrates fabricated using OAD did not exhibit significant SERS effects due to limited morphology control. However, by systematically adjusting the nanorod length and tilting angle, the corresponding SERS enhancement factor (EF) demonstrated significant changes. In the following discussion, SERS characterization was performed by drop-casting 1 μL droplet of the Raman probe molecule, trans-1,2-bis (4-pyridyl) ethylene (BPE, Aldrich, 99.9+%), dissolved in methanol at a concentration of 10^{-5} M, on the AgNR substrates. The SERS spectra were collected using an excitation wavelength of $\lambda_{ex} = 785$ nm.

Figure 3a shows the SERS EF of BPE on AgNR with different rod lengths L at varying vapor incident angles.[22] Here the underlayer thin film was fixed as a 500-nm Ag film. Two general trends were observed: (1) as the AgNR length (L) increased, the SERS EF showed an almost monotonic increase until reaching a critical length L_c, beyond which the SERS EF either remained constant or exhibited a slight decrease; (2) increasing the vapor deposition angle resulted in an increase in the SERS EF. This indicates that at the same length of AgNR, an increased tilting angle of the

nanorods significantly enhances the SERS EF. Specifically, for $\theta = 84°$, the maximum EF value reaches to 7.2×10^8 when L = 1100 nm.[22] It is expected that when the titling angle reaches 90°, the SERS EF will reach its maximum value.

The SERS EF is also strongly influenced by the growth temperature of the AgNRs. While there have been conflicting reports on the effect of substrate temperature,[23-25] it is generally believed that lower substrate temperature lead to better SERS substrates.[26] **Figure 3b** depicts the relationship between the SERS EF and deposition temperature, keeping the deposition angle and film thickness constant. Clearly, a lower deposition temperature results in a higher EF.[26] This effect is attributed to the morphological changes in the SERS substrates: at lower deposition temperatures, the nanorods not only become longer and thinner, but have more roughness, compared to those deposited at higher temperatures under the same deposition angle and thickness.

Furthermore, it has been discovered that the SERS intensity of the AgNR substrate is strongly influenced by the underlying film deposited prior to the AgNR deposition, particularly the reflectivity of the underlying thin film.[27] **Figure 3c** demonstrates how the SERS signal depends on the reflectivity, even when the materials for underlying films differ. The growth of AgNRs and the SERS measurements were conducted under identical conditions. It is evident that the SERS intensity increases monotonically with the reflectivity of the underlying film.[27] This reflectance effect has been theoretically explained by a simple model developed by Liu and Zhao, which considers the reflection of the underlying coating (see **Section 4.3**).[28] Therefore, all our SERS-related detection experiments were conducted using AgNRs deposited on 50- or 100-nm Ag films,

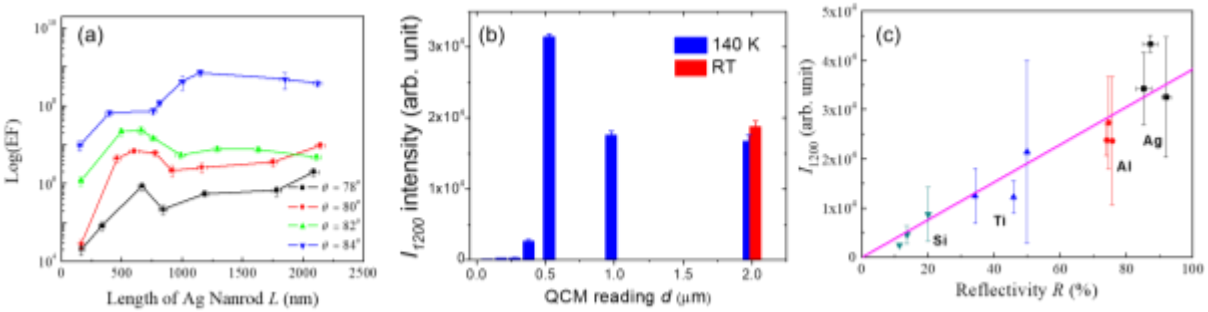

Fig. 3 (a) The SERS EF as a function of nanorod length L for samples deposited θ = 78°, 80°, 82°, and 84°, respectively; (Adapted with permission from Ref. 22. Copyright 2010 American Chemical Society.) (b) bar graph depicting the dependency of I_{1200} on the QCM reading for material deposited at a substrate temperature of 140 K; (Adapted with permission from Ref. 26. Copyright 2012 American Chemical Society.) and (c) the SERS peak intensity I_{1200} as a function of reflectance from the underlayer. (Adapted with permission from Ref. 27. Copyright 2010 American Institute of Physics.)

with an optimal nanorod length of approximately 1000 nm, deposited at $\theta = 86°$, with detailed structure illustrated in **Figure 2b**.

Various other conditions that can impact the growth of AgNRs have been explored. One such condition is the use of regular 2D templates to facilitate the growth of periodic arrays of AgNRs (or AuNRs) with varying spacing. The utilization of 2D regular templates, such as 2D regular Au[29] and Si[30] nanopost arrays created via electron-beam lithography, or nanoimprinted polycarbonate[31], has been investigated for guiding the growth of AgNRs (or AuNRs). However, there is no definitive conclusion regarding the influence of regularly spaced AgNR arrays on SERS performance. Based on our own experiments, we have observed that semi-ordered AgNR SERS substrates, resulting from these regular templates, exhibit inferior SERS performance compared to randomly grown AgNRs on clean glass substrates.[29]

The shape of AgNRs has been identified as another factor capable of modulating the SERS EF. While **Figures 3a-c** exclusively feature straight AgNRs, the unique nanorod topology achievable

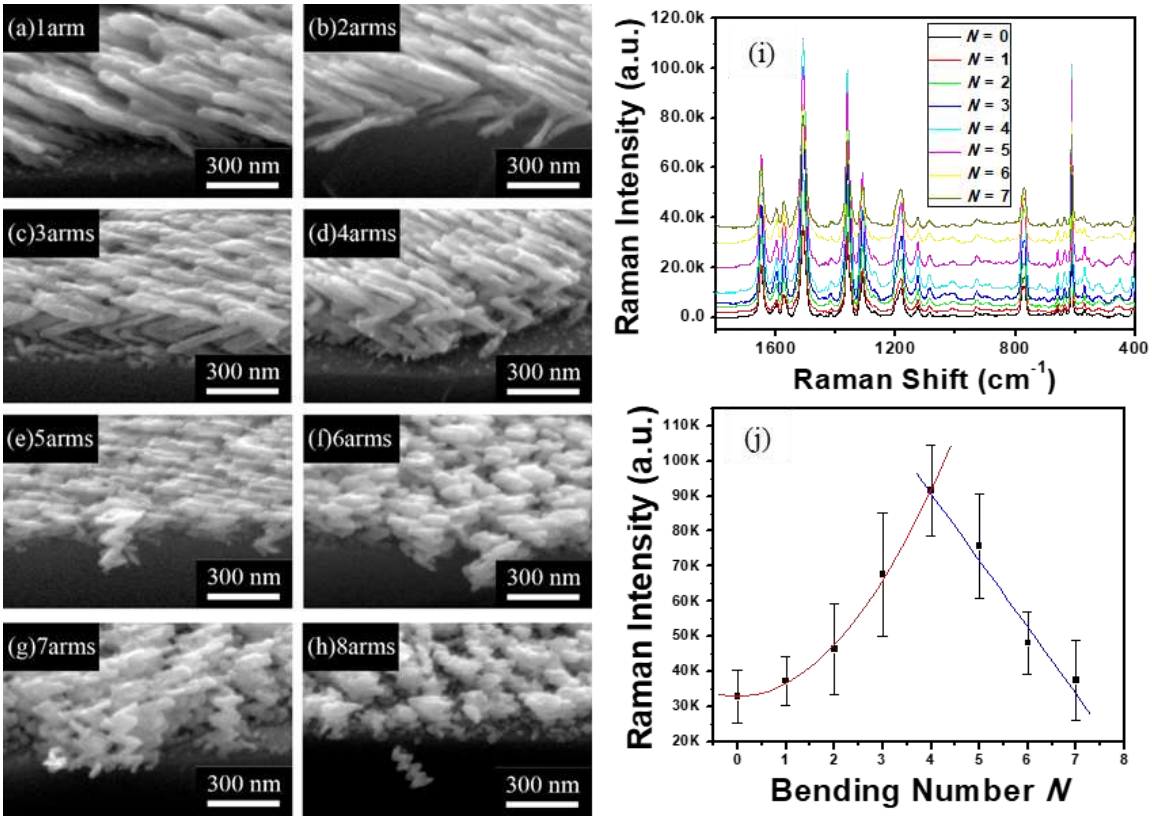

Fig. 4 (a)-(h) The representative SEM images of bent AgNR with different numbers of bending arms; (i) the SERS responses of the 3D substrates; and (j) the SERS intensity versus the number of bends. (Adapted with permission from Ref. 35. Copyright 2012 American Institute of Physics.)

through GLAD allows for the fabrication of Ag or Au nanorods with various shapes, including bent,[32-34] zig-zag,[35, 36] or helical structures.[37-39] Systematic investigations have been conducted to examine the SERS performance of these differently shaped nanorods. Remarkably, our research has revealed that folding straight AgNRs into zig-zag structures creates corners or bends that serve as potential "hot-spots" with exceptionally high local electric fields for SERS enhancement.[32, 35] In **Figure 4**, we present a comprehensive study on how the bending of AgNRs influences SERS performance. **Figures 4a-h** display representative SEM images of zig-zag AgNR arrays with different bending numbers (N) but a fixed total rod length. Additionally, **Figures 4i-j** provide SERS spectra based on Rhodamine 6G and compare the corresponding SERS intensities.[35] The SERS intensity increases as N varies from 1 to 4, and subsequently decreases for $N > 4$. Notably, at $N = 4$, the SERS intensity is approximately twice as high as that of straight AgNR substrates. This outcome suggests that appropriately folded 3D AgNR arrays can achieve superior SERS performance.

3. The Optical Measurement Configurations

The final collected SERS signals can be influenced by different optical incident and collection configurations due to the anisotropic shape of the AgNR substrates. Previous studies have examined the polarization-dependent SERS signals of short AgNR substrates, considering the impact of morphological anisotropy.[18] Later investigations focused on the polarization excitation[40, 41] and incident angle[41, 42] effects for long AgNR substrates. **Figure 5a** illustrates the definition of the polarization angle when the laser incident angle φ is 0°, with ψ representing the polarization

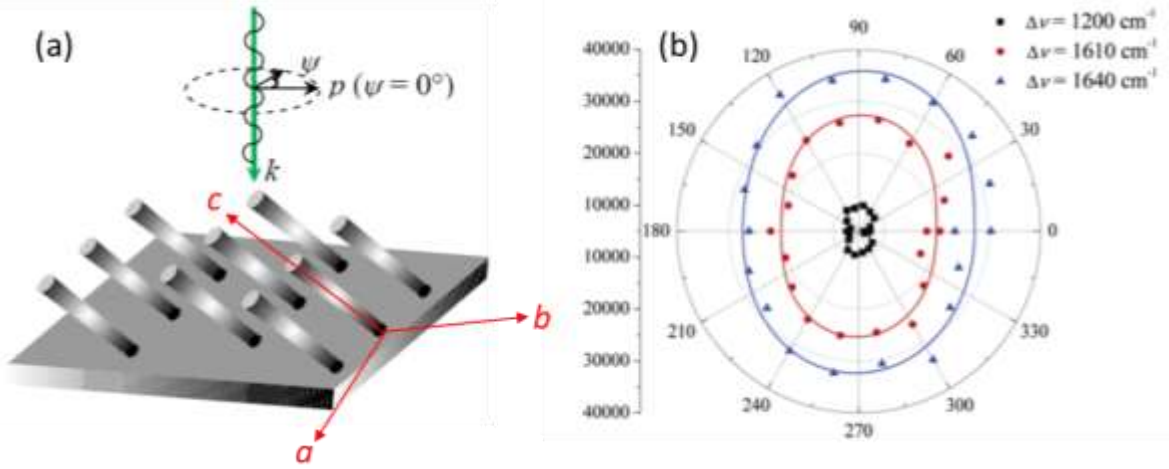

Fig. 5 (a) A diagram of definition of incident light polarization and the local coordinate for AgNR; and (b) the polar plots of the SERS peak intensity at Raman band $\Delta\nu$ = 1200, 1610, and 1640 cm^{-1} of BPE as a function of polarization angle ψ. (Adapted with permission from Ref. 40. Copyright 2006 American Chemical Society.)

angle when the excitation laser aligns with the nanorod direction (referred to as *p*-polarization).[40] **Figure 5b** presents a polar coordinate plot depicting the SERS peak intensity of BPE at bands $\Delta\nu$ = 1200, 1610, and 1640 cm^{-1} as a function of the polarization angle ψ. Within the range of ψ = 0° - 360°, the maximum intensity occurs at ψ = 90° or 270° (*s*-polarization), while the minimum intensity is observed at ψ = 0° or 180°. The polarization SERS behaviors in **Figure 5b** can be fitted with a function, $I_{SERS}(\psi) = I_0(1 + Ae^{-\frac{\psi}{\psi_0}}\sin^2\psi)$, with the ellipticities ($= (1 + A)^2$) for the three bands to be 1.25, 1.20, and 1.20, respectively.

The tilted orientation of AgNRs on a flat substrate breaks the reflection symmetry of the laser incident angle relative to the surface normal. Consequently, it is anticipated that the SERS response may differ when the excitation laser is incident along the nanorod direction compared to when it is incident in the opposite direction, even with the same incident angle. In the experimental setup, a positive incident angle φ is defined when the incident direction faces the nanorod tilting direction as depicted in **Figure 6a** (first quadrant in the incident plane). Conversely, a negative incident angle is assigned when the laser strikes the surface on the opposite side of the surface normal (second quadrant in the incident plane).[42] **Figure 6b** illustrates the SERS peak intensity as a function of the incident angle φ. As φ varies from -10° to +45°, the SERS peak intensity exhibits an increasing trend. However, for φ values exceeding +45°, the Raman peak intensity decreases monotonically. The maximum SERS intensity is observed at approximately φ = +45°, reaching a level approximately five times higher than that at φ = 0°.[42]

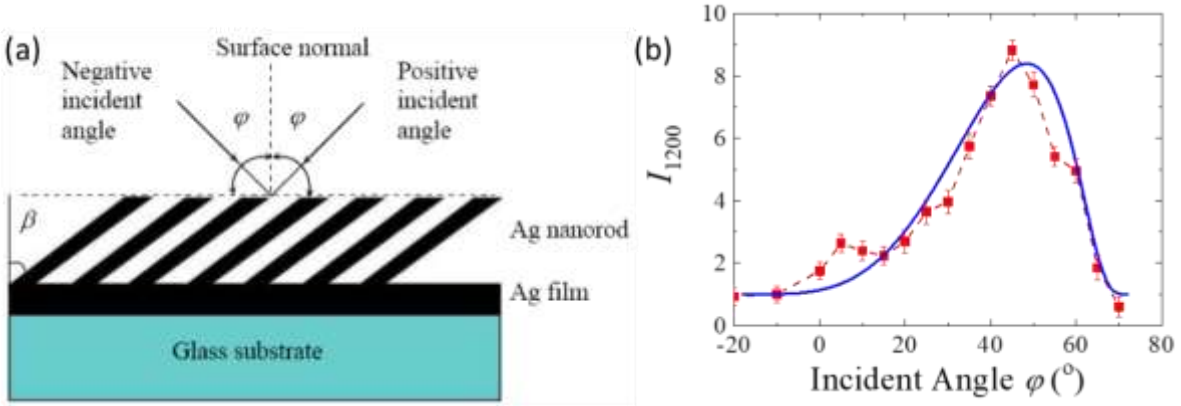

Fig. 6 (a) Illustration of Ag nanorod array and incident configuration (including the definition of φ); and (b) the integrated SERS intensity for the BPE band at $\Delta\nu$ = 1200 cm^{-1} plotted as a function of the incoming laser incident angle φ. (Adapted with permission from Ref. 42. Copyright 2006 American Institute of Physics.)

4. The SERS Mechanism of AgNR Substrates

4.1 The optical property of AgNR substrates

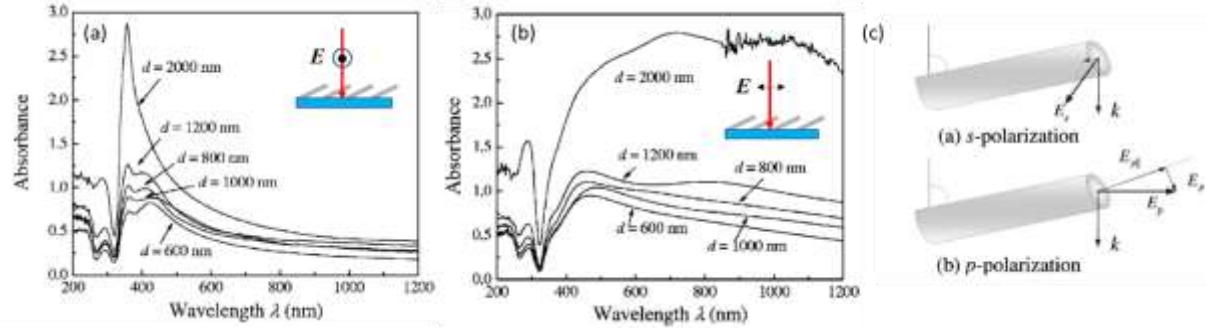

Fig. 7 The polarization dependent absorption spectra of AgNR substrates deposited at different thickness: (a) s-polarization and (b) p-polarization; (c) the possible LSPR modes excited by different polarized light. (Adapted with permission from Ref. 43. Copyright 2006 American Institute of Physics.)

Based on the two fundamental SERS mechanisms, namely electromagnetic (EM) and chemical enhancements, the dominant mechanism for most plasmonic structures is the EM mechanism. [1, 2] This mechanism can be indirectly revealed by probing the optical properties of the corresponding structures. **Figures 7a-b** show the polarization dependent absorption spectra of an AgNR grown at $\theta = 86°$ without an underlying Ag film, at different deposition thicknesses d (d = 2000 nm corresponding to thickness of the optimal AgNR SERS substrates discussed in **Section 2**), probed at $\psi = 0^o$ and $\psi = 90^o$.[43] The incident light polarizations are illustrated in the corresponding figures. For *s*-polarized light ($\psi = 90°$, also see **Figure 5a**), all the spectra in **Figure 7a** exhibit relatively narrow and strong absorption peaks between 300 to 500 nm. On the other hand, for *p*-polarization ($\psi = 0°$), a broad absorption plateau appears at wavelength greater than 450 nm, as shown in **Figure 7b**. As the deposition thickness d increases, the amplitude of the plateau becomes larger. The spectral features in **Figures 7a-b** can be explained by the excitation of different localized surface plasmon resonance (LSPR) modes of AgNR, as depicted in **Figure 7c**. In the case of *s*-polarization, only the transverse LSPR modes of the AgNRs are excited, resulting in spectra close to sharp peaks in **Figure 7a**. Conversely, for *p*-polarization, both transverse and longitudinal LSPR modes are excited, leading to the observation of a broad band spectrum in **Figure 7b**.

For AgNRs grown at $\theta = 86°$ on a 100 nm-Ag film, only reflection spectra can be measured, and the optical properties are significantly different from those presented in **Figure 7**. **Figure 8a** shows the typical polarization dependent reflection spectra of an optimal AgNR substrate. Apart from the maximum reflection amplitude, the *p*- and *s*-polarized spectra appear quite similar: the

reflection increases with wavelength when $\lambda < 500$ nm, and when $\lambda > 500$ nm, the reflection remains almost constant. Further analysis reveals that the coupling between adjacent Ag nanorods also plays a crucial role in determining the optical properties, particularly the electric quadrupolar coupling, as shown in **Figure 8b**.[44] By measuring the polarization-dependent light scattering of the AgNR substrates, one can determine the induced effective magnetic permeability tensor of the AgNRs, which arises from this coupling. Additionally, by performing azimuthal and incident angle-dependent spectroscopic ellipsometry, one can determine the dielectric tensor of an optimal AgNR SERS substrate.[45] The dielectric tensor is represented as $\begin{pmatrix} \varepsilon_c & 0 & 0 \\ 0 & \varepsilon_a & 0 \\ 0 & 0 & \varepsilon_b \end{pmatrix}$, with the *a*, *b*, *c* axes defined in **Figure 5a**.[45] **Figure 8c** plots the real and imaginary parts of ε_a, ε_b, and ε_c extracting from experiments. The ε_c behaves like that of a pure metal, whereas both ε_a and ε_b

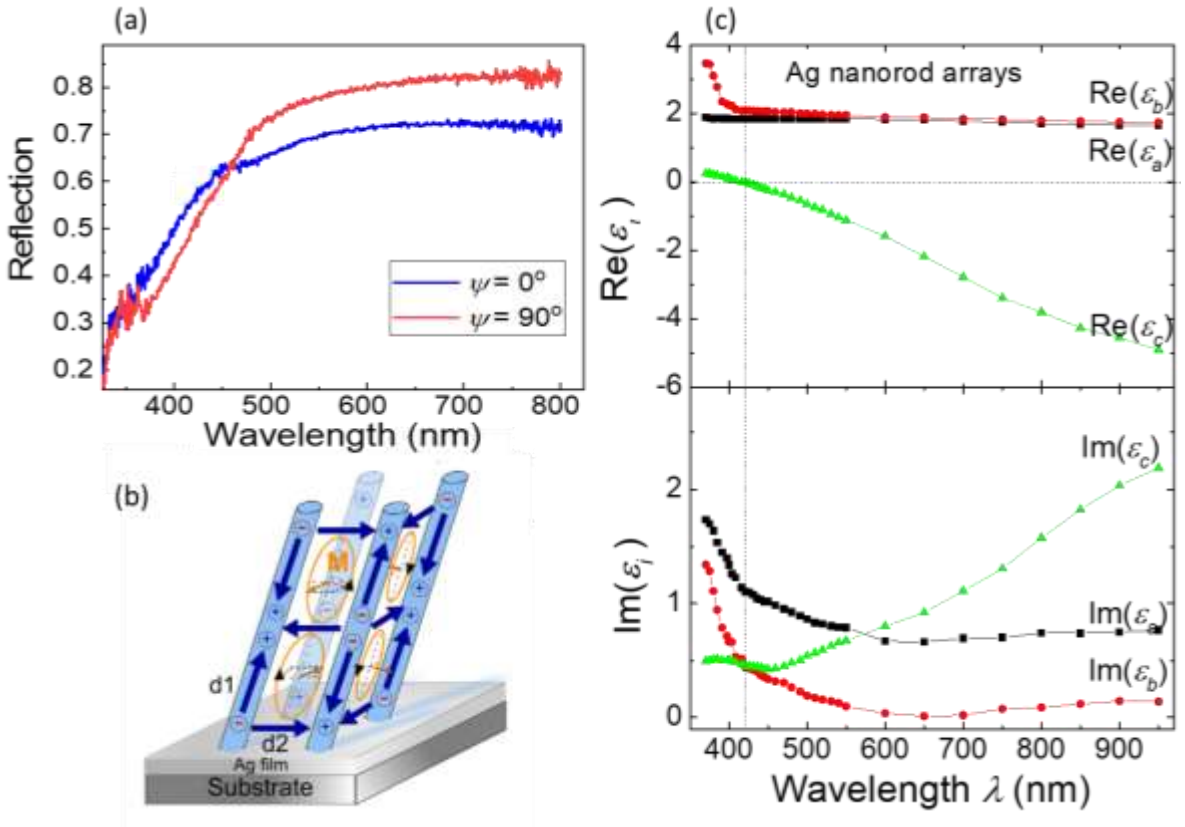

Fig. 8 (a) The polarization dependent reflection spectra of an optimal AgNR substrate. (b) The possible electric quadrupolar coupling among adjacent nanorods. (Adapted with permission from Ref. 44. Copyright 2010 Institute of Physics.) (c) The plot of dielectric tensor of an optimal AgNR substrates. (Adapted with permission from Ref. 45. Copyright 2020 Institute of Physics.)

exhibit characteristics similar to those of an absorption dielectric. This result further confirms the polarization dependent SERS behavior of AgNR substrates.

4.2 The SERS enhancement mechanism of AgNR substrates

As shown in **Figure 2** and other illustrative diagrams presented earlier, the optimal SERS substrates using AgNRs exhibit complex 3D plasmonic structures, consisting of an underlying Ag film and a randomly distributed array of tilted Ag nanorods. In comparison to plasmonic nanoparticle-based SERS substrates or other discrete nanostructure systems,[46] the AgNR substrates are considerably more intricate. **Figures 7c** and **8b** demonstrate that the plasmonic optical properties of AgNRs not only rely on the excited LSPR modes but also heavily depend on the coupling between neighboring nanorods. Furthermore, as indicated in **Figure 8b**, the combination of the underlying Ag film and adjacent Ag nanorods can give rise to cavity-like spaces. These spaces not only can securely capture analyte molecules or particles but also have the potential to form plasmonic cavities that generate stronger local electromagnetic fields. Further investigation reveals that the SERS intensity of the same analytes is strongly influenced by the

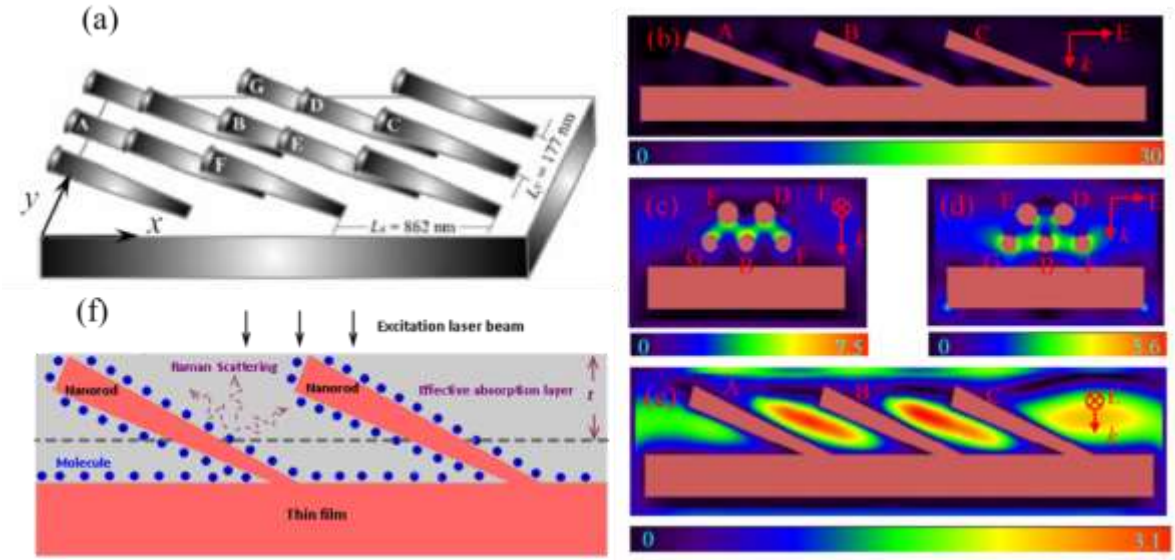

Fig. 9 (a) The schematics of AgNR SERS structure model used in the FDTD calculations. The local *E*-field magnitude distributions under different polarization incidences at different cross-sections: (b) *p*-polarization incidence and the cross-sections along the axis of nanorods A, B, and C; (c) *p*-polarization incidence and the cross-section parallel to *yz* plane crossing nanorods D, E, F, B, and G; (d) *s*-polarization incidence with the same cross-section as (c); and (e) *s*-polarization incidence with the same cross-section as (b). (f) The Raman scattering in nanorod array-film system (the dashed line) shows that the absorbance at different depths of the film may play an important role. (Adapted with permission from Ref. 49. Copyright 2009 American Institute of Physics.)

sample preparation strategy, as discussed in **Section 6**. For instance, under identical analyte concentrations, the immersion method yields significantly higher SERS signals compared to the drop-cast method. Additionally, drying the SERS analyte droplet dissolved in a high surface tension liquid on AgNR substrates produces superior SERS signals.[47] These findings collectively suggest that the potential mechanism underlying SERS enhancement could be quite complicated.

In 2009, a comprehensive theoretical and experimental study was conducted by Zhao and colleagues to elucidate the SERS mechanism of AgNR substrates.[48, 49] Utilizing a regular array of AgNRs, as shown in **Figure 9a**, finite difference time domain (FDTD) calculations were performed at an excitation wavelength of $\lambda_{ex} = 785$ nm. **Figures 9b-c** depict the distribution of the ratio of the magnitude of the local electric field to the incident excitation field ($|\vec{E}_{local}|/|\vec{E}_0|$) of AgNRs in two cross sections under *p*-polarization. The corners between the tilted nanorods and the Ag film exhibit the highest E-field magnitudes. Additionally, relatively strong E-fields are observed around each nanorod and on top of each nanorod. Under *s*-polarization, **Figures 9d-e** illustrate the E-field magnitude distribution, where the maximum E-fields are observed at the sides of each nanorod, and significant coupling occurs between adjacent nanorods in the horizontal direction. Therefore, the hot-spots for the Ag nanorod array are localized at the corners between the tilted nanorods and around each Ag nanorod.[48] These findings have been subsequently confirmed by other research groups.[31, 50] However, it should be noted that since the nanorods are elongated and the hot-spots are distributed throughout the entire depth of the nanorod thin film, when estimating the SERS EF under a specific polarization excitation (**Figure 9f**), the actual SERS intensity can be expressed as,[49]

$$I_{SERS} \propto \iiint_v n(e^{-\alpha_s z}|E^y_{local}|^4 + e^{-\alpha_p z}|E^x_{local}|^4)dv, \quad (1)$$

where *n* represents the uniform Raman molecule density, α_s and α_p are the absorption coefficients of AgNR substrate at both *s*- and *p*-polarization incidents, i.e., one needs to count all SERS signals emitted from the entire SERS active layer.

Subsequently, the following experiments was designed to investigate the impact of analyte molecule location on the SERS response in AgNR substrates, as shown in **Figure 10a**.[48] In the first case (Case I), a 500-nm Ag thin film was deposited on a glass substrate, and a 1 μL droplet of 10^{-4} M BPE was uniformly drop-casted onto the Ag thin film substrate, followed by measuring the SERS spectrum. Next, an Ag nanorod array, prepared through OAD, was deposited onto the BPE-coated Ag thin film substrate from Case I without adding any additional BPE (Case II), and

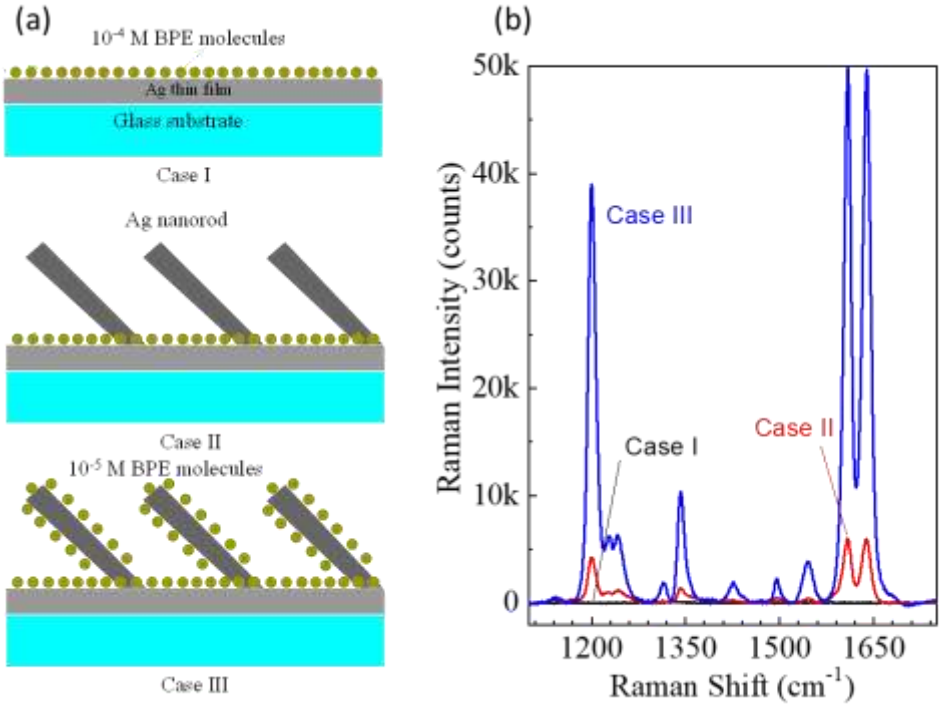

Fig. 10 (a) Cartoons to illustrate three cases for experimental design: Case I: A droplet of 10^{-4} M BPE was dispensed on the Ag film; Case II: Ag nanorods were deposited onto BPE-dispensed Ag thin film; Case III: a droplet of 10^{-5} M BPE was dispensed on the AgNR substrate from Case II. (b) The representative BPE spectra obtained from Cases I, II and III. (Adapted with permission from Ref. 48. Copyright 2009 American Chemical Society.)

the SERS spectra were obtained. Finally, a 1 μL drop of 10^{-5} M BPE was dispensed on the top of the AgNR substrate, and the SERS spectra were once again measured (Case III). **Figure 10b** displays representative SERS spectra obtained from Cases I, II, and III, respectively. The SERS spectrum from Case I (black curve) exhibits weak spectral features, while noticeable SERS peaks (red curve) are observed for Case II, indicating that the corners between the Ag nanorods and the planar Ag film serve as SERS hot-spots. In Case III, a remarkably strong SERS signal is obtained, approximately 10 times greater than that of Case II. Despite the concentration of BPE droplets in Case III being 10 times lower than in Case I, and the actual surface area of the AgNR substrates being over 10 times higher than that of the flat Ag thin film, the SERS signal in Case III is almost 10 times stronger than in Case II. This observation suggests that the application of 10^{-5} M BPE on the surfaces of Ag nanorods significantly enhances the SERS signal, indicating that both the side surfaces and tips of the Ag nanorods play a crucial role in enhancing Raman signals for AgNR substrates.[48]

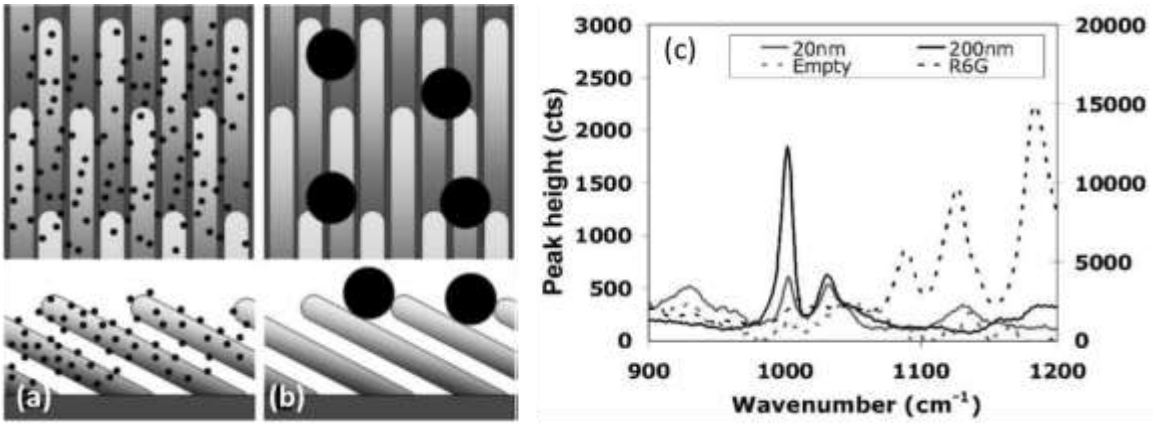

Fig. 11 (a) Schematic illustration (a) 20 nm diameter and (b) 200 nm diameter polystyrene beads on AgNR SERS substrates. (c) The representative SERS spectra obtained on both polystyrene bead samples and Rhodamine-6G (R6G) on (a) AgNRs (primary y-axis) and (b) flat silver substrates (secondary y-axis). (Adapted with permission from Ref. 51. Copyright 2013 SAGE Publications Inc.)

Alternatively, Marotta and Bottomley conducted an experiment utilizing polystyrene (PS) beads of different sizes as Raman probes to demonstrate the significance of Ag nanorod tips in enhancing the Raman signal.[51] They dispensed 5 µl aliquots of 2×10^{10} ml^{-1} 20 nm-diameter PS beads and 2×10^{7} ml^{-1} 200 nm-diameter PS beads onto the AgNR wells with identical areas. Considering the geometry of AgNR substrates, the 20 nm PS beads were distributed between the Ag nanorods (**Figure 11a**), while the 200 nm beads could only reside on the tips of Ag nanorods (**Figure 11b**). Based on calculations, the surface area of the beads in contact with the nanorods was found to be similar for both cases. SERS spectra were obtained under identical measurement conditions for the two scenarios, as shown in **Figure 11c**. Taking into account various factors that could influence the SERS intensity, such as the contacting surface areas of the beads with AgNRs and the uneven distribution of beads in the well, the researchers discovered that the SERS intensity of the 200 nm-diameter PS beads was approximately three times higher than that of the 20 nm-diameter beads, despite the number density of smaller beads being over 1000 times greater. These findings align with the results from **Figure 10** [48] and further suggest that the Ag nanorod tips may exhibit stronger enhancement, consistent with the lightning-rod theory[40].

4.3 A phenomenological model of SERS response of AgNR substrates

Despite the comprehensive understanding of the SERS enhancement mechanism in AgNR substrates discussed earlier, several experimental observations, such as polarization (**Figure 5**), excitation laser incident angle (**Figure 6**), and the underlying layer (**Figure 3c**), cannot be

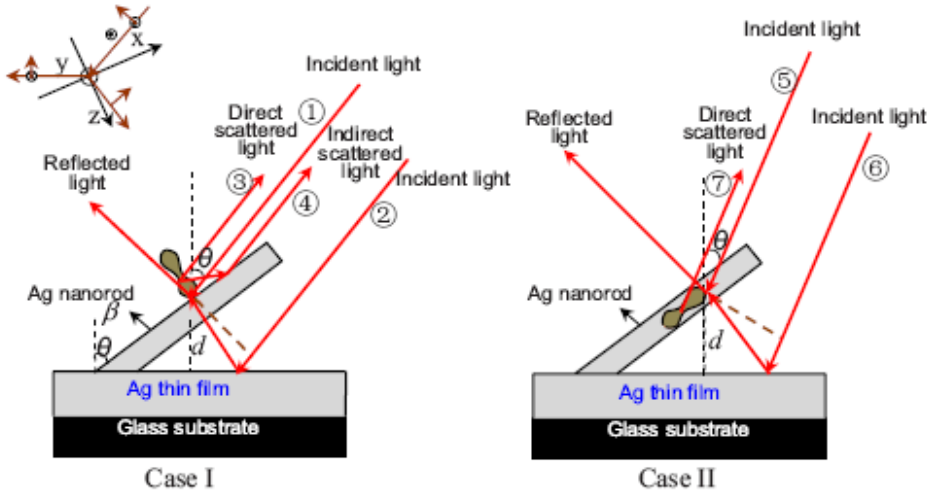

Fig. 12 A schematic illustration of the modified Greenler's model for AgNR substrates: Case I — the dipole of targeted molecule is in the incident plane; Case II — the dipole of targeted molecule is perpendicular to the incident plane. All the induced dipoles are perpendicular to the nanorod. (Adapted with permission from Ref. 28. Copyright 2008 American Physical Society.)

accurately predicted quantitatively or semi-quantitatively. This is due to the fact that SERS, unlike conventional Raman spectroscopy, requires the analyte molecules to attach to the SERS surface. Once the molecules are adsorbed, the scattering symmetry is disrupted, leading to modifications in the selection rules.[5] Additionally, the incident angles, polarization of the excitation laser, and optimal collection angles are influenced by this configuration. Greenler accounted for these effects by considering the adsorbed targeted analyte molecule as a simple oscillating dipole on a flat surface, which breaks the reflection symmetry for molecule vibrations.[52]

Based on the surface dipole model , along with the experimental results and conditions, Liu and Zhao proposed a modified Greenler's model to explain the dependence of incident angle, nanorod tilting angle, polarization, and substrate reflection on the SERS response of targeted molecules adsorbed onto AgNR substrates.[28] The model made several assumptions: 1) The surface of the Ag nanorod was treated as planar, neglecting any scattering effects of the nanorods, and only considering Raman scattering from a single nanorod. 2) The targeted molecules were assumed to adsorb on the side and top surfaces of the Ag nanorods. 3) The SERS effect of molecules on the top of Ag nanorods was neglected, focusing only on the SERS intensity from molecules adsorbed on the side surfaces. 4) Only the backscattering collecting configuration was considered. Since the targeted molecules can randomly adsorb on the AgNR surfaces, the model simplified the analysis by considering two cases: Case I, where the dipole of the targeted molecule is parallel to the

incident plane of the excitation laser, and Case II, where the dipole is perpendicular to the incident plane (**Figure 12**).

In Case I (**Figure 12**), the external field inducing forced oscillation of the targeted molecule dipole consists of three components: the direct incident laser beam ①, the laser beam reflected from the surface of the Ag nanorod ①, and the laser beam reflected from the Ag thin film ②. The forced oscillation of the molecular dipole emits Raman radiation, with part of the radiation ③ directly collected by the detector, while the remaining portion is reflected from the Ag nanorod surface ④ and subsequently collected by the detector. In Case II (**Figure 12**), only two beams contribute to the forced field for dipole oscillation: the incident light beam ⑤ and the laser beam reflected from the Ag thin film ⑥. The Raman radiation from the molecular dipole ⑦ is directly collected by the detector. The total Raman intensity is assumed to be the sum of the collected radiations from both Case I and Case II.

Taking into account the reflectivity of the incident laser beam on Ag surfaces using the Fresnel equations and considering the radiation distribution of a dipole moment, a pair of equations describing polarized (Eq. 31 in Ref. [28]) and unpolarized (Eq. 32 in Ref. [28]) Raman scattering intensity were derived. These equations incorporate the effects of polarization, incident angle of the excitation laser, reflectivity of the underlying thin film, and the tilting angle of the nanorods. They demonstrate excellent agreement with the experimental results, as depicted by the solid lines or curves in **Figures 3b**, **5b**, and **6b**.

5. Quality of AgNR substrates

The previous sections have focused on elucidating the fundamental properties of AgNR substrates and the underlying SERS enhancement mechanism. However, when considering practical applications, the quality of SERS substrates becomes a primary concern. In this section, we will examine these attributes primarily based on our own experience, while also considering relevant findings from the literature.

5.1 The quality and uniformity of AgNR substrates

The quality of AgNR substrates is influenced by various factors, including material purity, deposition chamber conditions, and substrate preparation. Based on our previous experience, we have found that the purity of the Ag evaporation material plays a crucial role. Ag with a purity of

99.999% yields significantly better SERS substrates compared to Ag with purities of 99.995% or 99.99%. Furthermore, contamination from the deposition chamber, especially if it has been used for other material depositions involving graphite crucibles, can greatly degrade the quality of the resulting AgNR SERS substrates. Therefore, whenever possible, it is advisable to use a dedicated AgNR substrate fabrication chamber.

Additionally, the preparation of the substrates is of utmost importance. The substrates used for AgNR deposition should be free from contamination and particles. The presence of foreign

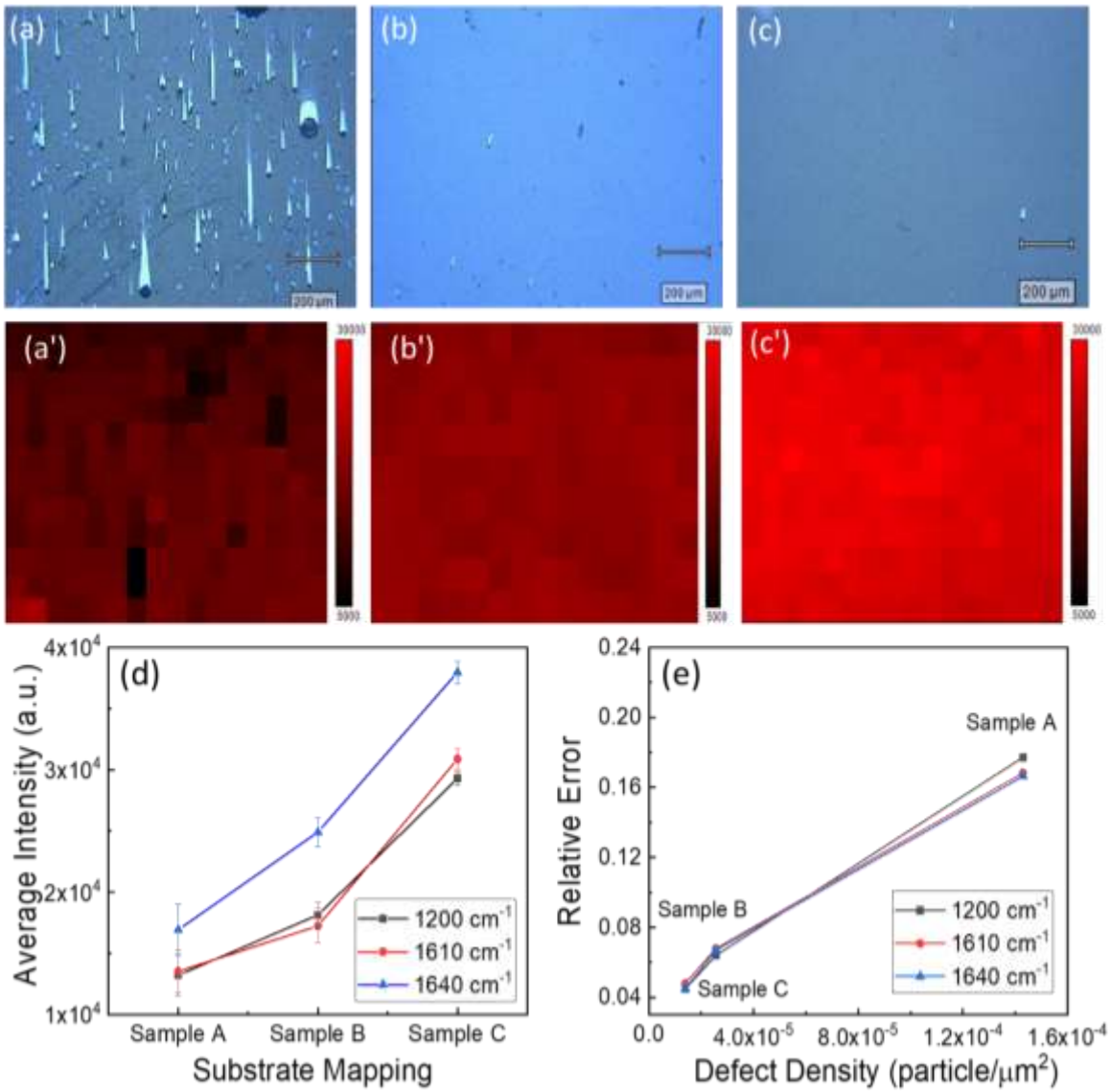

Fig. 13 Representative micrographs of AgNR substrates with varying defect densities: (a) high, (b) medium, and (c) low, and corresponding SERS intensity mappings of the 1200 cm^{-1} peak of 10^{-5}M BPE on corresponding substrates (a'-c'). The plots of (d) the average BPE SERS peak intensities and (e) the corresponding variations of these three samples.

particles on the flat substrates can lead to the generation of numerous defects due to the shadowing effect of OAD after AgNR deposition, resulting in significant variations in SERS measurements. **Figures 13a-c** display three typical photos of AgNR substrates with different defect densities: 1.4×10^{-4}, 2.5×10^{-5}, and 1.3×10^{-5} particles/μm^2. Higher defect densities are associated with greater morphological variations, as depicted in **Figures 13a'-c'**, which show the SERS intensity mappings of the $\Delta\nu = 1200$ cm^{-1} peak of 10^{-5} M BPE. It is evident that a high defect density sample exhibits substantial SERS intensity variation. To provide a clearer representation, **Figures 13d-e** present the average BPE intensity and the corresponding variations obtained from the mappings collected from the three substrates shown in **Figures 13a-c**. Clearly, substrates with high defect density not only exhibit lower SERS intensity but also have higher variation. Conversely, high-quality AgNR substrates with minimal defects display not only the highest intensity but also minimal variation across the entire substrate. These results emphasize the importance of preparing AgNR substrates in a cleanroom environment.

5.2 The reproducibility of AgNR substrates

Another critical aspect of AgNR production is the observed variation from batch to batch. Due to the involvement of different students working in the lab and changes in the Raman instrument utilized, we were unable to gather long-term data for this study. However, we were able to collect over one year of data from a single operator to analyze the batch-to-batch variations. **Figure 14a**

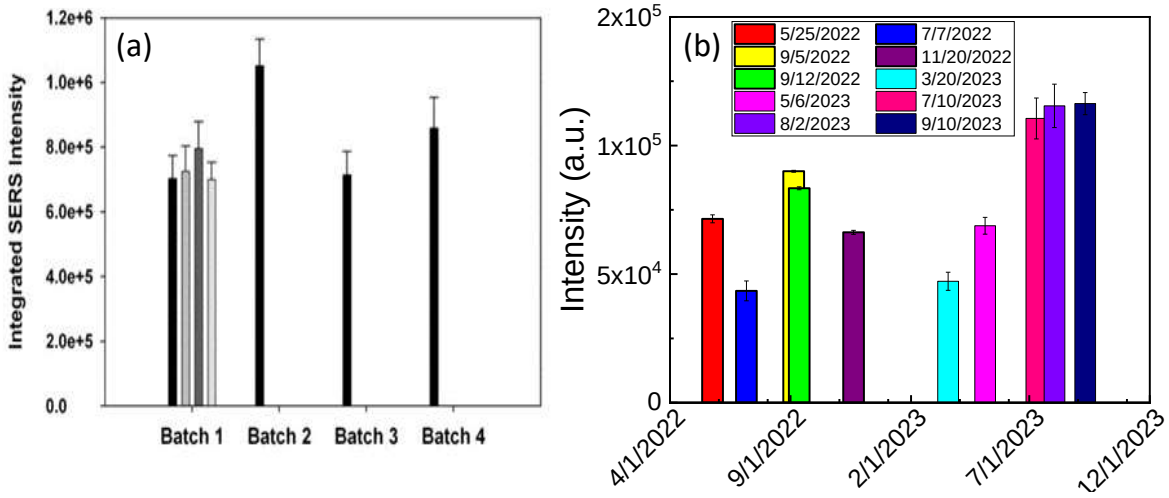

Fig. 14 The Integrated intensity of the BPE peak $\Delta\nu = 1200$ cm^{-1} peak for substrate prepared in the same batch and different batches: (a) 2008 results (Adapted with permission from Ref. 20. Copyright (2008) American Chemical Society) and (b) current result.

showcases the variations observed in AgNR SERS substrates produced in Ref. 20, while **Figure 14b** represents the variations observed in 2022-2023.

In the 2008 paper, it was reported that the reproducibility from substrate to substrate ranged from 6% to 13% for substrates prepared in the same batch, with a batch-to-batch reproducibility of less than 15%.[20] In principle, the quality of the substrates shall not depend on the operator as long as the standard procedures are followed, since the process is compatible to microfabrication for chips. However, in our current production (**Figure 14b**), the quality and consistency of the substrates were significantly influenced by the students' training and the working environment. Between May 2022 and May 2023, there was noticeable variation in substrate quality. It was only after implementing several measures, such as upgrading the lab's air handling system, enforcing stringent substrate cleaning protocols, and ensuring substrate packaging in a cleanroom environment (Class 1000), that the quality and uniformity of the substrates significantly improved from July 2023 to September 2023. These high-quality substrates now resemble Sample C in Figure 13. Consequently, the variation from one substrate to another is now less than 5%, and the reproducibility from batch to batch is below 15%.

It is important to note that the SERS measurement instrument and the BPE sample preparation conditions varied between the two figures. Despite these variations, the results highlight a remarkable level of consistency.

5.3 Air contamination for AgNR substrates

Due to their high SERS EF and the inherent chemical activity of Ag surfaces, AgNR substrates are susceptible to rapid adsorption of organic molecules from the surrounding air, leading to significant background SERS spectra.[53-56] These molecular contaminants can occupy active SERS hot-spots, impeding the adsorption of targeted molecules onto these hot-spots. Particularly, for analyte molecules with weak affinity for Ag surfaces, this contamination can hinder or even prevent their adsorption onto the contaminated surface. Furthermore, at extremely low concentrations, these surface contaminants or impurities can have a noticeable impact by generating anomalous SERS bands that overlap with the desired SERS signal of the target molecule. As a result, contamination not only reduces the sensitivity of AgNR-based SERS sensors but also introduces additional spectral features that interfere with the accurate interpretation of the acquired spectra. The issue of surface contamination is commonly encountered regardless of the fabrication method employed, and it can arise from the preparation procedure or from the ambient

atmosphere during storage. Typically, these contaminants primarily consist of organic (carbonaceous) substances that adhere to the Ag surface.[53-56]

The degree of contamination on AgNR substrates also heavily depends on the quality of the surrounding air. **Figure 15a** shows the time-dependent SERS spectra of a fresh AgNR before the

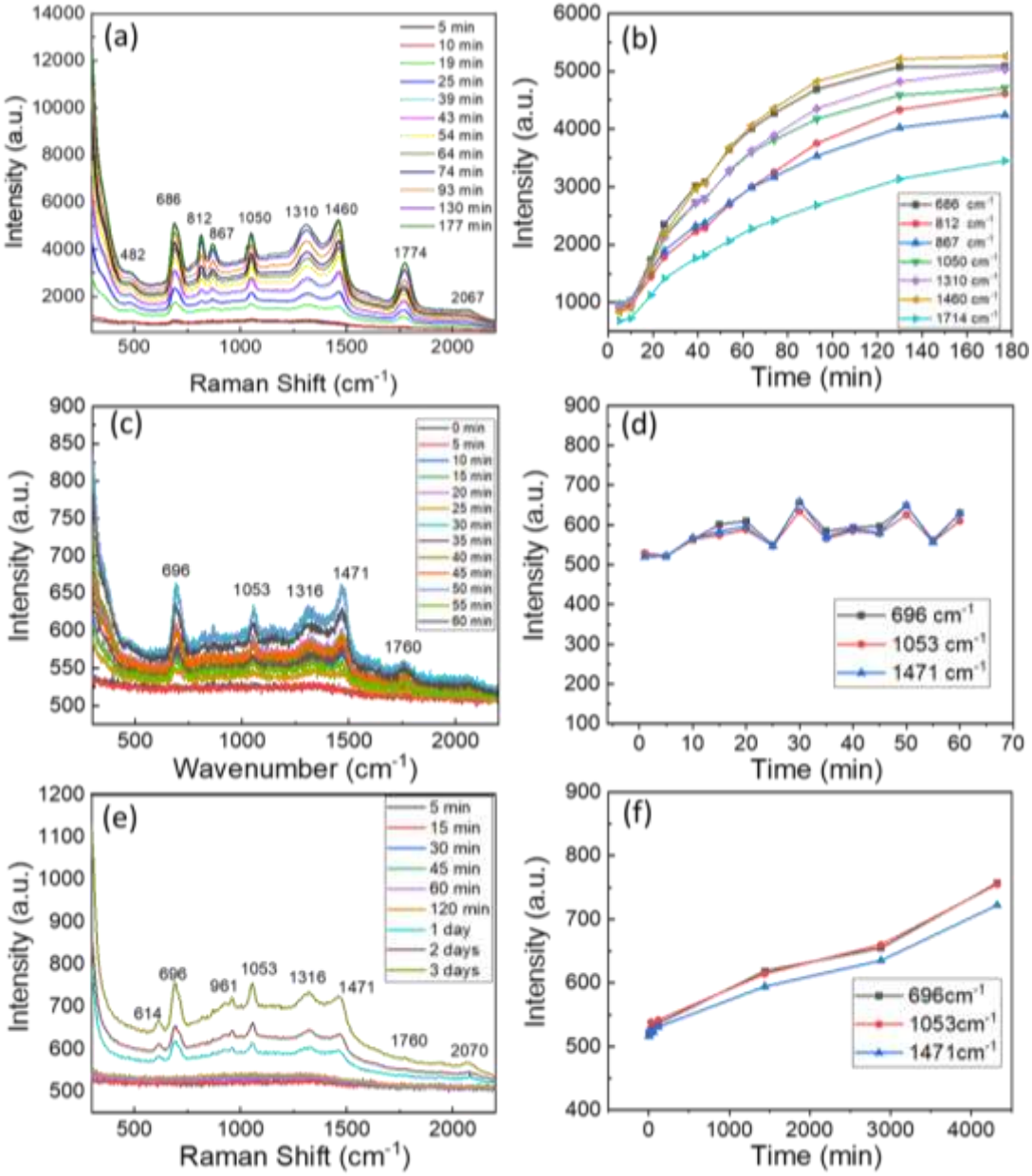

Fig. 15 (a) The time-dependent spectra of a fresh AgNR before the air-handling system was replaced, and (b) the corresponding plot of peak intensities versus time. (c) The time-dependent spectra of a fresh AgNR after the air-handling system was replaced, and (d) the corresponding plot of peak intensities versus time. (e) The time-dependent spectra of an AgNR substrate after Ar^+ plasma cleaning, and (f) the corresponding plot of peak intensities versus time.

air-handling system in our building was replaced. The initial spectrum, obtained approximately 5 minutes after removing the sample from the chamber, exhibits weak contamination peaks. However, after the sample was exposed to air for 19 minutes, a notable and significant increase in contamination peaks is observed. This trend continues throughout the 3-hour measurement duration, with the spectral intensity of contamination steadily increasing over time and eventually reaching saturation, as shown in **Figure 15b**, depicting the time-dependent intensities of the contamination peaks. However, after the replacement of the old air-handling system in the lab, the severity of contamination is significantly reduced. **Figure 15c** presents the time-dependent spectra of a fresh AgNR substrate after the air-handling system was replaced. In this case, after 60 minutes, the overall contamination spectra exhibit minimal changes compared to **Figure 15a**. **Figure 15d** plots the contamination peak intensities against time, further confirming our findings. Clearly, maintaining good air quality during fabrication is also of paramount importance. In addition, the plasma cleaned AgNR substrate (see **Section 5.5**) can be re-contaminated when exposed in ambient air for a long time, as shown by **Figures 15e-f**.

5.4 Storage of AgNR substrates

Considering that air contamination is unavoidable and accumulative, it is crucial to store AgNR substrates in a contamination-free environment or protect their surfaces with specialized coatings. Several studies have investigated the use of different coatings, such as polymer coatings[57] or thiol coating,[58] to safeguard SERS substrates. However, it is important to note that if these coatings are not thoroughly cleaned, they may introduce spectral features associated with the coating materials, which can be considered as additional sources of contamination.

A conventional way to prolong the shelf-life of AgNR substrates is to store the substrates in a clean environment, such as high vacuum.[59] In our research group, we have implemented a method of storing AgNR substrates using argon-filled pouches. **Figure 16a** shows a photo of such a pouch and its contents. Four 0.5”×0.5” AgNR substrates are securely attached to a glass slide using double-sided tape, and this glass slide is carefully inserted into a sturdy mailer box capable of accommodating multiple slides. To maintain optimal conditions, the mailer box is enclosed within a moisture-resistant bag and filled with argon gas, creating a controlled atmosphere. Finally, the bag is hermetically sealed using a vacuum sealer, effectively preserving the contents and protecting them against external influences. We employ a digital vacuum sealer (ACCVACS E200G) for this packaging process, as shown in **Figure 16b**.

We have been employing this packaging method for AgNR substrates since 2007. To assess the long-term efficiency of storage, we conducted standard SERS measurements of 10^{-5} M BPE using AgNR substrates that had been stored for varying durations, under identical conditions. The resulting SERS peak intensities, with and without plasma cleaning, are presented in **Figures 16c-d**, respectively. For the untreated AgNR substrates, the overall trend of the SERS intensities versus storage time indicates a monotonic decay, albeit with some fluctuations. However, for the plasma-cleaned substrates, the SERS intensity exhibits a continuous and monotonous decrease as the storage time increases. Such a decay can be attributed to slow Ag surface oxidation or adsorption of more contaminants. The data can be fitted with an exponential decay function, as shown by the solid curve in **Figure 16d**. From this analysis, we were able to determine that the shelf life of the

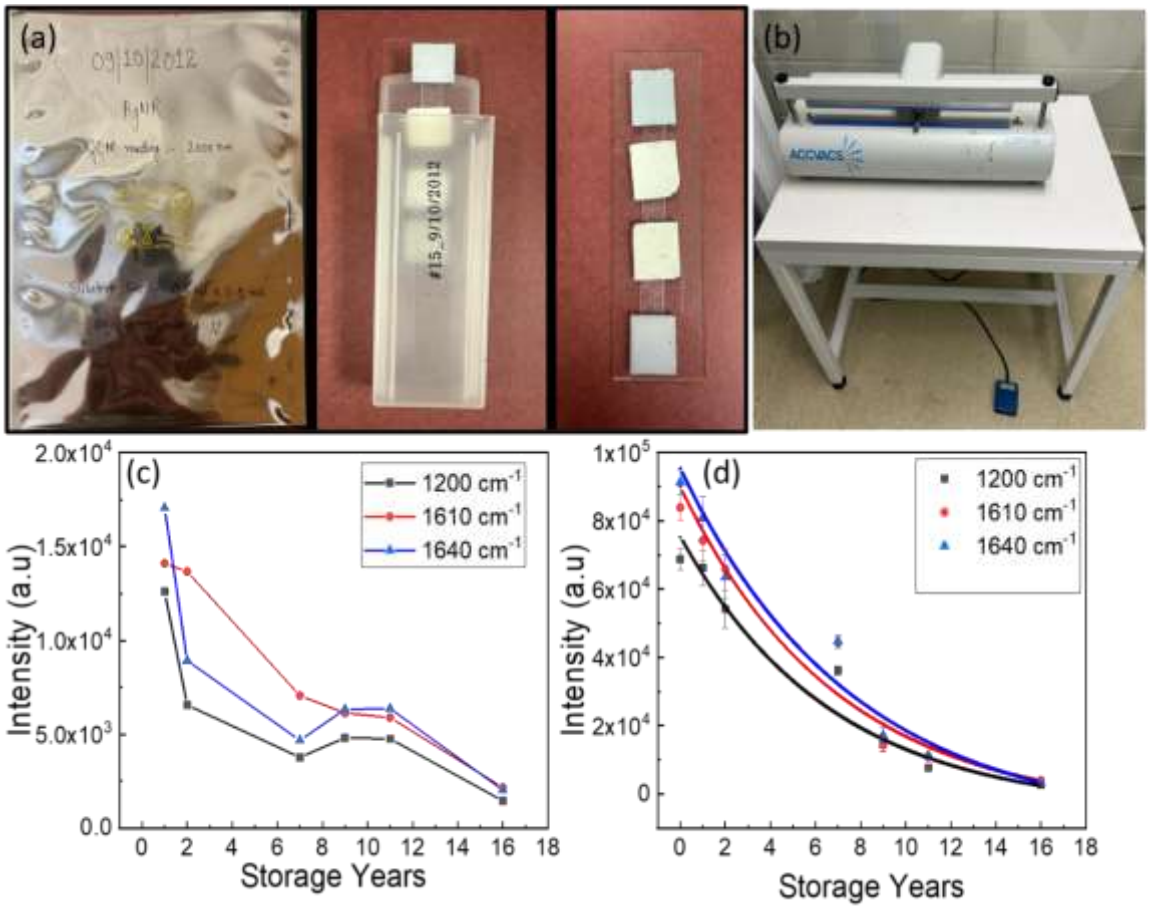

Fig. 16 Storage and protection of AgNR Substrates: (a) A photo of the Ar-filled pouch and the AgNR substrates in a glass-mailer stored in the pouch and (b) the digital vacuum sealer used for packaging the pouch. The SERS intensities of BPE peaks versus packaging duration plots of (c) un-cleaned substrates and (d) plasma cleaned substrates. The solid curves in (d) show the exponential decay fittings.

AgNR substrates (initial intensity decays to 1/*e*), in terms of maintaining their SERS performance, is approximately 7 years.

5.5 The cleaning of AgNR substrates

It is evident that contamination on AgNR substrates is unavoidable after storage.[60, 61] While it is acceptable to use these contaminated substrates directly if the targeted analyte molecules have a high SERS scattering cross-section, a strong analyte-surface affinity, and a large enough concentration, applications requiring high sensitivity may necessitate the removal of contamination before using the AgNR substrates for targeted detection. Currently, our preferred method for cleaning AgNR substrates is Ar plasma cleaning, based on the investigation conducted by Negri et al.[53]

Plasma cleaning with argon efficiently eliminates both the adsorbed analytes and original organic contaminants from the Ag nanorod substrate, as indicated by the absence of corresponding spectral features in the SERS spectrum after cleaning. The cleaned substrate retains approximately

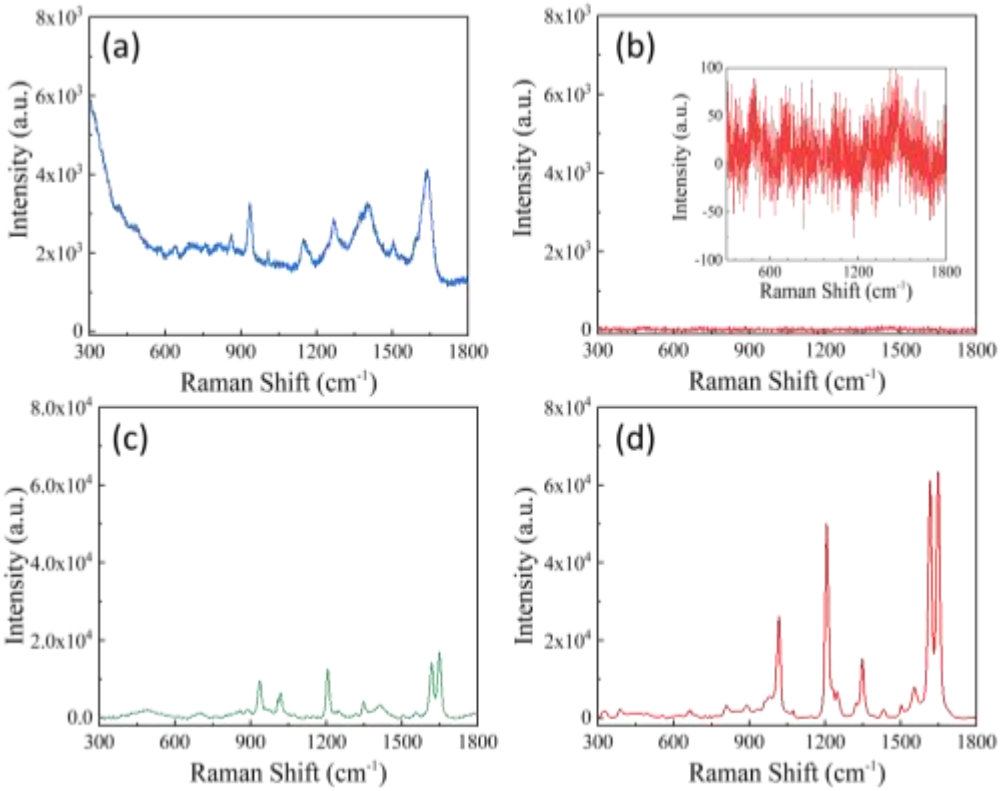

Fig. 17 The effects of plasma cleaning of an AgNR substrate: (a) the background SERS spectrum of an uncleaned AgNR substrate, and (b) the spectrum of a plasma-cleaned substrate. (c) The 10^{-5} M SERS spectrum of an uncleaned and (d) a plasma cleaned AgNR substrate.

60% of the SERS intensity when an analyte is reapplied, suggesting that the cleaning procedure reduces the observed intensity without altering the spectral characteristics of the analyte. **Figure 17a** shows a SERS spectrum of an AgNR substrate that has been exposed to air for an extended period. Several characteristic peaks, such as $\Delta v = 937, 1153, 1270, 1407, \text{and } 1640$ cm^{-1}, can be observed, which are likely due to organic contamination in the air, as discussed earlier; and the maximum intensity count reaches 6,000.

After subjecting the same substrate to 90 seconds of Argon (Ar^+) plasma cleaning, the resulting SERS spectrum becomes remarkably flat and featureless, as shown in **Figure 17b**. In fact, the SERS intensity varies between -100 to 100 counts, as indicated in the insert of **Figure 17b**. The quality of the AgNR substrate is also improved: **Figure 17c** shows a SERS spectrum of 10^{-5} M BPE dispensed on the uncleaned AgNR substrate. The highest peak intensity occurs at $\Delta v = 1640$ cm^{-1}, with $I_{1648} \approx 20{,}000$. In contrast, for the plasma-cleaned substrate under the same measurement conditions, as shown in **Figure 17d**, the maximum intensity becomes $I_{1648} \approx 63{,}000$, which is three times the intensity observed in **Figure 17c**. Furthermore, when comparing the spectral shapes in these two figures, the spectrum in **Figure 17c** exhibits higher background intensity. Note that most of AgNR substrates used in our studies, if not otherwise stated, were Ar^+ plasma cleaned.

When AgNR substrates are removed from the vacuum chamber, a thin layer of Ag_2O naturally forms on the surface, which is expected to attract contaminants. Therefore, a simple method to clean the AgNR substrates is to remove this oxide layer, which can be easily achieved through a chemical reaction. One effective approach is the use of a very dilute nitric acid (HNO_3) solution to remove Ag_2O on AgNR, as demonstrated in Ref. [62]. **Figure 18** presents the results of a systematic investigation: 1 cm × 1cm AgNR substrates are immersed in HNO_3 solution ranging from 0.02 μM to 0.25 μM by mixing 65% HNO_3 with anhydrous methanol for 5 minutes, and the SERS spectra of the cleaned substrates are measured, as shown in **Figure 18a**. With different HNO_3 treatments, SERS peaks at $\Delta v = 891, 966, 1039, 1407, \text{and } 1635$ cm^{-1} appear with varying intensities. The peak at $\Delta v = 1039$ cm^{-1} may arise from $AgNO_3$,[63] while the other peaks may be associated with hydrocarbons or other contaminants. Although the treated substrates exhibit higher background signals, when droplets of 2 μL of 10^{-5} M BPE are drop-casted onto these cleaned AgNR substrates, the resulting BPE spectra show significant different behavior. **Figure 18b** compares the five main peaks of BPE SERS spectra. Among the different HNO_3 treatments,

the 0.05 μM HNO_3 treatment yields the highest intensity for all Raman bands, followed by the 0.02 μM HNO_3 treatment. These results demonstrate that a dilute HNO_3 treatment can effectively clean the AgNR substrates.

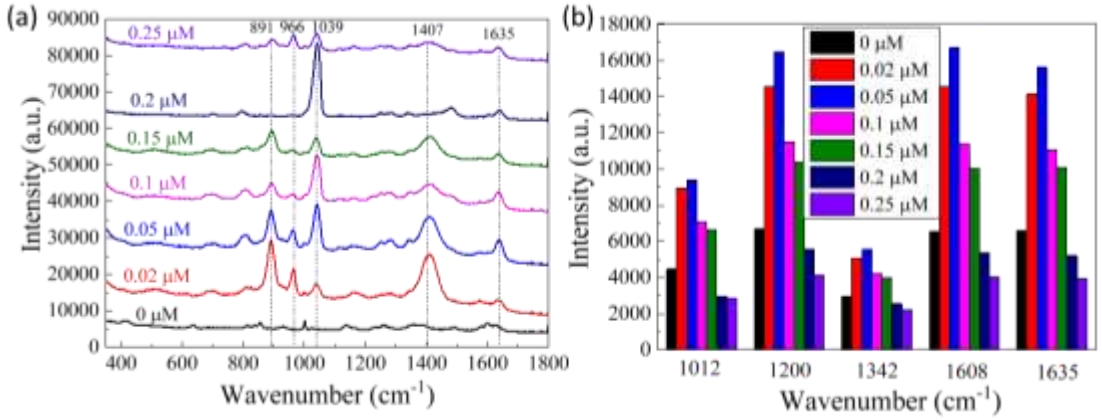

Fig. 18 (a) The SERS spectra of AgNR substrates treated by different HNO_3 solutions. (b) The comparison of the five main peaks of BPE SERS spectra from AgNR substrates by different HNO_3 treatments.

6. AgNR Substrate Based SERS Measurements

In **Section 5**, we extensively covered the quality and preparation of AgNR substrates for SERS measurements. Now, in this section, we will discuss various aspects related to conducting SERS measurements using AgNR substrates. We will first discuss how to prepare samples for SERS measurements and then consider how different optical conditions affect the SERS measurements.

6.1 Sample preparation on AgNR substrates: drop-cast and immersion

Sample preparation plays a critical role in obtaining reliable and accurate SERS measurements, particularly when utilizing AgNR substrates. The quality of sample preparation directly affects the interaction between the analyte molecules and the substrate, thereby impacting the resulting SERS signal. Several factors, including the concentration, volume, and distribution of analyte molecules, can significantly influence the SERS measurements. It is important to achieve a uniform distribution of the analyte molecules across the substrate surface to obtain consistent and reproducible results.

In general, there are two commonly used sample preparation methods for AgNR substrates: the drop-cast method and immersion method. The drop-cast method, as shown in **Figure 19a**, involves several steps: 1) preparing a desired concentration of analyte, 2) preparing a AgNR SERS

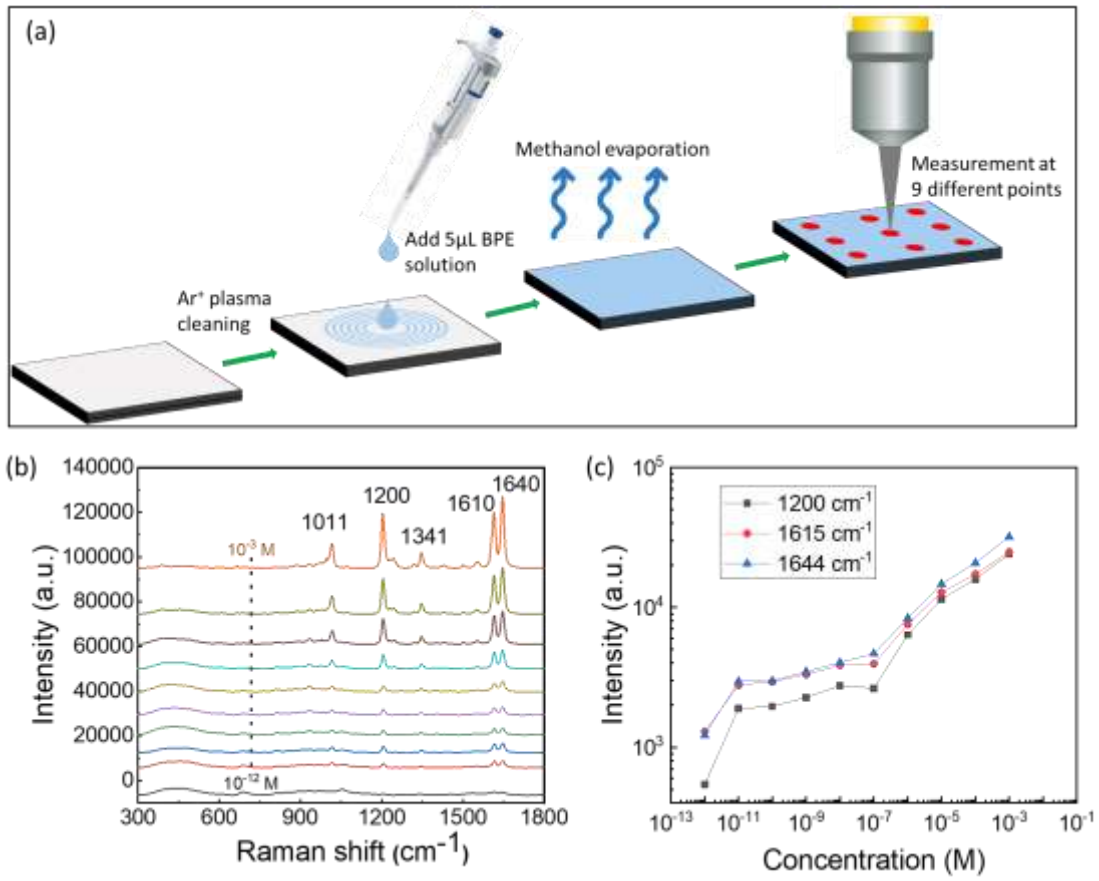

Fig. 19 (a) A cartoon showing the drop-casting sample preparation process; (b) the concentration dependent SERS spectra of 10^{-12} – 10^{-4} M BPE solutions; and (c) the SERS peak intensity I_{SERS} at $\Delta\nu = 1200, 1610,$ and 1640 cm^{-1} of BPE spectra versus BPE concentration.

substrate with an appropriate area, 3) dispensing an appropriate amount of analyte solution on the substrate, ensuring the droplet spreads uniformly across the entire substrate, and 4) acquiring multiple SERS spectra at different locations of the substrate to obtain an average spectrum and assess variations. The drop-cast is a dynamic and non-equilibrium process influenced by various factors, including the uniformity of droplet spreading, the spreading and evaporation dynamics of the droplet, the adsorption of the target analyte molecules in hot-spots, etc. If we consider a droplet of analyte solution with a volume V and a concentration C_b uniformly spread onto an AgNR substrate with an area of A_s, and the excitation laser beam has a probe area of A_p, the number of analyte molecules N_p can be probed is,

$$N_p = \frac{VC_b}{A_s} A_p. \quad (2)$$

However, it is important to note that the actual number of probed analyte molecules may deviate from N_p due to the fact that only the analytes located in SERS hot-spots can contribute to

the final SERS spectrum. **Figure 19b** shows example of BPE spectra obtained from 5 µl 10^{-12} – 10^{-3} M. BPE was prepared in methanol, which were dispensed on 1 cm × 1cm AgNR substrates. Given the low surface tension of methanol, the sample droplet rapidly spreads and completely covers the entire AgNR substrate, evaporating quickly and resulting in uniform and consistent SERS spectra. In fact, **Figure 13c** showcases the outcome of uniformly spreading of BPE methanol solution. According to our measurements, when the BPE concentration is 10^{-12} M, the estimated number of BPE molecules within the excitation laser beam is approximately 0.9, effectively one molecule. As the concentration increases to 10^{-11} M, the estimated number of BPE molecules rises to around nine. Consequently, as shown in **Figure 19c**, the AgNR substrate demonstrates the capability of single molecule detection. Additionally, it becomes evident that with increasing concentration, the spectral peak intensities at $\Delta v =$ 1200, 1610, and 1640 cm^{-1} increase monotonically with the BPE concentration. In a log-log plot (**Figure 19c**), the relationships are linear, with the slope representing the apparent sensitivity of the detection, measured as 0.16 ± 0.01 lg(counts)/lg(M).

However, if the analyte solution does not exhibit good wetting properties with the AgNR substrate, a phenomenon known as the coffee ring effect (CRE) can occur, leading to non-uniform distribution of the analyte molecules on the spreading area.[64, 65] The underlying principle of the coffee ring effect can be attributed to a combination of capillary flow and particle migration, as illustrated in **Figure 20a**. As the liquid droplet evaporates, the liquid at the droplet's edges experiences higher curvature compared to the liquid at the center. This disparity in curvature triggers capillary flow, causing the liquid to migrate from the center towards the edges of the droplet. Alongside this flow, suspended particles or solutes present in the liquid are carried towards the droplet's periphery. These particles/solutes, being larger and less volatile than the liquid, do not evaporate as rapidly and consequently accumulate near the edges of the droplet as evaporation progresses, resulting in the formation of a darker and more concentrated ring. Various factors influence the CRE, including droplet size, solute concentration, liquid surface tension, contact angle between the liquid and the solid surface, and evaporation rate.

When the BPE is dissolved in deionized (DI) water, the water droplet does not spread well on the AgNR surface, as shown in **Figure 20b**. Upon drying, a ring-like mark is left on the AgNR substrate surface, as shown in **Figure 20c**. When SERS spectra are measured across this water-induced mark and the SERS intensity is plotted as a function of the measurement location, as

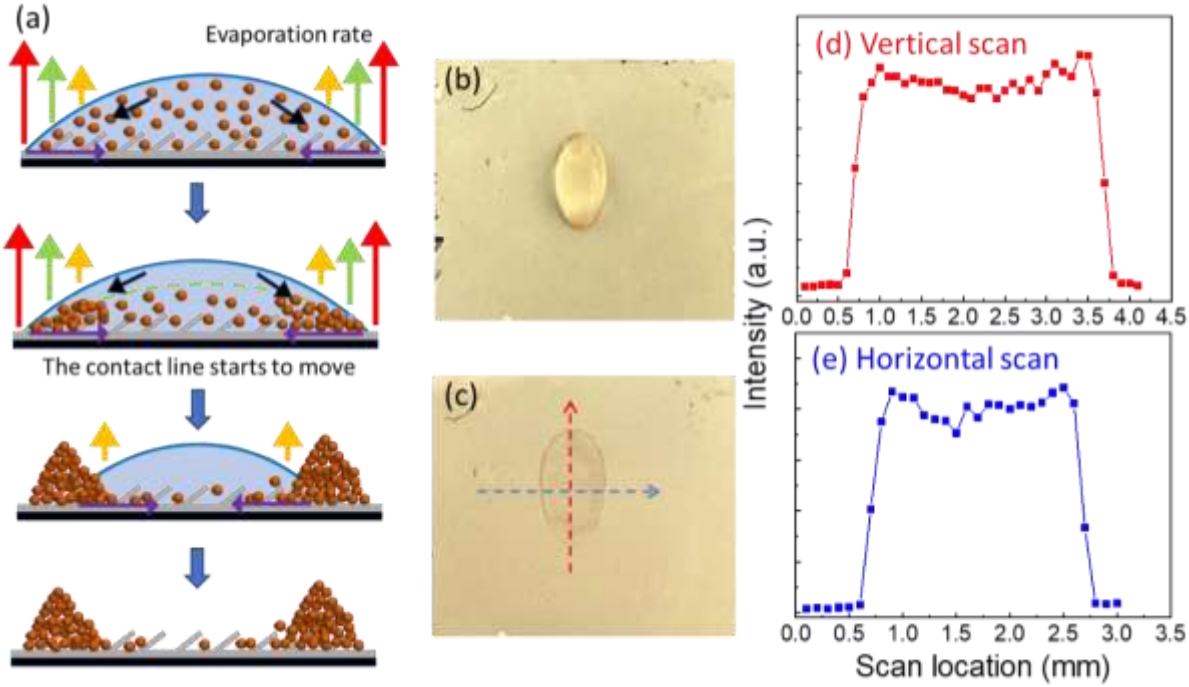

Fig. 20 (a) The principle of coffee ring effect. (b) A photo of analyte droplet and (c) a photo of the coffee ring formed. (d) and (e) the position dependent BPE peak ($\Delta v = 1200$ cm^{-1}) intensities across vertical and horizontal directions over the coffee ring.

shown in **Figures 20d-e**. It is observed that the spectral intensity is higher at the edges of the mark, regardless of the scanning direction (horizontal and vertical scans). This is attributed to the higher concentration of the analyte at the edges. Therefore, when evaluating the uniformity of a SERS substrate, it is crucial to ensure that the sample preparation procedure does not introduce additional non-uniformity.

The second sample preparation method is the immersion method, where the AgNR substrate is immersed in a large volume of analyte solution or soaked in a confined well. SERS measurements can be conducted while the substrate is immersed in the solution (*in-situ* real-time measurement) or after the substrate is removed from the solution and dried (immersion-drying measurement). Once the AgNR substrate is immersed in the analyte solution, a dynamic process of adsorption and desorption of analyte molecules onto the Ag surfaces is initiated. As a result, the number of analyte molecules gradually increases with immersion time. **Figure 21a** shows an example of time-dependent SERS peak intensities when an AgNR substrate is immersed in a 10^{-5} M BPE solution. The SERS peak intensity follows a saturation relationship with immersion time, which can be attributed to the dynamics of analyte molecules' adsorption and desorption on the Ag

surface. The equilibrium time to reach an equilibrium, t_e, can be determined by fitting the experimental data in **Figure 21b** using the equation:

$$I_{SERS}(t) = I_0(1 - e^{-\frac{t}{t_e}}), \quad (3)$$

where I_0 is the maximum SERS intensity achieved at equilibrium. For the data in **Figure 21a**, we obtain t_{e1} = 16 min for 1200 cm^{-1} and t_{e2} = 15 min for 1610 cm^{-1}. It is evident that, for the immersion-drying measurement, the immersion time period, t_{in} , is crucial. Typically, one would use $t_{in} \gg t_e$ or at least $t_{in} = 2t_e$ to ensure consistent and reliable quantitative spectral relationships. Therefore, determining t_e for all immersion-drying measurements is highly important. When the adsorption-desorption equilibrium is reached, the SERS intensity attains a saturation value that is dependent on the initial concentration of BPE due to the mechanism of analyte adsorption. **Figure 21b** plots the saturated peak intensities at Δv = 1200, 1610, and 1640 cm^{-1} of BPE against the BPE concentration in a log-log scale. Similar to what observed in **Figure 19c**, linear relationships are observed with an average slope of 0.38 ± 0.07 lg(counts)/lg(M). This slope value is higher than the one obtained from **Figure 19c**, suggesting that the immersion method may provide higher sensitivity. This conclusion might be limited to BPE.

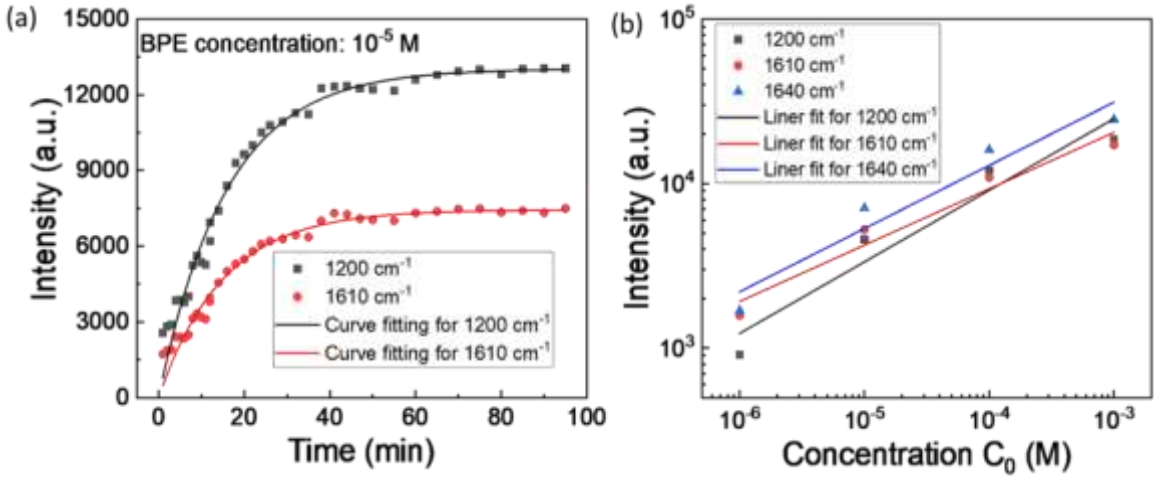

Fig. 21 (a) The time dependent BPE peak intensities (Δv = 1200 cm^{-1} and 1610 cm^{-1}) versus immersion time and (b) the saturation BPE peak intensity versus BPE concentration.

The above discrepancy can be attributed to fundamental differences in the sample preparation methods. In the immersion method, the sample is directly immersed in the solution of interest, allowing ample time for better interaction and more analytes to be chemically adsorbed on the

substrates. This facilitates a more efficient and uniform distribution of the analyte on the surface, resulting in a steeper slope in the calibration curve (**Figure 21b**). On the other hand, the drop-cast method involves placing a small droplet of the analyte solution onto a solid substrate. While this method is relatively simple, it entails non-equilibrium processes such as droplet spreading, evaporation, flow convection, and potential chromatographic phenomena due to the porosity of the AgNR substrates. Analyte adsorption becomes considerably complex: some molecules might undergo chemical adsorption on the surface, while many others may be physically adsorbed. These varied analyte adsorption behaviors could contribute differently to the SERS signal, resulting in less analytes chemically adsorbed on the AgNR surface. In addition, the non-equilibrium process can lead to uneven spreading of the droplet and less chemisorbed analytes on the SERS substrate. Consequently, a less homogeneous distribution of the analyte on the surface can result in a less pronounced slope in the calibration curve (**Figure 19c**) compared to the immersion method. However, due to the intricate non-equilibrium processes involved in the drop-cast method, determining the exact amount of analytes adsorbed on the surface becomes challenging. Hence, establishing a direct quantitative relationship between the SERS intensity and the bulk concentration of the analyte is difficult.

6.2 The effect of solvent wetting/dewetting on AgNR SERS measurements

Based on the description in **Section 6.1**, both the drop-cast method and the immersion-drying measurement involve two crucial interfacial physics processes: liquid wetting (spreading) and dewetting. During these processes, the capillary phenomenon plays a significant role as the liquid infiltrates between Ag nanorods, and the narrow gaps between the nanorods generate substantial capillary forces that mechanically deform them. This capillary-induced morphological change, known as the nano-carpet effect, has been observed by our group and others.[66, 67] The formation mechanism of this effect has been extensively investigated.[67-69]

In fact, in the SERS community, the nano-carpet effect is well-known for creating hot-spots.[70-72] Our group has designed an experiment to show how the nano-carpet effect could change the SERS response of AgNR substrates.[47] An AgNR substrate was incubated with mercaptophenol (MPh) vapor in a sealed container for several minutes, then the SERS spectra were measured. Surprisingly, only a weak MPh SERS signal was observed initially (**Figure 22a**). However, when the same AgNR substrate was immersed in water, the SERS intensity decreased by approximately 50% compared to the initial dry signal. Finally, upon drying the AgNR substrate, the SERS signal

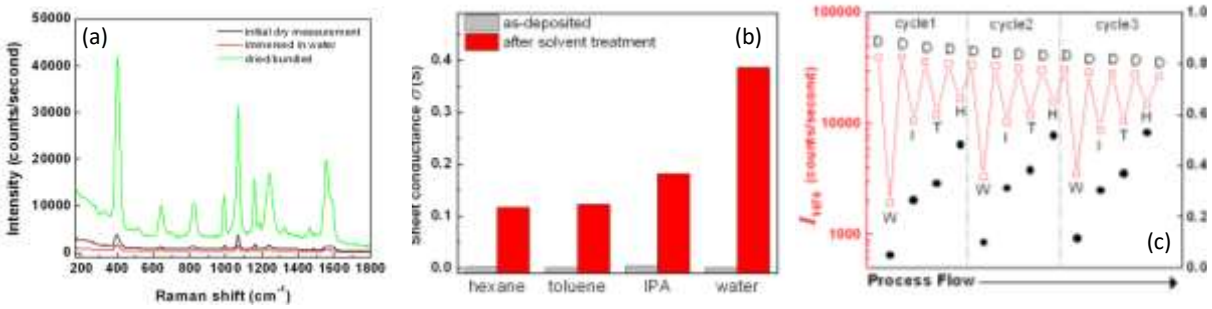

Fig. 22 (a) SERS spectra of MPh vapor-deposited onto a AgNR film. Each spectrum represents the measurement on the same substrate: in air after the initial vapor deposition (black), while immerse in water (red), after drying (green). (b) Sheet conductance σ of as-deposited AgNR films and after treatment with different solvents. (c) SERS intensity of MPh-modified AgNR acquired in air (I_{dry}) or while immersed in solvent (I_{wet}) for three cycles: D = dry, W = water, *I* = IPA, T = toluene, and H = hexane. "□" representing the measured I_{dry} and I_{wet} values (left *y*-axis), and "●" denoting the ratio I_{wet}/I_{dry} for different solvents (right *y*-axis). (Adapted with permission from Ref. 47. Copyright (2014) Royal Society of Chemistry.)

increased by up to 10-fold compared to the vapor-treated substrate. This change in SERS signal strength indicates the possibility of AgNR bundling, which was supported by measurements of the substrate's electrical conductivity before and after solvent treatment (**Figure 22b**).

Further experiments revealed that the bunding effect was reversible. A MPh vapor coated AgNR substrate was sequentially immersed in different solvents: water (followed by drying), isopropanol (IPA) (followed by drying), toluene (followed by drying), and hexane (followed by drying). SERS measurements were performed during each solvent immersion (I_{wet}) and after drying (I_{dry}), and the process was repeated three times. Note that all the solvent treatments do not involve additional thiol solution. **Figure 22b** shows the results of the three cycles. The I_{dry} only slightly decreased as the substrate was consecutively treated in different solvents and dried, while the MPh surface coverage remained relatively constant. However, I_{wet} strongly depended on the solvent used, with the trend $I_{wet}^{water} < I_{wet}^{IPA} < I_{wet}^{toluene} < I_{wet}^{hexane}$. Similarly, the I_{wet}/I_{dry} ratio for each solvent increased accordingly. Such a behavior was reproducible for at least three cycles. The same experiment conducted with another thiol, mercaptohexanol (MH), yielded nearly identical results to those obtained with MPh.[47] This phenomenon is attributed to the change of the Ag nanorod de-bundling during the re-immersion process due to the differences in the surface tension and polarity index of the solvents. At 20°C, water, IPA, toluene, and hexane have surface tension values of 72.8, 21.8, 28.4, and 18.4 mN/m, respectively, and corresponding polarity indices of 10.2, 3.9, 2.4, and 0.001. The degree of Ag nanorod de-bundling follows the order of increasing polarity

index and roughly surface tension values. Re-immersion in solvent with higher polarity index and surface tension results in larger gaps among adjacent Ag nanorods, leading to reduced hot spot intensity. However, establishing direct experimental evidence for this conclusion presents significant challenges.

Therefore, these findings confirm that the presence of SERS hot-spots in AgNR substrates depends on the gap between adjacent nanorods. The nano-carpet effect induced by capillary forces during wetting and drying processes significantly affects the SERS response and provides valuable insights into the optimization of SERS measurements using AgNR substrates.

6.3 The use of AgNR substrates in different biological buffers

SERS is expected to have significant applications in biological detection and medical diagnostics, particularly in the field of biomedical research. In biomedical applications, specimens are often collected and handled in biological buffer or culture media such as phosphate-buffered saline (PBS), phosphate buffer (PB), Dulbecco's Modified Eagle's Medium (DMEM), Roswell Park Memorial Institute (RPMI) 1640, etc. These solutions are designed to maintain specific ionic strength and pH levels, ensuring the biological specimens remain biochemically active or provide necessary nutrients for cell growth.

Biological buffers and culture media contain various ions such as Cl^-, PO_4^-, Na^+, K^+, and Ca^{2+}, as well as other components like glucose, amino acids, and vitamins. Each component may have a different influence on the properties of AgNR substrates and the resulting SERS spectra. For instance, Cl^- ions can react with Ag surface, potentially impacting the SERS EF of the substrate. On the other hand, glucose, amino acids, and vitamins present in the media may contribute to the background SERS spectra, leading to interference with the spectrum from the target analyte. Therefore, it is crucial to understand the properties and stability of AgNR substrates in commonly used biological buffers.

In this section, we will discuss the effects of four specific buffers on the properties of AgNR substrates: PBS, PB, DMEM, and RPMI 1640. By examining the interactions between these buffers and AgNR substrates, we can gain insights into their compatibility and suitability for SERS measurements. Understanding the behavior of AgNR substrates in these buffers is essential for reliable and accurate SERS analysis in biological and biomedical applications.

6.3.1 The SERS spectra of different buffers

Figure 23 shows the SERS spectra of AgNR substrates subjected to two different treatments: (1) immersing the substrates in the buffer for 20 minutes, followed by blow-drying with N_2 flow, and (2) creating a small well on the AgNR substrate (see **Section 7.3**), filling the well with 20 µl of buffer, and allowing it to dry overnight. In **Figure 23a**, regardless of the treatment, the SERS features observed after PBS treatment are very small. Conversely, in **Figure 23b**, PB treatment results in prominent SERS peaks at $\Delta\nu = 563, 921, \text{and } 1052\ \text{cm}^{-1}$, which may be attributed to contaminants on the substrates (as discussed in **Figure 15**). The substrates treated with DMEM and RPMI 1640 (**Figures 23c-d**) exhibit multiple peaks, potentially due to the presence of amino acids[73, 74] and vitamins[75, 76].

Comparing the spectra of substrates treated for 20 minutes and overnight, it can be observed that the spectra treated for 20 minutes generally have higher intensity than those treated overnight. This indicates that the duration of buffer treatment can impact the quality of AgNR substrates.

During the experiments, fractal-like crystals were observed when the buffers were dried on the surface of AgNR substrates. **Figure 24a** presents a typical photo of multiple fractal crystals formed

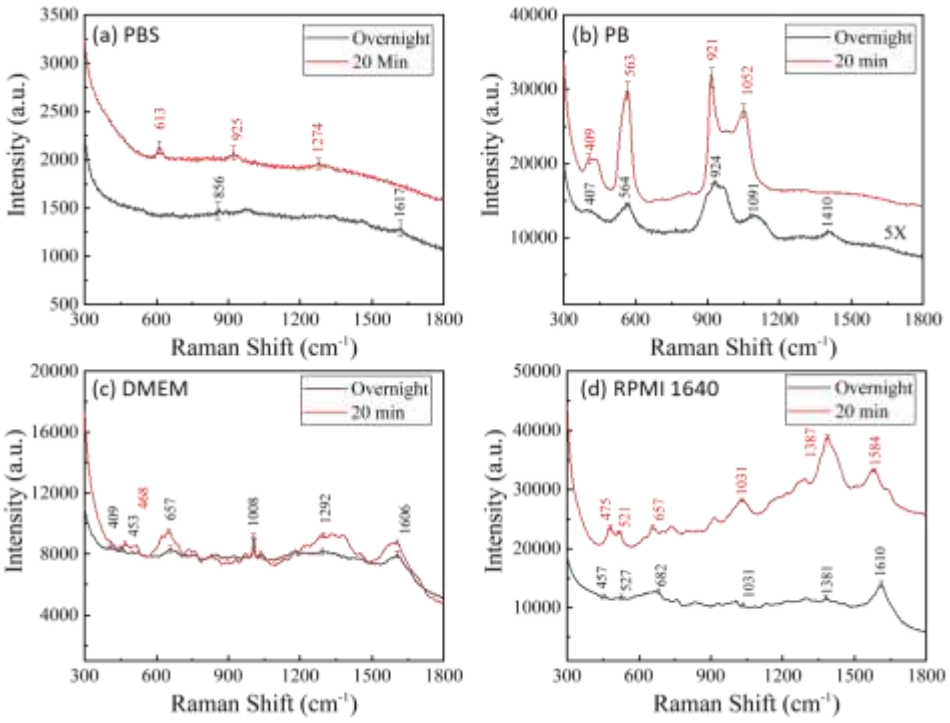

Fig. 23 The SERS spectra of the AgNR substrates after immersed in buffers for 20 minutes & blow dry and after dried overnight: (a) PBS, (b) PB, (c) DMEM, and (d) RPMI 1640.

after PBS buffer drying on an AgNR substrate. In **Figure 24b**, it can be seen that different spectra are obtained when the excitation laser beam is focused on or off the crystals. Despite slight differences in the spectra (mostly changes in amplitude), the spectral features remain similar, suggesting that the crystals do not significantly affect the SERS measurements.

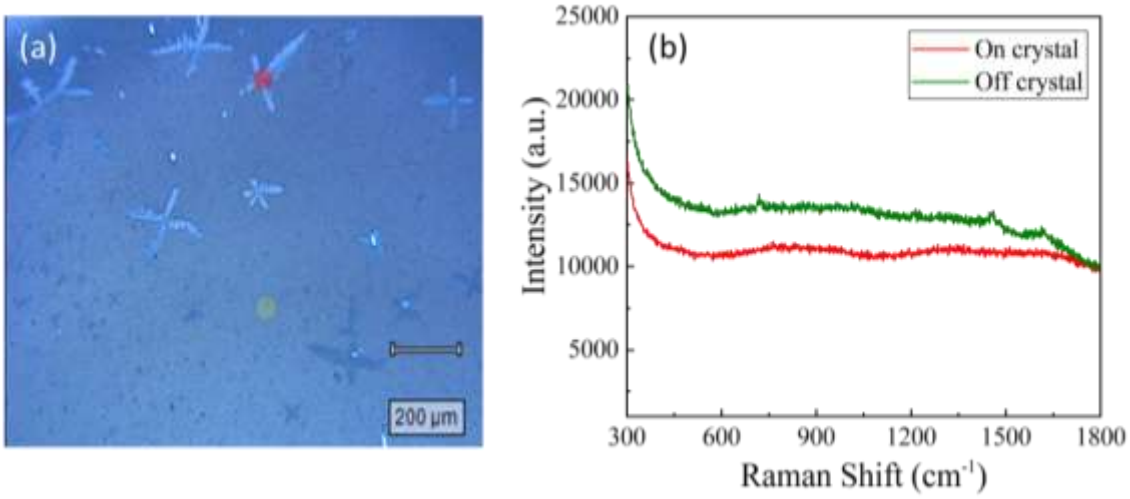

Fig. 24 (a) A photo of salt fractal crystals formed on the surface of a AgNR substrate and (b) the comparison of SERS spectra when the excitation laser beam focused on a crystal and off a crystal.

6.3.2 The stability of AgNR substrates in buffers

Figure 23a demonstrates that the duration of buffer treatment has varying effects on the background SERS signal, suggesting that certain buffers may degrade the AgNR substrates. To further investigate this effect, a time-dependent PBS treatment experiment was conducted. Fresh AgNR substrates were immersed in PBS solution for a fixed duration, followed by rinsing with DI water and blow-drying with N_2. Subsequently, a 5 μl 10^{-5} M BPE solution was drop-casted onto the dried AgNR substrate. **Figure 25a** illustrates the time dependent BPE spectra. As the immersion time in PBS increases, the intensity of the BPE spectrum progressively decreases. When the peak intensities are plotted against the immersion time on a log-log scale (**Figure 25b**), a power law relationship is observed for all major BPE peaks, with exponents ranging from -0.9 to -0.5. This degradation in SERS performance of the AgNR substrates may be attributed to the continuous reaction of Cl^- ions or other ions with Ag_2O or Ag surfaces.

The interaction or reaction between the AgNR substrates and different buffers can vary due to variations in their chemical compositions. **Figure 25c** presents the BPE SERS spectra obtained

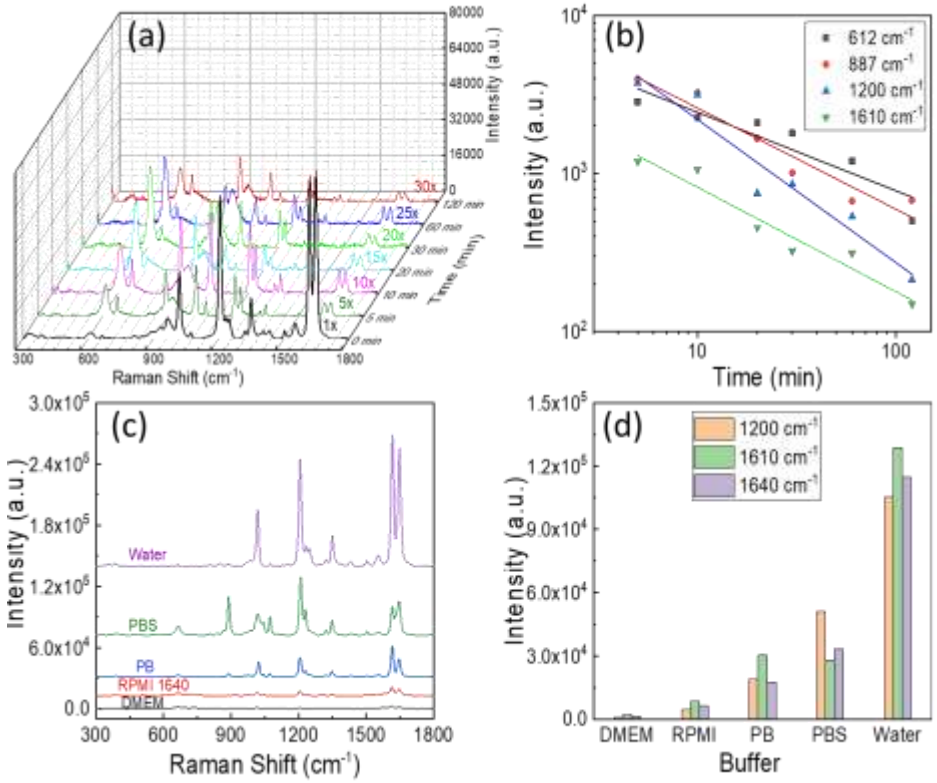

Fig. 25 The time-dependent degradation of the AgNR substrate after treated by PBS: (a) Time dependent BPE spectra and (b) the log-log plots of the SERS peak intensities from spectra in (a) against the treatment time. The effect of different buffer treatment on the property of AgNR substrates: (c) The BPE spectra taken after the AgNR substrates were treated by buffer for 3 hr and (d) the comparison of the BPE peak intensities for different buffers.

after treating the AgNR substrates with different buffers for 3 hours, followed by rinsing with DI water and drying with N_2 flow. The water-treated substrate is used as a reference. Comparing the BPE SERS peaks for different buffer treatments (**Figure 25d**), it is evident that the influence of the buffer on the quality of AgNR substrates follows the order: DMEM > RPMI > PB > PBS > water.

The observed degradation in SERS performance, as influenced by different buffer treatments, raises concerns regarding the long-term stability and reliability of AgNR substrates in biomedical applications.

6.3.3 Ultra-thin Oxide coating on AgNR substrates

One effective method to mitigate the high reactivity of AgNR with buffers or biological fluids and enhance the stability of AgNR substrates is to apply an ultra-thin oxide layer on their surfaces.

Two approaches have been developed for coating AgNRs with ultra-thin layers of SiO_2, Al_2O_3, and TiO_2: hydrolysis [77-79] and low temperature atomic layer deposition (ALD) [80, 81].

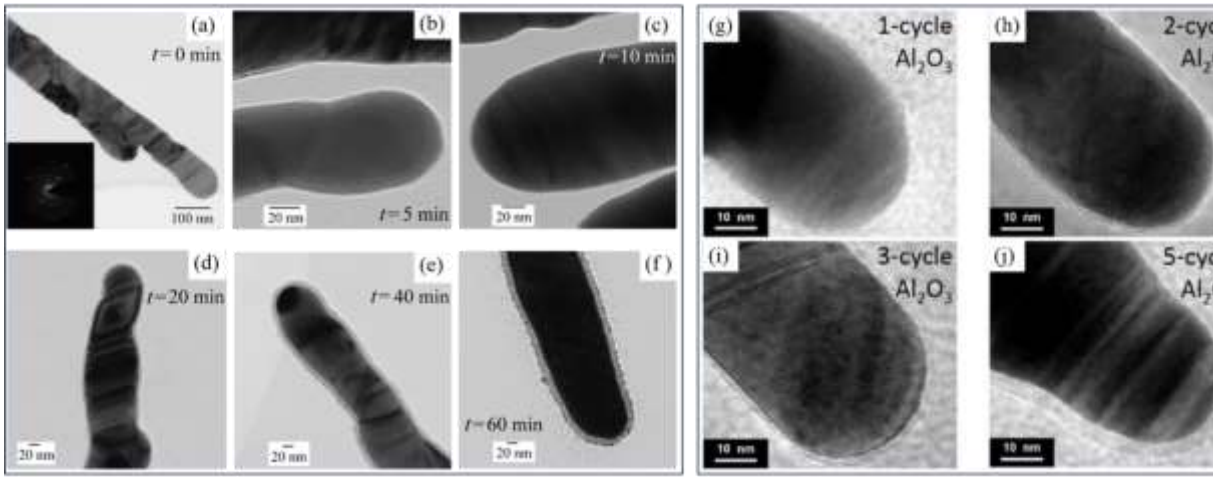

Fig. 26 (a)-(f) Typical TEM images of the AgNR samples before and after coating with a layer of SiO_2 for different hydrolysis reaction times. (Adapted with permission from Ref. 77. Copyright 2012 American Chemical Society.) (g)-(j) High resolution TEM images of the AgNRs coated with Al_2O_3 layers by 1, 2, 3 and 5 ALD cycles. (Adapted with permission from Ref. 80. Copyright 2015 Nature Portfolio.)

For hydrolysis SiO_2 coating, the AgNR substrates are immersed in a homogeneous mixture of 30 mL of EtOH, 4 mL of H_2O, and 500 μL of tetraethoxysilane for 20 minutes under stirring. The SiO_2 coating process is initiated by adding 560 μL of ammonium hydroxide. After 5 minutes, the AgNR substrates are removed from the reaction solution, rinsed with water, and dried with N_2 gas. Under these conditions, a 2-nm conformal SiO_2 coating is expected on the AgNRs. **Figures 26a-f** show the typical TEM images of the AgNR samples before and after SiO_2 coating for different reaction times.[77] These images demonstrate that all AgNRs are uniformly and conformably coated with an amorphous and nanoporous SiO_2 layer. Further experiments have shown that these 2-nm SiO_2-coated AgNR substrates exhibit excellent stability in various buffer solutions.[78, 79]

An alternative approach to achieve ultra-thin oxide coatings is through low-temperature ALD.[82, 83] Zhang's group from Tsinghua University has successfully implemented this strategy to coat ultra-thin Al_2O_3 and TiO_2 layers on AgNR substrates at substrate temperatures of 50°C and 80°C, respectively.[80, 81] **Figures 26g-j** show the TEM images of individual AgNRs coated with Al_2O_3 layers using 1, 2, 3 and 5 ALD cycles.[80] These images reveal amorphous coating layers of different thicknesses, ranging from less than 1 nm to approximately 4 nm, fully encapsulating the nanorods. The authors have demonstrated that these coatings can maintain the morphological integrity of AgNRs up to 400°C, effectively passivating the AgNR surfaces to stabilize SERS

activity in air, while minimally impacting the SERS sensitivity.[80] For TiO_2-coated AgNR substrates, photocatalytic degradation of adsorbed molecules under ultraviolet irradiation and water dilution enables self-cleaning, making the SERS substrates reusable.[81]

6.3.4 Au replaced AgNR substrates

Au is known to be more chemically stable and inert compared to Ag. While AuNR substrates can be directly fabricated through the OAD method,[84] the cost associated with such fabrication is considerably higher than that of AgNR substrates. Therefore, a cost-effective and reliable approach to enhance the stability of AgNR-based SERS substrates is to replace Ag with Au.

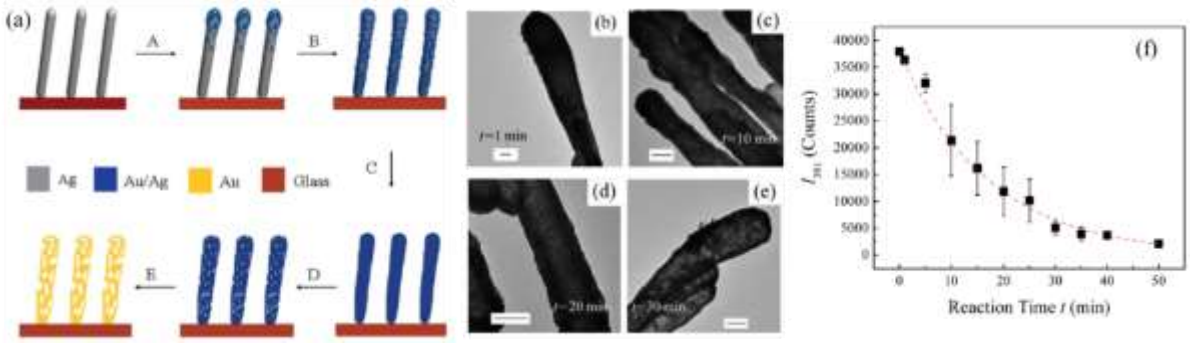

Fig. 27 (a) A schematic diagram of the five stages of the morphology evolution during the Au GRR; (b)-(e) Typical TEM images of the AgNR samples before and after the GRR with $HAuCl_4$ for different reaction time t = 1, 10, 20, and 30 min, respectively. The scale bar in the figures represents 100 nm. (f) The SERS intensity I_{391} ($\Delta\nu = 391$ cm^{-1}) of MPh versus reaction time t. The dashed curve is an exponential decay fitting. (Adapted with permission from Ref. 85. Copyright (2012) Royal Society of Chemistry.)

To achieve this, we have developed a galvanic replacement reaction (GRR) that allows for the deposition of a thin and conformal layer of Au onto the AgNR substrates, as described by the following equation: $3Ag(s) + HAuCl_4 \rightarrow Au(s) + 3AgCl(s) + HCl(aq)$.[85] The morphology and structure evolution during the Au GRR is schematically shown in **Figure 27a**. As the reaction progresses, a porous Au layer conformally coats the surfaces of the AgNRs, while the Ag content gradually decreases with reaction time t. **Figures 27b-e** present some typical TEM images to show the development of porous Au structures on the surface, with increasing pore size observed as the reaction time t progresses. Furthermore, when these coated substrates are immersed in a 1 mM MPh aqueous solution, the intensity of the characteristic SERS peak at $\Delta\nu = 391$ cm^{-1} of MPh exhibits an exponential decrease with reaction time t, as shown in **Figure 27f**.

6.3.5 SAMs coating on AgNR substrates

Previous experiments have demonstrated that thiol molecules can displace adsorbed contaminants from AgNR surfaces and form a stable SAM layer.[86] Later, De et al. conducted a comprehensive study to investigate how thiol coatings affect the long-term stability of AgNR substrates.[58] They functionalized the AgNR substrates with a range of organic thiols, including carboxythiophenol (CTP), methoxythiophenol (MTP), aminothiophenol (ATP), nitrothiophenol (NTP), thiophenol

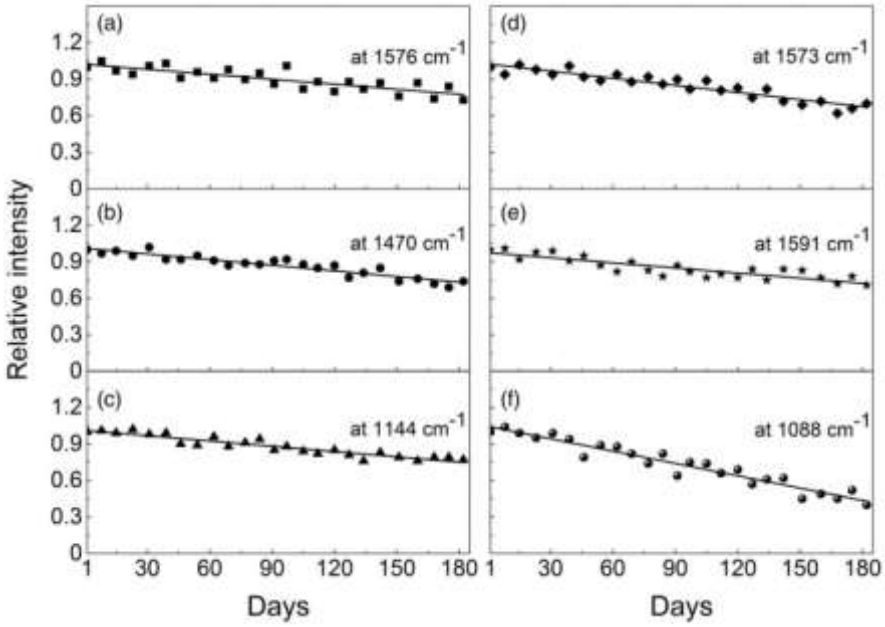

Fig. 28 Lifetime plot showing long-term stability of AgNR array substrates functionalized by (a) NTP, (b) ATP, (c) CTP, (d) TP, (e) MTP, and (f) PT. Functionalized substrates were stored in surfactant solution. (Adapted with permission from Ref. 58. Copyright 2016 SAGE Publications Inc.)

(TP), and propanethiol (PT), which varied in hydrophilicity and hydrophobicity. To assess the stability of these functionalized substrates, they were stored in different environments: (i) ambient laboratory atmosphere, (ii) a moisture-free vacuum chamber with minimized light exposure, and (iii) an aqueous surfactant solution. The substrates stored in the ambient laboratory atmosphere exhibited stability for approximately three months. **Figure 28** illustrates the long-term stability of all six thiol-functionalized substrates stored in the aqueous surfactant solution for an extended period. Very slow SERS intensity decays were observed. Similar results were obtained when the substrates were stored in a moisture free, external light minimized vacuum chamber. These results demonstrate that under these conditions, the functionalized substrates are stable for more than six months.

6.4 Raman excitation wavelength effect on AgNR substrates

The optical configuration during SERS measurements, including the excitation wavelength, laser power, illumination duration, and other parameters, plays a crucial role in obtaining reliable and accurate SERS spectra from AgNR substrates. Starting from this section, we will explore how these factors influence the SERS measurements.

The excitation wavelength is a well-known parameter that significantly affects the intensity of the SERS spectrum. It has been established by Van Duyne and others that the excitation laser wavelength should be close to the LSPR wavelength of the plasmonic structures to maximize the SERS signal.[87-89] This near-resonance excitation generates strong local electric fields within the

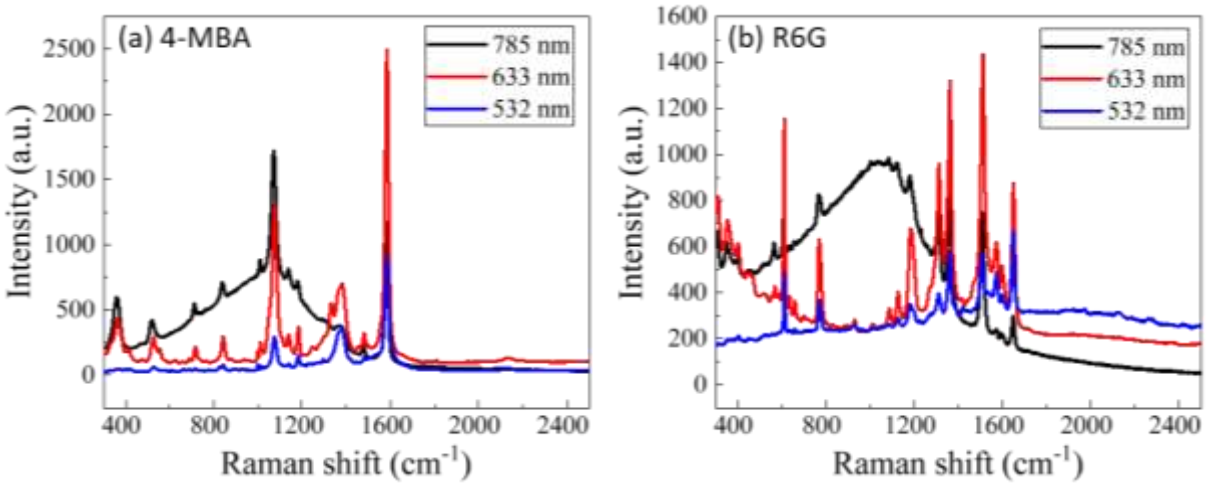

Fig. 29 The incident power normalized SERS spectra of (a) 10^{-5}M 4-MBA and (b) 10^{-5}M R6G on the AgNR substrates probed by three excitation wavelengths $\lambda_{ex} = 532, 633$, and 785 nm, respectively.

plasmonic structure, thereby enhancing the SERS signal by promoting the formation of SERS hot-spots. However, the AgNR substrate, as discussed in **Section 4**, is a quasi-3D structure composed of interconnected Ag nanostructures. Locating a specific excitation wavelength that matches the LSPR of the entire structure is challenging. **Figures 7a-b** demonstrate the broad absorption spectrum of the AgNR substrate. Therefore, it is expected that multiple excitation wavelengths can be employed to generate significant SERS signals from the AgNR substrates. Although we tested only three excitation wavelengths ($\lambda_{ex} = 532, 633$, and 785 nm) due to limited access to the Raman instrument, it provides valuable insights.

Figure 29 shows the original SERS spectra of 4-MBA and R6G from the same AgNR substrates measured using the three excitation wavelengths on a Renishaw system. These spectra

are normalized by the corresponding incident power. Several interesting observations can be made: 1) Background signals vary with different excitation wavelengths. The $\lambda_{ex} = 532$ nm exhibits a relatively flat background, while the $\lambda_{ex} = 785$ nm excitation shows a broad peak background. 2) Even with the same excitation wavelength, the background signals for different target analytes can differ. This is particularly evident in the spectra obtained using $\lambda_{ex} = 633$ nm excitation (**Figure 29**). 3) Although most characteristic peak locations of the same analytes are consistent across different excitation wavelengths, the relative peak intensities vary. For example, in the 4-MBA spectra, the most prominent peak at $\Delta v = 1586$ cm^{-1} is observed for $\lambda_{ex} = 532$ and 633 nm, whereas for $\lambda_{ex} = 785$ nm excitation, the peak appears at $\Delta v = 1071$ cm^{-1}. Additionally, for $\lambda_{ex} = 532$ nm excitation, peaks with $\Delta v < 1071$ cm^{-1} are barely discernible, while for $\lambda_{ex} = 633$ and 785 nm excitations, the peaks at $\Delta v = 365, 523, 717,$ and 844 cm^{-1} are more pronounced.

These observations highlight the significant influence of the excitation wavelength on SERS measurements. While near-resonance excitation is desirable, the broad absorption spectrum of the AgNR substrate necessitates exploring multiple excitation wavelengths to achieve optimal SERS signals. Furthermore, the background signals and relative peak intensities can vary, not only with different excitation wavelengths but also with different target analytes. Hence, careful selection of the excitation wavelength and interpretation of the resulting SERS spectra are vital to obtain accurate and meaningful results.

6.5 The effect of laser power or measurement duration for AgNR substrates

In general, the SERS signal from a thin-film substrate, such as the AgNR substrate, can be written as,

$$I_{SERS} = G_{SERS} F_H N_{AH} \sigma_{SERS} I_0, \quad (4)$$

where G_{SERS} is the apparent SERS EF at the hot-spot location, F_H is the fraction of photons emitted by the SERS specimen and collected by the microscopic objective, N_{AH} is the total number of analyte molecules/particles in SERS hot-spots in the measurement area, σ_{SERS} is the SERS scattering cross-section at a particular wavenumber, and $I_0 = I_0(\lambda_{ex})$ is the incident intensity of the excitation laser with a wavelength λ_{ex}. According to **Eq. 2**, $N_{AH} \propto N_p \propto A_p$, i.e., I_{SERS} is proportional to the area of excitation laser beam A_p and the surface density $\frac{VC_b}{A_s}$ of analyte molecules (or distribution of analyte molecules on the surface). Typically, when obtaining the

SERS spectra of an analyte on an AgNR substrate, multiple randomly selected locations on the substrate are measured, employing a point-to-point sampling approach. The average spectrum and the corresponding spectral variation are reported to account for the potential nonuniform distribution of analyte molecules on the surface, as discussed in **Section 6.1**.

However, due to the small size of the excitation laser beam, typical in the order of 1-10,000 μm^2, each spectrum obtained from a sampling location represents only a very small area of the entire analyte-covered AgNR substrate. As a result, the variation in SERS measurements can be significant. To achieve better statistical measurements, a relatively large number of locations on the substrate may need to be sampled. Alternatively, the laser beam size can be increased by defocusing the laser while maintaining the laser intensity, allowing more analyte molecules to be probed in a single measurement. However, this approach requires a significant increase in incident laser power, and the signal collection configuration may need to be adjusted (e.g., F_H may be changed).

Another approach to improving statistical measurements is to increase the integration time of the measurement, which reduces noise generated from the instrument and improves the signal-to-noise ratio (SNR). However, since the λ_{ex} is selected to near the resonant absorption wavelength of the plasmonic structures, a good portion of the laser beam will be absorbed by the SERS substrate and turned into heat. Therefore, this strategy poses a potential issue of photothermally-induced changes or variations in the SERS measurement when a single sampling spot on a substrate is continuously exposed to laser excitation. Previous studies have shown that the SERS intensity can exhibit irreversible decreases or significant fluctuations as the cumulative excitation time or power density increases.[90-93] These changes in signal intensity have been attributed to factors such as photo-thermal degradation of the substrate or analyte, or ablation of the analyte from the substrate surface.

To address these issues, a rastering/translating method can be employed, where the laser spot rapidly moves across the substrate surface during excitation/measurement without altering the optical signal collection configuration.[90-94] This method increases the measuring area by dynamically rastering or translating the laser spot during the measurement, while keeping the SERS instrument configuration intact. By reducing the residence time of the laser at a particular location and simultaneously generating a signal that is essentially a summed average of multiple locations on the substrate, this approach significantly improves quantitative SERS analysis. It

mitigates the effects of photo-thermal heating from the excitation laser, reduces signal loss, spectral fluctuation, and substrate damage.

Abell et al. conducted a detailed investigation on how dynamic/rastering measurements could impact the analytical performance of AgNR substrates for quantitative SERS analysis.[93] They mounted AgNR substrates onto an optical chopper, with the excitation laser spot positioned at an offset distance *r* from the axis of rotation, and systematically tuned the frequency *f*. For each experiment, multiple measurements ($n = 5$ or 9) were collected on each AgNR substrate. They first examined how the spot-to-spot intensity variation of the AgNR substrates could be improved by dynamic rastering measurement. They found that the relative standard deviation (RSD) for rastering measurements ranged between 1.9% and 7.7%, whereas for static measurements, the RSD ranged from 2.4% to 52%. This indicates that the variation in rastering measurements was significantly smaller than that in static measurements.

Furthermore, the effect of the two critical parameters for rastering measurement, *r* and *f*, were systematically studied. As shown in **Figure 30a**, at a fixed rotation frequency $f = 10$ Hz, the RSD of the rastering measurements decreased monotonically with an increase in *r*. This can be understood as more analyte molecules being measured with increasing *r*, resulting in a smaller RSD based on the law of large numbers in statistics. The RSD of the rastering measurements versus the rotation frequency *f*, at a fixed $r = 1.0$ mm, plotted in **Figure 30b**, remained almost constant. This was expected since the number of analyte molecules in the measurements did not change (due to the fixed *r*).

Finally, the effect of continuous excitation exposure on the SERS intensity for static and rastering measurements was investigated. **Figure 30c** shows the normalized SERS intensity versus cumulative exposure time *t* for multiple continuous measurements at a fixed sampling point. For all the static measurements, the data demonstrated a monotonically increasing SERS intensity with respect to exposure time *t*. However, long-time rastering measurements exhibited a completely different trend. **Figure 30d** shows the normalized SERS intensity versus *t* for substrates undergoing continuous rastering measurements at $r = 1$ mm and $f = 0.5$ Hz and 10 Hz, respectively. The change in SERS intensity associated with cumulative *t* was virtually eliminated in the rastering measurements.

Clearly, the dynamic/rastering measurement method significantly improves the analytical merits of AgNR substrates for quantitative SERS analysis. It reduces spot-to-spot intensity

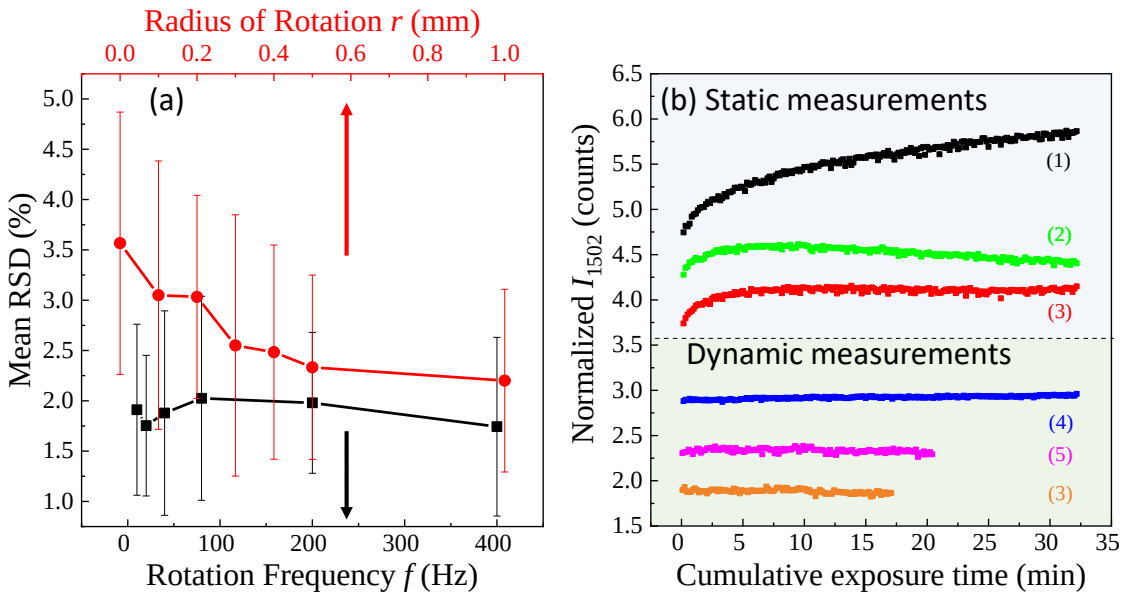

Fig. 30 (a) The average RSD versus rastering radius *r* (red) (*f* = 10 Hz) and frequency f (black) (*r* = 1 mm) from six substrates. (b) The normalized SERS intensity I_{1052} versus cumulative exposure time *t* for static and rastering measurements (*r* = 1 mm and *f* = 0.5 or 10 Hz) on AgNR substrates exposed to repetitive excitation of λex= 785 nm laser for ~15-30 minutes. All intensities have been normalized with respect to the intensity measured at *t* = 0 min, and plots have been vertically offset for clarity. (Replot from Ref. 93.)

variations, eliminates photothermally-induced changes in SERS intensity, and improves measurement accuracy.

6.6 Other advanced measurement techniques

6.6.1 Polarization modulation measurement

Based on the polarization property of the AgNR substrate shown in **Figure 5**, Vo-Dinh's group has developed a polarization modulation strategy to effectively eliminate fluorescence background from SERS measurements.[95] In this measurement strategy, the excitation laser's polarization is modulated using a half-wave liquid crystal variable retarder so that the polarization of the laser can be alternated periodically between being parallel and perpendicular to the nanorod's long axis direction as shown in **Figure 31a**. During this modulation process, the SERS signal experiences significant changes, as indicated by the red curve in the insert of **Figure 31a**, while the background florescence signal remains relatively unaffected, as shown by the blue curve in the insert. Thus, by measuring the amplitude of the modulated SERS signal, the authors propose that the background signals could be removed effectively.

To demonstrate the effectiveness of this idea, a SERS measurement was conducted on a functionalized AgNR substrate immersed in a fluorescence solution containing a 1 μM concentration of Cyanine 5 dye. The normal SERS spectrum obtained with a $\lambda_{ex} = 633$ nm excitation, as shown in **Figure 31b**, exhibits a strong fluorescence background. However, upon applying the polarization modulation, as shown in **Figure 31c**, a significant portion of the fluorescence background is successfully eliminated.

The researchers also showcased the background extraction technique under LED illumination during SERS measurements. This methodology, enabling the extraction of SERS signals from a robust background, holds promise for in-situ SERS measurements involving diverse background solutions or varying illumination conditions.

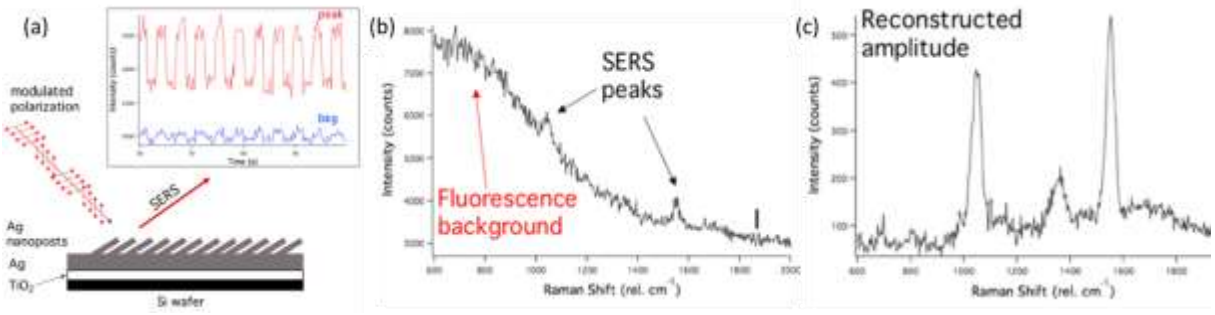

Fig. 31 (a) The cartoon illustrates the polarization modulation and the insert shows the SERS signal modulated by this method. The SERS spectrum of the functionalized AgNR substrate under (b) the normal measurement condition and (c) under polarization modulation. (Adapted with permission from Ref. 95. Copyright 2019 American Chemical Society.)

6.6.2 Dual SERS-SPR measurement

Redundancy is a widely adopted strategy in high sensitivity sensors to promote reliability by using multiple sensors to detect the same analyte.[96] This approach not only improves the robustness of detection but also enhances precision. However, redundant detection strategies have been rarely explored in the realm of SERS-based sensors.[97, 98] To achieve accurate and reliable detection, it is envisioned that integrating two plasmonic sensing modes into a single sensor or sensing system could effectively leverage their respective advantages while compensating for their limitations. Fortunately, various plasmonic sensing strategies, such as SERS and LSPR, share similar principles, making a redundant sensing strategy feasible.

Potara et al. demonstrated the combination of SERS and LSPR by harnessing the engineering of local hot-spots.[99] Building upon this concept, our recent work involved modifying the underlayer to create plasmonic nanohole arrays for AgNR deposition, resulting in the development of a dual-mode biosensor based on SERS and SPR.[100] **Figures 32a-b** show the representative top view and cross-section view SEM images of the Ag nanohole (NH) and Ag nanorod on nanohole (NR-NH) arrays. The Ag NH array features a hole diameter of D = 339 ± 9 nm, a lattice spacing L = 500 ± 10 nm, and a height of h = 85 ± 2 nm. In the Ag NR-NH array, randomly distributed tilted Ag NRs with a NR length l = 151 ± 40 nm and a NR density η = 53 ± 6 NR/μm^2 are exclusively grown on the ridges of the nanoholes or Ag thin film area, with no NRs present inside

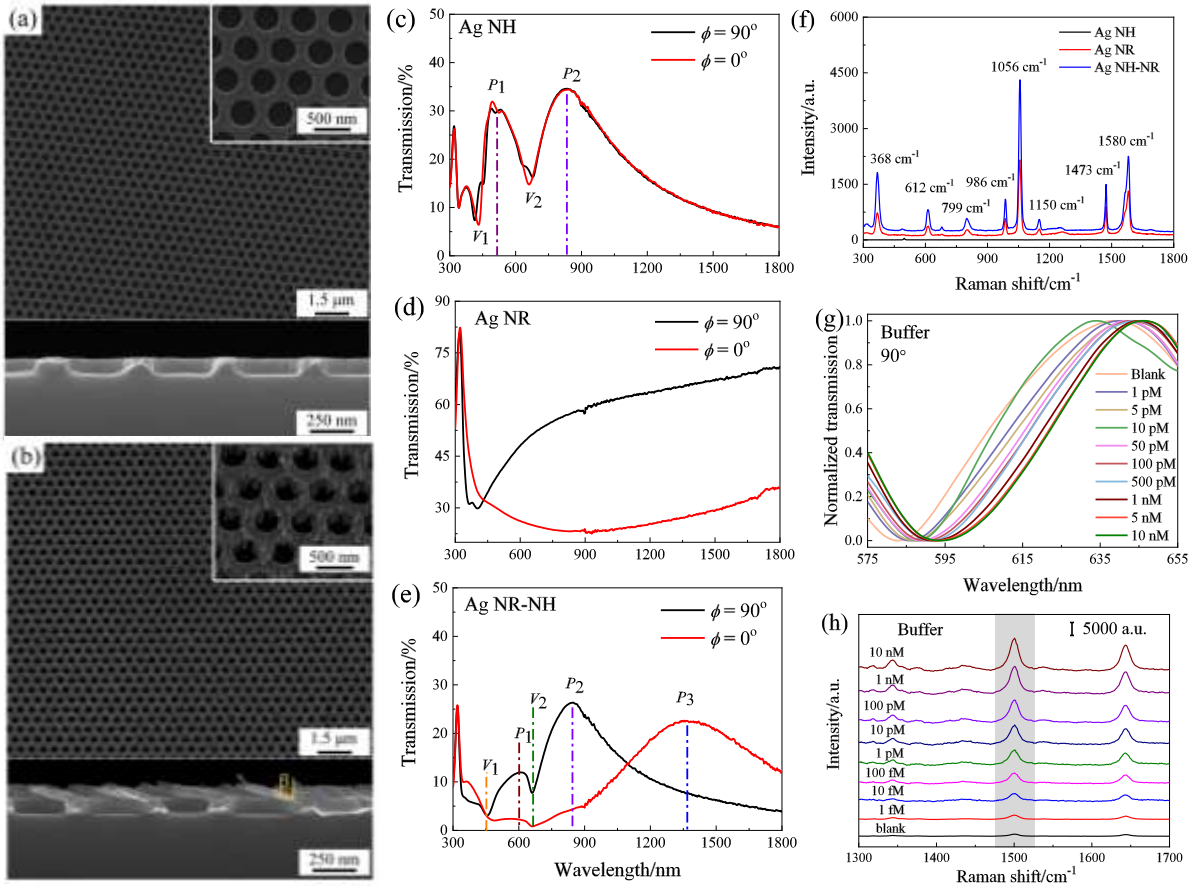

Fig. 32 Top-view (inset: magnified image) and the cross-section view (bottom) SEM images of (a) Ag NH and (b) Ag NR-NH arrays. The transmission spectra of Ag NH (c), Ag NR (d), and Ag NR-NH (e) recorded at the polarization angle ϕ = 0° and 90°, respectively. (f) The SERS spectra of MPH obtained from Ag NH, Ag NR, and Ag NR-NH arrays, respectively. (g) The DNA concentration-dependent normalized transmission spectra under the 90° polarized light and the (h) the corresponding SERS spectra from Ag NR-NH arrays. (Adapted with permission from Ref. 100. Copyright 2020 American Chemical Society.)

the nanoholes. The polarization-dependent transmission spectra of three different substrates, namely Ag NH, AgNR, and Ag NR-NH, are illustrated in **Figures 32c-e** under similar sample preparation conditions. While the Ag NH array exhibits no polarization-dependent spectra, both the AgNR and Ag NR-NH substrates demonstrate strong anisotropic optical properties.

The SERS spectra of these three substrates immersed in MPh are shown in **Figure 32f**. It becomes evident that the Ag NR-NH array produces a superior SERS signal compared to the AgNR array directly deposited on a Si wafer without nanoholes. In fact, the SERS EF of the Ag NR-NH was determined to be 4.02×10^6. By surface modifying the substrates with tetrahedral DNA probes, we demonstrated highly sensitive dual detection of DNAs. **Figure 32g** plots the normalized optical transmission spectra when the Ag NR-NH substrate was immersed in different concentrations of targeted DNA solutions, clearly showing a red-shift in the dip wavelength, enabling a limit of detection (LOD) of 0.180 pM. Simultaneously, the changes in SERS spectra were also measured and shown in **Figure 32h**. Although the spectral shapes are quite similar, the SERS peak intensity increases with increasing target DNA concentration, yielding an LOD of 0.379 fM. Clearly the combination of SERS together with another detection method can greatly improve the reliability of the detection.

6.7. Quantification in AgNR-based SERS measurements

The quantification of targeted analyte solutions is of great importance in many SERS-based detections. Typically, the concentration of an analyte solution is characterized by its bulk concentration C_b. However, SERS-based detection is a surface detection method, meaning that only a certain amount of analyte molecules on a surface is probed, as shown in **Eq. 2**. Therefore, the actual number of molecules probed by the excitation laser N_p is proportional to C_b. However, according to **Eq. 4**, not all the analyte molecules located within the excitation laser beam will produce the SERS signal. Only a fraction of the molecules N_{AH} out of N_p contributes to the final SERS signals, and N_{AH} is not necessarily proportional to N_p. Thus, there could be complicated relationships between the SERS intensity I_{SERS} and the bulk concentration C_b of the analyte. Furthermore, the methods used to prepare the SERS samples, such as drop-cast or immersion-drying, as well as the spatial distribution of hot-spots, also play a crucial role in determining the $I_{\mathrm{SERS}} - C_b$ relationship.

During the use of AgNR substrates for different analyte quantifications, we have observed six quantitative relationships: linear,[101] power law, [102] semi-log,[103] saturation,[104] peak,[105] and long-range[106] relationships. **Figure 33** presents typical experimentally measured $I_{\mathrm{SERS}} - C_b$ relationships from various analyte solutions using AgNR substrates. In all these experiments, the samples were prepared by drop-cast method. It is clear that based on **Eq. 2** and **Eq. 4**, $I_{SERS} \propto N_{AH}$, and the relationship between N_{AH} and C_b, under the adsorption equilibrium assumption, shall be determined by different types of adsorption isotherms of analytes molecules adsorbed on AgNR surfaces.[107] But the variations in the $I_{\mathrm{SERS}} - C_b$ relationship across different experiments indicate that, in addition to analyte adsorption/desorption, other fundamental physical and chemical mechanisms, such as wetting/dewetting dynamics in drop-cast process, competing adsorption, substrate morphology, optical attenuation, etc., may play important roles in determining the $I_{\mathrm{SERS}} - C_b$ relationship in practical applications.

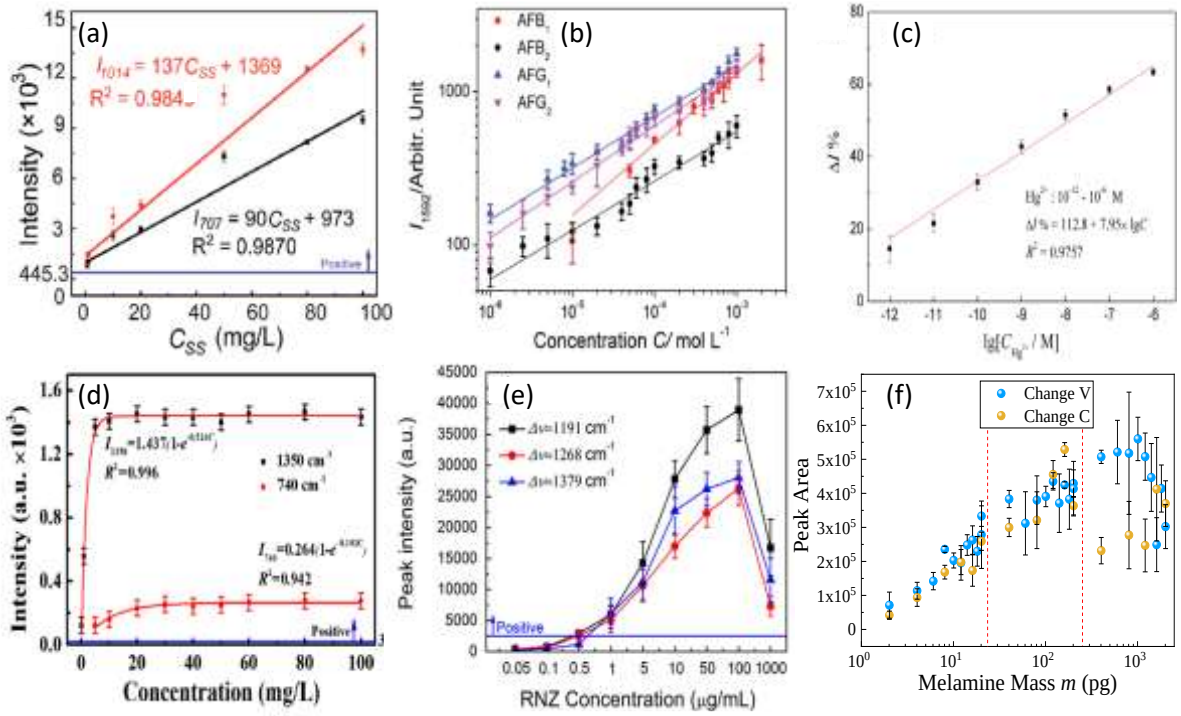

Fig. 33 (a) A linear relationship observed from SERS based Sodium saccharin detection. (Adapted with permission from Ref. 101. Copyright 2017 Elsevier.) (b) A log-log (or power laws) relationship found for aflatoxin detection. (Adapted with permission from Ref. 102. Copyright 2012 Royal Society of Chemistry.) (c) A semi-log relationship discovered in mercury ion detection. (Adapted with permission from Ref. 103. Copyright 2017 Elsevier.) (d) A saturation relationship measured in flavin mononucleotide detection. (Adapted with permission from Ref. 104. Copyright 2019 SPIE.) (e) A peaked relationship produced in the detection of ronidazole; (Adapted with permission from Ref. 105. Copyright 2014 Elsevier.) (f) A large range concentration relationship for melamine detection. (Replot from Ref. 106)

7. Manufacture and Device Design of AgNR Substrates

7.1 Large scale fabrication of AgNR substrates

The OAD method, being a physical vapor deposition technique, offers convenience in producing a large quantity of small SERS substrates with consistent quality. For instance, as shown in **Figure 34a**, a 5" × 6" rectangular substrate holder can accommodate over 116 pieces of 0.5"×0. 5" small AgNR substrates in a single deposition. The variation among the AgNR substrates, whether from the bottom to the top or from left to right, is less than 10%. Moreover, we have developed a specialized umbrella-like multiple substrate holder (**Figure 34b**) that enables the simultaneous deposition of 10 pieces of 1" × 3" or 2" × 3" AgNR substrates. This holder allows for azimuthal rotation while maintaining the vapor incident beam direction at the center, ensuring uniform deposition across all substrates.

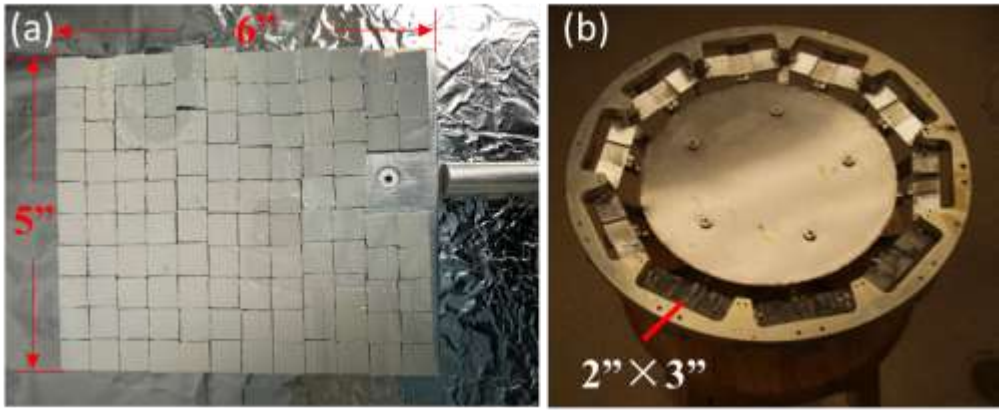

Fig. 34 Large scale AgNR SERS substrate fabrication: (a) multiple 1 cm × 1 cm samples on a 3"-diamter substrate holder; (b) special substrate holder designed to hold 10 pieces of 2" × 3" glass slide substrates.

7.2 The fabrication of flexible AgNR substrates

Since the AgNR substrate fabrication can be carried out under the room temperature, the limitation of the use of different types of substrate materials will be less stringent compared to other SERS substrate fabrication techniques. Flexible AgNR SERS substrates can be created using plastic materials such as polyethylene terephthalate (PET) or polydimethylsiloxane (PDMS) as host substrates. **Figure 35a** shows a photo of a PET AgNR substrate, where the deposition conditions were optimized as determined in **Section 2**.[108] These flexible SERS substrates exhibit remarkable resilience, tolerating tensile strains up to 30% without compromising SERS performance. However,

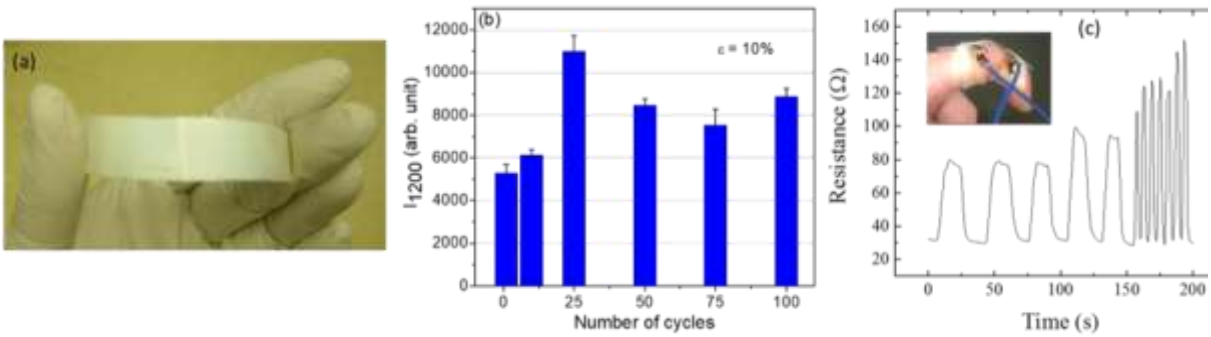

Fig. 35 (a) a photo of flexible AgNR substrate. (b) A bar graph of the SERS intensity I_{1200} versus the number of tensile loading cycles for a pre-defined 10% tensile strain. (Adapted with permission from Ref. 108. Copyright 2012 Royal Society of Chemistry.) (c) The flexible AgNR substrate as a stress sensor as well as a SERS sensor. (Adapted with permission from Ref. 109. Copyright 2016 American Chemical Society.)

bending strains of a similar magnitude lead to a reduction in SERS performance by approximately 13%.

One important consideration for flexible sensors is their ability to withstand cyclic deformation. **Figure 35b** shows the variation in SERS intensity of BPE as a function of the number of tensile cycles at a pre-specified tensile strain (ε) value of 10% for a PDMS substrate. The SERS intensity remains stable for over 100 cycles, with instances where an increase in SERS intensity is even observed. These disposable and flexible SERS substrates can be integrated with biological substances, offering a practical and innovative approach to facilitate biosensing applications. For instance, Bradley et al. have successfully transferred AgNRs onto a PDMS sheet, resulting in a flexible conductive sheet capable of performing SERS measurements.[109] This sheet exhibits a piezoresistive effect, with its resistance changing when subjected to bending. Such a structure serves as both a motion sensor and a chemical sensor. **Figure 35c** demonstrates the resistance versus time plot for an AgNR PDMS sheet attached to a person's finger, showcasing the correlation between the bending motion of the finger, the change in resistance, and the rate of change and peak value of the resistance. This system enables the monitoring of both mechanical and chemical environment changes through SERS measurements.[109] In addition, flexible AgNR substrates have been successfully applied to detect pesticide residues from fruits and vegitables.[110, 111]

7.3 The fabrication of multi-well AgNR substrates

The OAD process, as depicted in **Figure 34**, enables the production of large-area and uniformly distributed AgNR SERS substrates. This unique feature provides the opportunity to perform

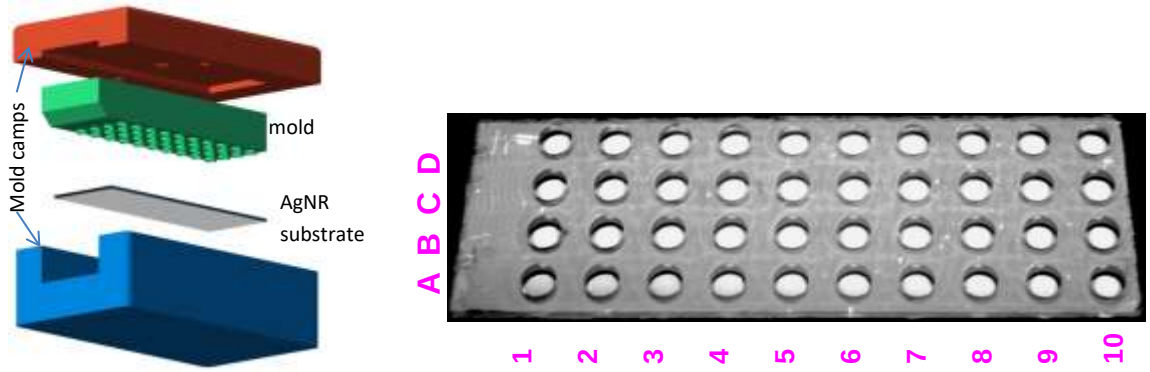

Fig. 36 A molding process to produce multi-well SERS chip (left) and the resulting chip (right). (Adapted with permission from Ref. 112. Copyright 2009 Elsevier.)

multiple sensing tests at different locations on the same substrate. However, to ensure accurate results and avoid interference between tests or potential contamination, it is necessary to confine the sensing area within small wells. In our laboratory, we have developed a molding process to fabricate multi-well SERS substrates on a 1" × 3" AgNR substrate, as shown in **Figure 36**.[112] This approach involves loading the AgNR substrate into an aluminium mold designed to create a 4×10 array of SERS-active wells. Each well has a diameter of 4 mm and a height of 1 mm, allowing for the containment of up to 20 µl of liquid sample (**Figure 36**). Further details can be found in Ref. 112. This design effectively confines the liquid samples to specific areas, facilitating the simultaneous screening of 40 samples. It is worth noting that alternative well formats, such as 48 or 96 wells, can also be fabricated. Our subsequent experiments have revealed that it is not necessary to mold the AgNR substrate and PDMS together. Instead, a PDMS sheet with wells can be fabricated separately and tightly placed onto the AgNR substrate, creating well-defined sensing areas.

7.4 The integration of AgNR substrates into fiber optical SERS sensor

Fan and Zhao demonstrated the coating of AgNRs onto the side surface of a cylindrical object, such as a taped cylindrical object, thereby opening up the possibility of creating an AgNR SERS-based optical fiber sensor.[113] Building upon this work, we developed a technique in which multiple optical fibers were simultaneously polished and installed into the OAD system. This enabled the direct deposition of AgNR arrays onto the polished fiber tips or the outer surface of a tapered fiber, as shown in **Figure 37**.[114] These AgNR-coated fiber tips can be seamlessly integrated into a Raman

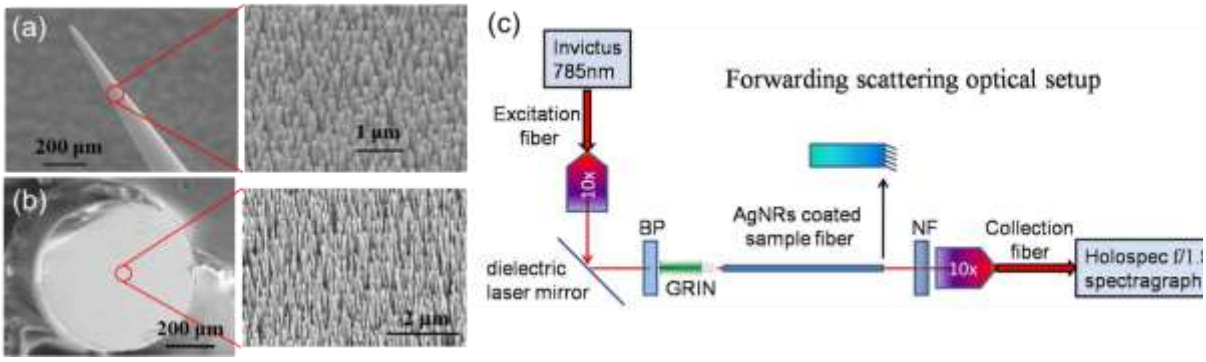

Fig. 37 The representative SEM images of AgNR arrays on (a) a taped fiber tip and (b)a polished fiber end, and (c) a setup for the fiber SERS probe. (Adapted with permission from Ref. 113. Copyright 2011 Elsevier.)

system, allowing them to function as SERS fiber probes. The performance of these AgNR fiber probes is discussed in detail in Ref. [114].

7.5 The integration of AgNR substrates into flow cell sensors

The integration of the AgNR substrate into a flow cell enables the real-time monitoring of specific chemical composition changes within a flow system. **Figure 38a** shows an example of such a system, where a circular disk-shaped AgNR substrate is fitted into a specially designed flow cell featuring a top window for optical measurements. The liquid sample is injected into the flow cell system, and the SERS spectra of BPE are measured in situ as a function of flow time. The measured results are shown in **Figure 38b,** demonstrating a continuous increase in SERS intensity with flow time. The dynamic process can be effectively modeled using **Eq. 3**, as shown by the solid red curve in **Figure 38b**. However, there are many challenges in such an in-situ measurement, which will be discussed in **Section 10**.

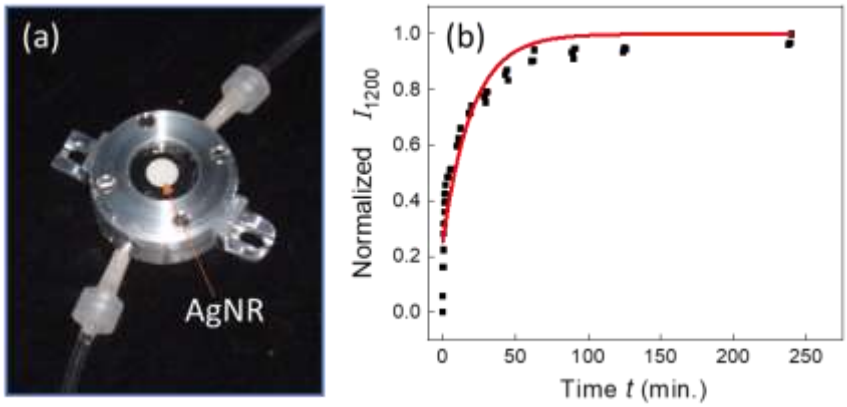

Fig. 38 (a) A photo of a SERS flow cell and (b) the SERS intensity versus time plot for a flow of BPE solution.

7.6 The integration of AgNR substrates into electrochemical cell sensors

Electric-field assisted detection (EFAD) has proven to be highly useful for specific applications. For instance, when dealing with nucleic acids, which possess an intrinsic negative charge, the application of an external electric field can facilitate control over their transport, hybridization, and dehybridization processes, thus aiding in their detection.[115-117] Additionally, for molecules that exhibit no or weak affinity to SERS substrate surfaces, the use of electro-potential bias on the SERS substrate has been suggested as an effective means to enhance the SERS signal at an appropriate bias potential.[118] Consequently, there is a demand to utilize the SERS substrate as an electrode for electrochemical settings while simultaneously measuring SERS signals.

The optimal AgNR substrate, characterized by its thin Ag layer coating, possesses electric conductivity and can serve as the working electrode (WE). To serve as the counter electrode, a pre-fabricated ITO-coated glass slide is employed due to its conductivity and transparency, which is advantageous for SERS signal collection. **Figure 39a** shows a diagram of an electro-cell composed of an AgNR substrate and an ITO slide. This configuration essentially forms a parallel-plate capacitor, generating a uniform electric potential gradient within the cell.[119] Care must be taken during SERS measurements to set an appropriate bias potential. The bias potential applied

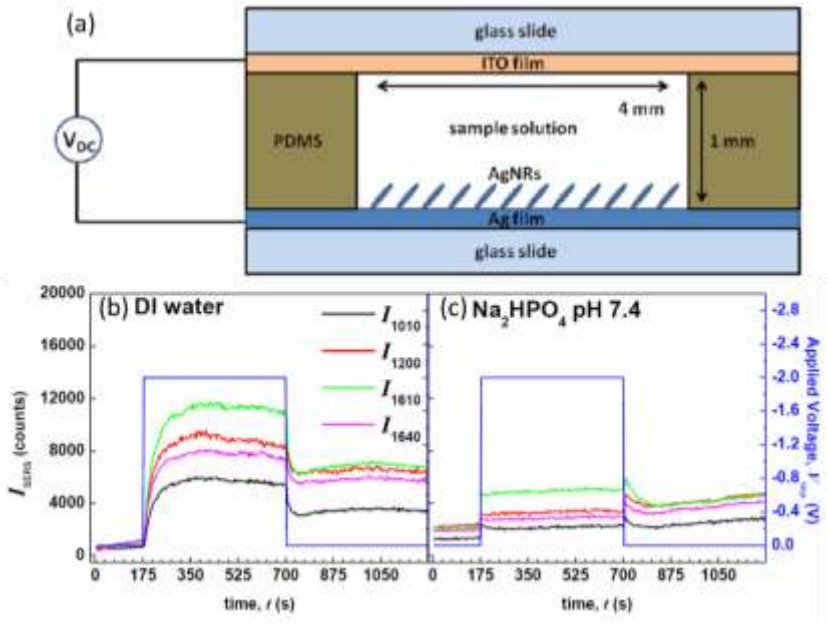

Fig. 39 (a) A schematic diagram of an electrocell made of AgNR substrate and ITO glass slide. The SERS intensity of four BPE peaks (1010, 1200, 1610, and 1640 cm^{-1}) vs time *t* and with a step bias potential V_{step} = -2.0 V for BPE dissolved (b) DI water and (c) Na_2HPO_4. The *I*SERS is scaled by the left y-axis, and the V_{step} is scaled by right y-axis. (Adapted with permission from Ref. 119. Copyright 2012 The University of Georgia.)

to the WE should be smaller than AgNR's oxidation potential (+0.2 V) [120, 121] and larger than its reduction potential (-5 V)[119]. The electrochemical behavior of the AgNR substrate can be found in Ref. [122]. **Figures 39b-c** show the change in SERS intensity as a function of bias time when 1×10^{-5} M BPE was dissolved in DI water (no electrolyte) and 100 mM HNa_2PO_4 pH = 7.4 buffer under a bias potential V_{step} = -2.0 V. Notably, their time-dependent behaviors exhibit distinct differences. A detailed analysis and the effects of bias potentials can be found in Ref.[119].

Furthermore, we have demonstrated the integration of the AgNR substrate into a microfluidic system, where it serves as both a microelectrode and a SERS substrate simultaneously. The detailed fabrication and integration process can be seen in **Figure 40a**, and further information can be found in Ref.[119]. The design entails a 1 mm diameter circular WE encircled by a "C"-shaped counter electrode with a 2.5 mm diameter. To facilitate electrical connectivity, 200 μm-wide wires extend from these electrodes to contact pads positioned at the edge of the glass slide. An array of ten such electrode configurations is constructed along the length of the microscope slide. The resulting device and its corresponding microstructures are shown in **Figure 40b**, illustrating the successful integration of the AgNR substrate into the microfluidic system. Further details and analysis can be found in Ref. [119].

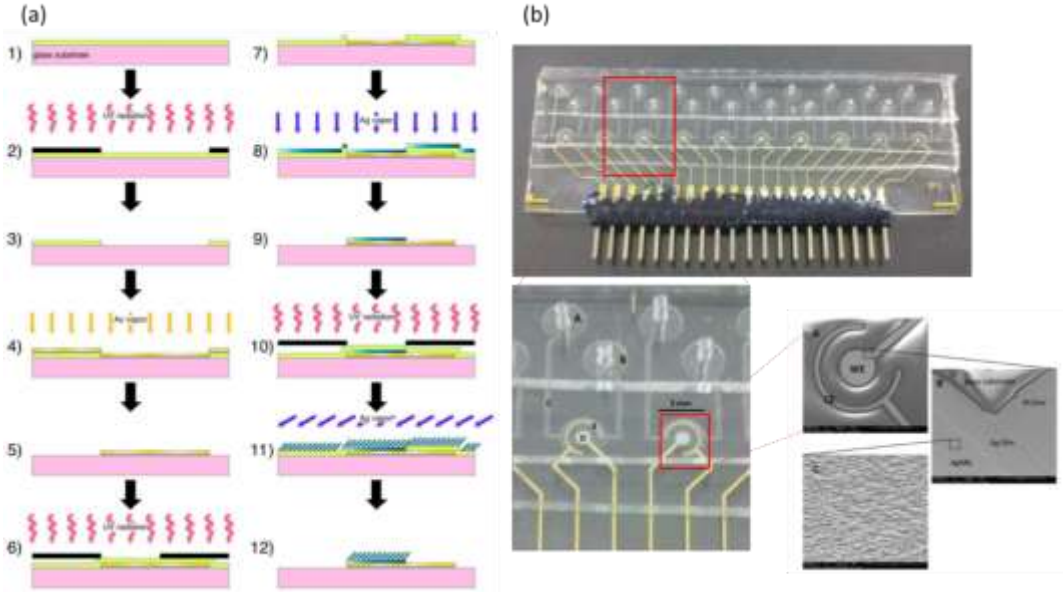

Fig. 40 (a) The fabrication process flow for integrating AgNR substrates into a microfluidic system and serving as microelectrodes. See main text for description (b) The microfluidic-electrochemical-SERS system made by AgNR substrate. (Adapted with permission from Ref. 119. Copyright 2012 The University of Georgia.)

7.7 The use of AgNR substrates for ultra-thin layer chromatography

As discussed in **Sections 6.1** and **6.2**, capillary forces among the Ag nanorods of liquid samples play a significant role not only in sample preparation but also in enhancing SERS signals. The strong capillary force, driven by wetting of the AgNR surfaces, facilitates rapid spreading of the liquid inside the Ag nanorods. This observation suggests that the AgNR substrate can be utilized as a separation device based on the principles of thin-layer chromatography (TLC)[123], with a particular focus on ultra-thin layer chromatography (UTLC) due to the AgNR substrate's thinness (< 1 μm) [124, 125]. Moreover, since the AgNR substrate is SERS-active, it can serve as both a separation and detection/diagnostic device simultaneously. **Figure 41a** shows the general procedure for the SERS-UTLC process using the AgNR substrate. This approach has been successfully applied to separate and detect a mixture of melamine-dye solution. The

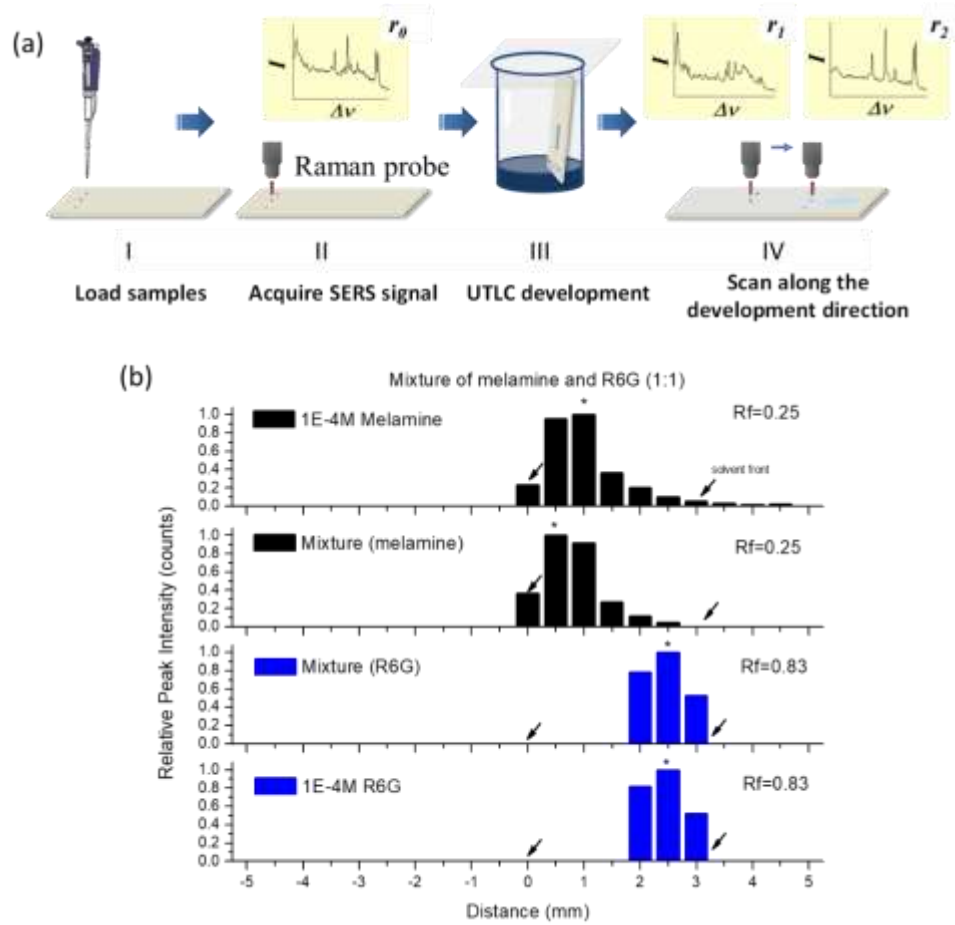

Fig. 41 (a) The SERS-TLC process on an AgNR substrate, and (b) the separation and detection of a mixture of melamine and R6G by AgNR UTLC. (Adapted with permission from Ref. 125. Copyright 2012 Royal Society of Chemistry.)

chromatograms of melamine and R6G from a 1:1 mixture, utilizing their spatially resolved unique Raman peaks, are presented in **Figure 41b.** Despite the dominance of the melamine SERS signal in the mixture's SERS spectra, the UTLC technique enables clear resolution of the R6G signals. A similar strategy has also been employed for the detection of polycyclic aromatic hydrocarbons (PAH) in cooking oil.[126]

7.8 The integration of AgNR substrates with handheld Raman systems

The combination of SERS with a handheld Raman system presents a promising solution for various point-of-care (POC) applications. The integration of the AgNR substrate with portable Raman spectroscopy systems can be easily achieved by making slight modifications to the sample holder of the instrument. **Figure 42a** shows an example of single AgNR chip detection using the Thermo Scientific FirstDefender RM instrument. An adapter is specifically designed to securely hold a chip of AgNR substrate mounted on a glass slide. By rotating the adapter along the instrument's thread, the distance between the AgNR chip and the instrument can be adjusted, ensuring proper alignment with the focal point of the excitation laser. This integrated system has been successfully employed for the measurement and differentiation of various influenza viruses,[127] as well as for identifying bacteria on fresh produce[128]. Another example involves the integration of a linear AgNR well (1×4) with a RAPID ID system, as shown in **Figure 42b**. Each well can be easily inserted into the circular opening of the holder and subsequently measured by the Raman system. To enable sampling at five different locations within the same well, a knob is designed to finely adjust the laser beam position. This configuration allows for efficient and precise analysis of multiple samples using the Raman system.

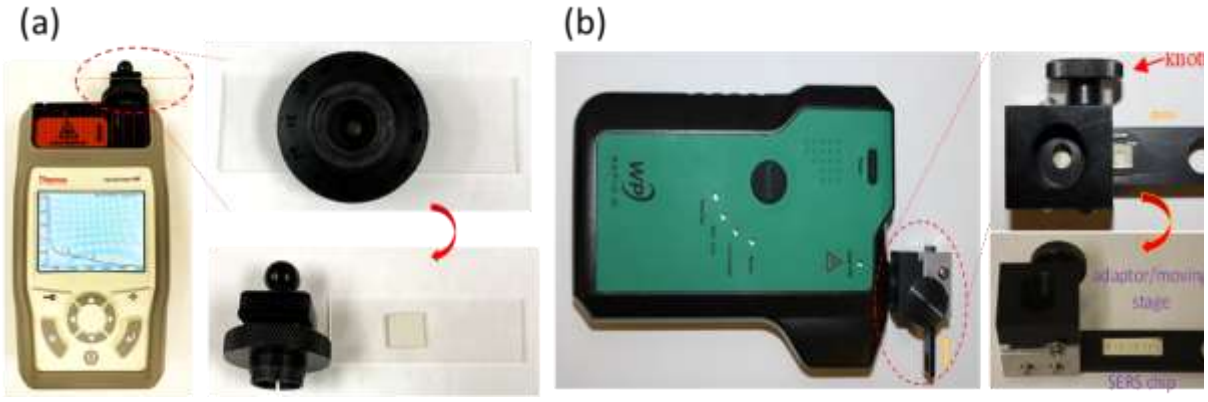

Fig. 42 (a) A photo of the AgNR substrate integrated with a FirstDefender system; and (b) a photo of an array of AgNR wells integrated with a RAPID ID system.

8. A Brief Summary of Applications

Since the discovery of the high SERS performance properties of the AgNR substrates, they have been used for various chemical and biological detections, covering applications in a wide spectrum of areas, such as biomedical diagnostics, veterinary diagnostics, food safety, environmental monitoring, national defense, etc. [12-14] **Table 1** summarizes all the applications we could find in the literature. We will not go into the details for specific applications, and some particular summaries can be found in previous reviews[129] or book chapters.[12, 130] Below we would like to address issues that might be encountered in different applications. Please note that the topics we are about to address primarily pertain to biological-based detection. However, it is important to emphasize that similar issues can also arise in other chemical sensing applications.

Table 1 A summary of applications of AgNR SERS substrates.

	Types of Analytes	Analytes	Strategy	AgNR	Applications	Ref.
Chemical detection	Vapors	4-aminobenzenethiol vapor	Direct	LT OAD	Environmental	131
		VOC gas	Direct	RT OAD	Environmental	132
		2-naphthalenethiol (2-NaT) and 2-mercaptopyridine (2-MPy)	Capture	HfO_2 coated	Environmental	133
		H_2S	Direct	RT OAD	Environmental	134
		Benzene	Direct	RT OAD	Environmental	135
		Uranyl ion	Direct	RT OAD	Environmental	136
	Metal ions	Uranyl ion	Direct	Al_2O_3 coated	Environmental	137
		Uranyl ion	Direct	HfO_2 coated	Environmental	138
		Mercury ion	Indirect	T-component oligonucleotide modified	Environmental	103
		Melamine	Direct	RT OAD	Food safety	106, 62
	Food additives	Sodium saccharin	Direct	RT OAD	Food safety	101
		Allura Red	Direct	RT OAD	Food safety	139
		Acesulfame potassium	Direct	RT OAD	Food safety	140
		Butylated hydroxyanisole	Direct	RT OAD	Food safety	141
		Antioxidants	Direct	RT OAD	Food safety	142
		PAH	Direct	RT OAD	Food safety	143
	Harmful substance in food	PAH	UTLC	RT OAD	Food safety	126
		Aromatic amines	Direct	Au nanostar coated	Food safety	144
		Capsaicin	Direct	RT OAD	Food safety	145
		2-, 3-, and 4-chlorobiphenyls	Direct	RT OAD	Environmental	146
	Pollutants	2,3,3', 4,4'-pentachlorinatedbiphenyl	Direct	RT OAD	Environmental	147

		Polychlorinated Benzene	Direct	Vertically aligned AgNR	Environmental	[148]
		Polychlorinated Biphenyls	Direct	RT OAD	Environmental	[149]
		1, 4-Benzenedithiol, 2-Naphthalenethiol, 4-Mercaptobenzoic acid, & 4-Mercaptopyridine	Direct	Al_2O_3 coated AgNRs	Environmental	[150]
		2-Naphthalenethiol & 4-Mercaptopyridine	Direct	Al_2O_3 coated AgNRs	Environmental	[151]
		3,3',4,4'-tetrachlorobiphenyl and 4-chlorobiphenyl	Direct	MXene modified AgNRs	Environmental	[152]
		2,3,7,8-Tetrachlorodibenzo-p-dioxin	Direct	Au NP modified AgNR	Environmental	[153]
		4-chlorobiphenyl & 3, 3′ , 4, 4′ - tetrachlorobiphenyl	Direct	Graphene-embedded AgNR	Environmental	[154]
		Benzo[a]pyrene	Direct	RT OAD	Environmental	[155]
		Methyl Parathion	Direct	RT OAD	Environmental	[156]
		Chlorpyrifos	Direct	RT OAD	Food safety	[130]
	Pesticide/ herbicide	Thiram	Direct	Flexible AgNR	Food safety	[110]
		Disulfide & thiabendazole	Direct	Flexible AgNR	Food safety	[111]
		Acetamiprid	Direct	RT OAD	Food safety	[157]
		Tetramethylthiuram disulfide & thiabendazole	Direct	Flexible AgNR	Food safety	[158]
		Methyl viologen	Direct	Au NP modified AgNR	Food safety	[159]
		Methyl parathion and fenthion	Direct	LT AgNR	Food safety	[160]
		Benzidine and 4-aminobiphenyl	Direct	Au NP modified AgNR	Food safety	[144]
		Aflatoxins	Direct	RT OAD	Food safety	[102]
	Toxins	Aflatoxins	Direct	AgNR UTLC	Food safety	[161]
		Metronidazole & ronidazole	Direct	RT OAD	Environmental	[105]
	Antibiotics	Tetracycline hydrochloride	Direct	O-g-C_3N_4 coated AgNR	Environmental	[162]
		Glucose	Capture	4-mercaptophenylboronic acid modified	Medical diagnostics	[163]
Biological detection	Biomarkers	Pyocyanin, biomarker of *P. aeruginosa*.	Direct/Indirect	RT OAD	Medical diagnostics	[164]
		Vitellogenin, biomarker for endocrine system	Direct/Indirect	Vertical AgNR	Medical diagnostics	[165]
		Methamphetamine for a central nervous system	Direct/Indirect	AuNR	Defense	[84]
		Endotoxins for bacteria	Direct/Indirect	AgNR	Food safety	[166]
		Bilirubin for Hyperbilirubinemia	Direct/Indirect	Boron nitride nanosheets on AgNR	Medical diagnostics	[167]

		Mycolic acids for tuberculosis	Direct/Indirect	RT AgNR	Medical diagnostics	[168]
		Endotoxins for bacteria	Direct/Indirect	AgNR	Food safety	[78]
		Flavin mononucleotide	Direct/Indirect	RT OAD	Medical diagnostics	[169]
		Human IgG	Sandwich	AuNP + AgNR	Medical diagnostics	[170]
	Antibody/antigen	Anthrax protective antigens	Sandwich	Aptamer modified AuNR+ AuNP&BPE tag	Defense	[171]
		Thymosin-β4	Direct	RT OAD	Medical diagnostics	[172]
	Protein	Lysozyme and cytochrome c	Direct	RT OAD	Medical diagnostics	[173]
		Influenza viral nucleoproteins	Capture	Aptamer modified	Medical diagnostics	[174, 175]
		NS1 protein for Dengue	Direct	RT OAD	Medical diagnostics	[176]
		microRNAs	Direct	RT OAD	Medical diagnostics	[177]
	DNA/RNA	microRNAs & mixtures	Direct	RT OAD	Medical diagnostics	[178]
		microRNAs	Direct	RT OAD	Medical diagnostics	[179]
		microRNA hybridization	Capture	DNA probe modified	Medical diagnostics	[86]
		Single strained DNA	Direct	RT OAD	Medical diagnostics	[180]
		DNA hybridization	Capture	DNA probe modified	Medical diagnostics	[181]
		RNA of Flu	Capture	DNA probe modified	Medical diagnostics	[182]
		microRNAs	Capture	DNA probe modified	Medical diagnostics	[183]
		DNA	Capture	Probe modified	Medical diagnostics	[184]
		DNA	Capture	Probe modified, dual sensors	Medical diagnostics	[100]
		microRNAs	Sandwich	DNA probe modified with AuNPs	Medical diagnostics	[185]
		CoV-2 virus RNA	Capture	DNA probe modified	Medical diagnostics	[186]
		DNA	Capture	Double-Tetrahedral DNA Probe	Medical diagnostics	[187]
		microRNA	Capture	CRISPR/Cas13a	Medical diagnostics	[188]
		Respiratory syncytial virus (RSV) Rhinovirus Adenovirus Human immunodeficiency virus (HIV) Influenza (flu)	Direct	RT OAD	Medical diagnostics	[189, 190]
	Viruses	RSV	Direct	RT OAD	Medical diagnostics	[191]
		RSV, HIV, Rotavirus	Direct	RT OAD	Medical diagnostics	[192]
		Avian influenza virus (AIV)	Direct	RT OAD	Medical diagnostics	[112]
		Measles virus (MeV)	Direct	RT OAD	Medical diagnostics	[193]
		Rotavirus	Direct	RT OAD	Medical diagnostics	[194]
		Flu	Direct	RT OAD	Medical diagnostics	[195]

		Flu	Capture	DNA probe modified	Medical diagnostics	196
		HIV	Direct	RT OAD	Medical diagnostics	197
		13 Respiratory viruses	Direct	SiO_2 coated	Medical diagnostics	79
		E. coli *S. aureus* *Salmonella*	Direct	RT OAD	Medical diagnostics Food safety	198
	Bacteria	*M. pneumoniae*	Direct	RT OAD	Medical diagnostics	199-202
		Salmonella *E. coli* *S. aureus*	Direct	RT OAD	Food safety	128, 203
		E. coli	Direct	RT OAD	Food safety	204
		P. aeruginosa	Direct	Flexible AgNR	Medical diagnostics	205
		E. coli	Capture	Functionalized AgNR	Food safety	206
		27 bacteria	Capture	Vancomycin modified AgNR	Medical diagnostics Food safety	207
		A. baumannii *E. coli* *K. pneumoniae* *P. aeruginosa* *S. aureus*	Direct	RT OAD	Medical diagnostics	208
		S. Typhimurium	Capture	Aptamer modified	Food safety	209
		Malaria	Direct	RT OAD	Medical diagnostics	210
	Other Diseases	Glioma brain tumors	Direct	RT OAD	Medical diagnostics	211

* LT: low temperature RT: room temperature VOC: volatile organic compound

8.1 Detection strategies

Like other SERS based detection, based on the ways to measure the target analytes, four different detection strategies are used for AgNR SERS based detections, as shown in **Figure 43**: direct detection, indirect detection, capture/conjugation/hybridization method, and sandwich method.

The direct detection method (**Figure 43a**) involves directly applying the solution of target analytes onto AgNR substrates and measuring their intrinsic SERS spectra. In this method, the detection relies solely on the characteristic SERS spectrum of the analyte, and the sensitivity or LOD depends on the EF of the analyte molecules on the SERS substrates. Direct detection is a simple and straightforward approach as it involves direct interaction without additional steps. It allows for quick analysis and is suitable for simple sample matrices, such as pure analyte solutions. Many AgNR-based SERS detections described in **Table 1** utilize the direct detection method. However, in complex sample matrices like buffers or biofluids, the presence of other molecules can compete with the target analyte molecules to adsorb onto the SERS hot-spots (see **Section 6.3**). This can have several consequences: 1) the reduced number of target analyte molecules adsorbed onto the hot-spots may lower the sensitivity or increase the LOD of the detection; 2) other molecules can introduce background SERS signals and decrease the relative intensity of the

intrinsic SERS spectrum of the target analytes, thereby affecting the sensitivity and specificity of the detection; 3) the background SERS spectrum introduced by other molecules can complicate the direct classification and quantification of the target analytes, potentially requiring additional target analyte separation processes or advanced data processing methods.

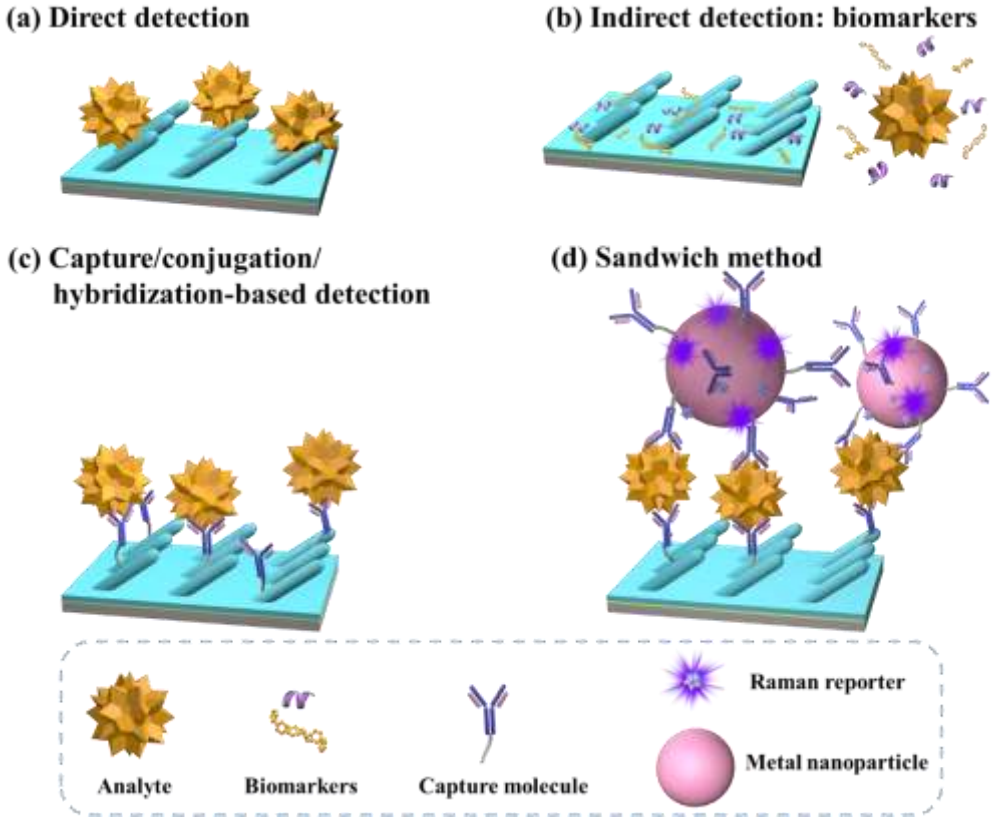

Fig. 43 The schematics for different SERS based detection strategies: (a) Direct detection; (b) Indirect detection; (c) Capture/conjugation/hybridization-based detection; and (d) Sandwich detection.

The indirect detection strategy involves measuring the SERS spectra of biomarkers associated with the target analytes or specific biological or health processes. Biomarkers, including proteins, nucleic acids, and metabolites, act as indicators of biological processes, conditions, or disease states. They are not a portion of the target but are generated due to specific chemical and biological reactions within the system the target is part of. Examples include antibodies or microRNAs, which are produced during the immune response to an infection, and mycotoxins released by specific pathogenic bacteria. In cases where the analyte particles are too large to be adsorbed around the side surfaces of AgNRs, as will be discussed in **Section 8.2**, resulting in low SERS EF, the sensitivity of the detection can be enhanced by measuring the SERS signals of biomarkers instead

of directly measuring the analytes. Compared to the target analytes, the SERS signals from their associated biomarkers may exhibit higher enhancements due to their sizes. However, unlike the definition of "direct detection" mentioned earlier, there can be multiple biomarkers associated with a particular target analyte. For example, in cancer detection, multiple microRNA biomarkers and protein biomarkers may be associated with a specific type of cancer.[183] This introduces the complexity of multiplexing detection, which may involve multiple processing steps, including the separation of different biomarkers from complex sample matrices.

In situations where the sample matrices become highly complex and the intrinsic SERS spectra of the target analytes are overshadowed by other molecules, the capture/conjugation/hybridization method can be employed. This method involves functionalizing specific capture or conjugation molecules onto the SERS substrate, and the detection is fulfilled via the affinity interactions, such as antibody-antigen binding or DNA hybridization, to selectively bind the target analytes. The affinity interaction enables the specific extraction of the target analytes from the complex sample matrices, offering high specificity and selectivity. The target analytes can include the target itself, a portion of the target, or biomarkers. The detection is based on analyzing the change in SERS spectra before and after the capture of the target analytes. For example, in DNA/RNA-based detection, a capture DNA is designed to be covalently immobilized on the AgNR substrate.[86, 181, 182] However, this method requires additional steps for capturing or conjugating the target analytes, which can increase the complexity and analysis time. The effectiveness of the method depends on the efficiency of the capture or conjugation process. Additionally, due to the distance effect in SERS enhancement mechanisms,[212] the spectral changes induced by affinity interactions may not be significant, especially at low concentrations of target analytes, limiting the sensitivity or LOD of the detection.

To address the issue of signal strength in the capture detection method, a more complex approach known as the sandwich method is proposed. This method involves two additional steps: first, SERS tags or reporter molecules with unique Raman spectral signatures, along with specific capture molecules (e.g., antibodies or aptamers) that selectively bind to the target analytes, are functionalized or conjugated to Au or Ag NPs; then, the functionalized NPs are incubated with AgNR substrates that have already captured the target analytes, forming a sandwich complex on the SERS substrate. Upon laser excitation, the SERS substrate enhances the Raman scattering signal from the SERS tags, enabling specific and sensitive detection of the target analytes. This

strategy offers high specificity, and the reporter molecule-tagged NPs generate significantly enhanced SERS signals. For instance, DNA probe-modified Au NPs have been used to detect microRNA cancer biomarkers for lung cancer.[185] However, this method involves a complex capture/conjugation process with two procedures. The conjugation of SERS tags to capture molecules requires careful optimization to ensure efficient and specific binding, which can be time-consuming, technically challenging, and economically expensive. Moreover, in complex sample matrices, the presence of interfering substances can affect the binding efficiency and detection sensitivity, necessitating additional sample preparation or purification techniques. Lastly, the specificity of the sandwich method relies on the specificity of the capture molecules, and cross-reactivity or nonspecific binding can lead to false-positive or false-negative.

Clearly, each of these detection methods has its own advantages and limitations. The choice of method depends on the specific requirements of the application, including sensitivity, selectivity, complexity of the sample matrix, and the desired level of assay development. One must carefully consider the pros and cons of each method to select the most appropriate strategy for their specific SERS-based detection needs.

8.2 The effect of target analytes

The detection strategy to be employed for AgNR substrates depends on the physical size of the target analytes and the sample preparation method used. As shown in **Figure 44**, the size of the analytes determines whether they can permeate into the gaps of the AgNRs and attach to the side surfaces. Both the side surfaces and the tips of the AgNRs contribute to the SERS signals from the substrate, as discussed in **Section 4**. The sample preparation method also plays a crucial role in this context.

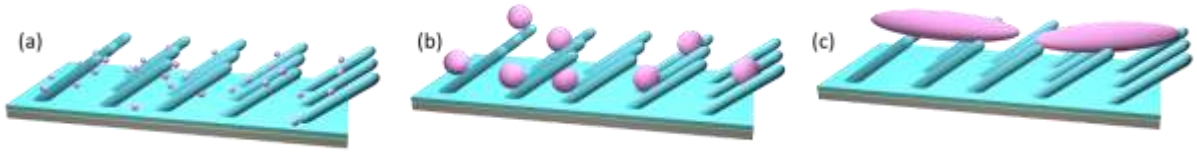

Fig. 44 A schematics of analyte size effect on an AgNR substrate: (a) very small size; (b) size comparable to the gap; and (c) huge size comparable to the gap.

In the case of the drop-cast method as the sample preparation technique, very small molecules like BPE or other molecular analytes with sizes smaller than 1 nm can readily adsorb onto the side surfaces of the AgNRs without significantly affecting the spacing between them (**Figure 44a**). As a result, these detections can achieve maximum enhancement. However, if the surfaces of the

AgNRs become hydrophobic (either due to contamination or surface functionalization), the nanorod array will make the surface more hydrophobic and prevent the sample droplet permeating into the gaps of the nanorods.[213, 214] Therefore the analyte can only reside on the tips of the AgNR, induced an analyte concentrating phenomenon, which could either increase or decrease the SERS intensity, depending on the competing between concentration increasing and the change of EF (only tip enhancement). There should be no dewetting-induced bundling effect in this case. If the adsorption of analyte molecule can alter the wettability of the surface of AgNRs, making the surface hydrophobic, then the dewetting-induced bundling effect will change (reduced) and a decrease in SERS enhancement shall be observed.

On the other hand, when the analyte molecules are larger, such as proteins or DNAs, they physically occupy a certain size between the AgNRs, as shown in **Figure 44b**, and the wetting-induced bundling effect becomes size-dependent. Additionally, the natural aggregation configuration and denatured configuration of proteins and DNAs, along with the buffer used and the specific wetting process, can influence the final adsorption results. An illustration is shown in **Figure 45**, where the possible adsorption configurations of folded and unfolded proteins are demonstrated. Clearly different protein folding configurations could generate different spectral features, which introduces extra spectral variations for the same analyte. Under different conditions, the SERS EF for different vibrational modes of the analytes may vary, potentially being less than that of small molecules, and the spectra obtained may also differ.

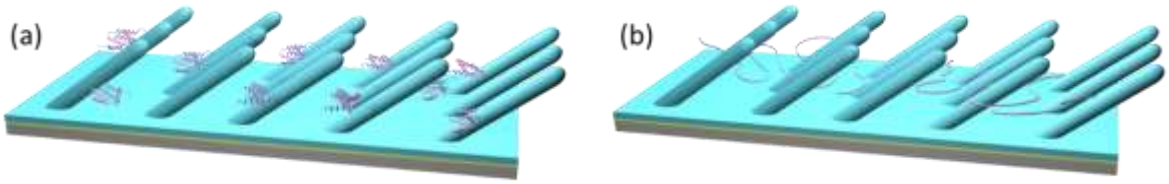

Fig. 45 The potential effect of (a) folded and (b) unfolded proteins on an AgNR substrate.

For even larger analytes such as viruses, which have sizes comparable to the gaps between the nanorods, if the viral particles can fall in-between the nanorods, there may be no wetting-induced bundling effect due to their size matching the gap size. However, for larger analytes like bacteria with sizes around micrometers as shown in **Figure 44c**, they cannot fall into the gaps between the nanorods and can only reside on the top surface of the AgNRs. In this case, only the tips of the

AgNRs contribute to the enhancement. It is expected that the EF in this scenario would be significantly different from the rest.

However, it is important to note that there is currently no systematic understanding of how the size of analytes precisely affects the final results of SERS measurements. Further research is needed to establish a comprehensive understanding of this relationship.

8.3 The effect of the quality of SERS spectra

In the SERS based detection, it is very important to understand the final obtained SERS spectra. The SERS signal from any measurement can be generally expressed as,

$$I_{total}(\Delta v) = R(\Delta v)(I_{SERS} + I_{Raman} + I_{FLU} + I_{FL} + I_{bk} + I_{medium}) + I_{noise} \quad (5)$$

where $R(\Delta v)$ is the instrument response function, which includes the quantum efficiency of the detector and the spectral response of each optical components in the instrument; the SERS intensity I_{SERS} from the analyte in SERS hot-spots can be written as **Eq. 4**; the normal Raman intensity can be expressed as

$$I_{Raman} = F_R N_R \sigma_{Raman} I_0, \quad (6)$$

with fraction F_R of photons collected, the total number N_R of analyte molecules contributed to Raman scattering, and the Raman scattering cross-section σ_{Raman}; I_{FLU} is the fluctuation SERS or Raman signal coming from the fluctuations of N_H and N_R due to the measurement configuration; I_{FL} is the potential florescence signal from the analyte, contaminants or other non-target molecules in specimen and solvent; I_{bk} and I_{medium} are potential SERS spectra from background molecule or medium molecule adsorption in SERS hot-spots or other optical spectral response; and I_{noise} is the electronic noises resulted from the Raman instrument. All the six intensities, $I_{SERS}, I_{Raman}, I_{FLU}, I_{FL}, I_{bk},$ and $I_{medium},$ are collected from the optical system in the instrument while I_{noise} is intrinsic to the electronics of the instrument and independent of the optical response of the instrument.

Therefore, the final SERS spectrum obtained from a Raman instrument is influenced by several factors that need to be considered for accurate analysis. These factors include: 1) *The instrument*: The spectral response of the Raman instrument itself can modify the true SERS spectrum. 2) *The excitation laser*: Parameters such as wavelength, incident angle, and polarization of the laser impact the excitation process. 3) *Measurement configuration*: The scattering angle and collection solid angle during data acquisition influence the collected signal. 4) *SERS substrate*: The size, shape, topology/morphology of the active SERS structure on the substrate, as well as its uniformity,

contamination, and dynamic effects, can greatly influence the shape and amplitude of the final spectrum. 5) *Analyte properties*: The size of the analyte molecules/particles, their intrinsic Raman scattering cross-section, potential fluorescence signals, and optical response affect the measured SERS spectrum. 6) *Adsorption property of analytes*: The adsorption affinity, distance to the SERS substrate, orientation, and equilibrium or non-equilibrium adsorption of analyte molecules impact the amplitude and potentially the shape of the observed spectrum. 7) *Contamination or medium*: If the SERS analyte is dissolved in a solution or medium containing other molecules, these background molecules may adsorb at the hot-spot locations and generate additional SERS signals. Many of these factors have been discussed in the previous sections.

To ensure that the obtained SERS spectra contain the specific spectral fingerprints of the analytes for a given application, it is crucial to analyze the spectra carefully. In simple sample matrices, the final measured spectra should exhibit obvious peaks representing the vibrational modes of the target analytes. In complex sample matrices, distinguishing characteristic peaks from the analytes can be challenging. However, advanced spectral analysis methods (see **Section 8.5**) can be employed to identify the important peaks that characterize the target analytes and differentiate them from the background buffer or medium.

The signal-to-noise ratio (SNR) of the SERS spectrum plays a significant role in SERS-based detection. SNR is typically defined as the ratio of the average peak height above the baseline to the standard deviation of the peak height.[215-217] The contribution of noise is not only due to the dark and shot noises from the instrument, i.e., I_{noise}, as seen from **Eq. 5**, various other factors, including variations in hot-spots, sample preparation, and number of analyte molecules in hot-spots, can also contribute to SERS intensity variation. Since a SERS spectrum has many different vibrational peaks, the SNR will be different for different peaks of the same spectrum. In practice, an alternative definition of SNR is the peak height above the baseline relative to the baseline noise or the root mean square (RMS) signal of a flat region of the spectrum.[218, 219] This definition is easier to implement and can be used to assess the quality of each individual SERS spectrum, but it is not really rigorously defined unless the baseline intensity is at the same order of the peak intensity. In general, for most intrinsic detections, a good detection is represented by an SNR value of at least 3, where the strongest peak in the SERS spectrum should be three times the RMS of the baseline noise. This 3σ-law is commonly used to determine the LOD in SERS-based detection. [128,

[164, 203, 204] However, it is important to note that the spectrum can be smoothened using advanced algorithms, which can improve the SNR virtually by reducing random noise effects.[215, 220, 221]

8.4 Baseline removal for SERS spectra

Baseline removal is a crucial step in SERS spectra analysis as it helps eliminate unwanted information contained in the spectra, such as background signals, nonuniform analyte distributions, and instrument effects. In recent years, with the rapid development and widespread application of SERS[222], particularly in combination with advanced machine learning algorithms[223-225], the importance of baseline removal has become even more significant (see **Section 8.5**).

The baseline in SERS spectra can originate from various sources, as indicated in **Eq. 5**, and can be categorized as intrinsic and extrinsic origins. Intrinsic baselines may arise from fluorescence and Rayleigh scattering from the analyte molecules, particularly biomolecules,[226] as well as surface plasmon-induced mechanisms.[227-229] Extrinsic baselines include contributions from scattering or absorption by the SERS substrate, such as morphology of nanostructures, environmental contamination molecules, background illumination, and instrument response.

Two main strategies have been proposed for baseline removal in Raman and SERS spectra. One approach involves hardware modifications, such as wavelength shifting and time grating,[230-234] which require adjustments to the instrument setup. For AgNR-based SERS detection, as discussed in **Section 6.6.1**, a polarization modulation method has been suggested for hardware-based baseline removal.[95]

The other widely used strategy is mathematical baseline removal. Currently, the most popular methods for baseline removal are polynomial methods, where the featureless baseline is approximated by a polynomial function. In a commonly employed method called ModPoly, baselines are fitted using the least squares method.[226] This iterative process fits the next baseline to the data points corresponding to the previously fitted baseline or the spectral data if it has lower intensity. However, successive iterations can result in an underestimation of the correct intensity due to the polynomial function. Modified versions of ModPoly, such as IModPoly[235] and ZhangFit[236], have been proposed to improve the performance compared to ModPoly. Additionally, many Raman instrument companies provide baseline removal software based on polynomial fitting. For example, the Windows-based Raman environment (WiRE^{TM}) supplied with Raman instruments from Renishaw Inc. applies an order 11 polynomial function to fit the spectra using a proprietary intelligent fitting technique.

While polynomial functions are simple to use and can represent a wide range of shapes with few variables, they may sometimes lack physical meaning in the context of the sources of the SERS baseline. **Figure 46** demonstrates the baseline fittings of the same SERS spectrum using polynomial functions of different orders. The resulting baseline-removed spectrum strongly depends on the order of the polynomial function used, indicating the potential for ambiguity in the interpretation of the baseline.

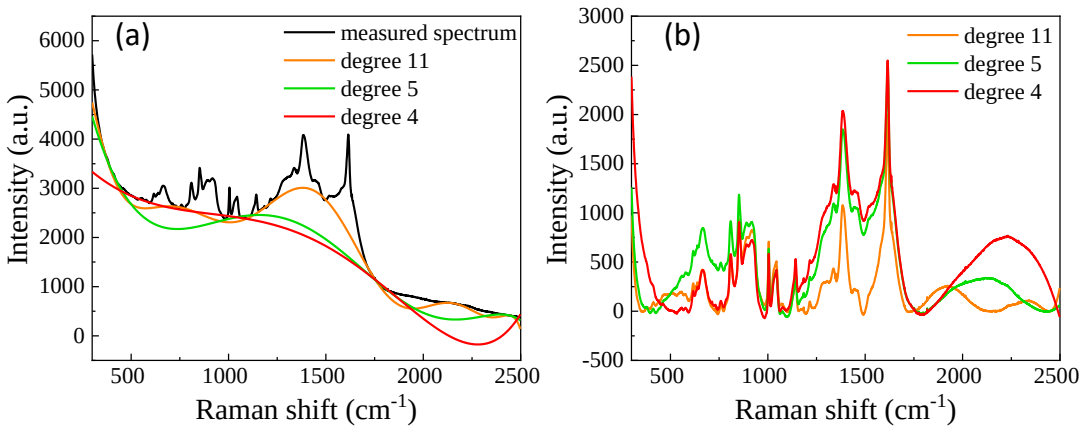

Fig. 46 (a) The SERS spectrum with baseline fitted by three polynomial functions with different orders. (b) The SERS spectra after removal of baseline using three polynomials shown in (a).

Thus, the choice of a "good" baseline removal method depends on the criteria set for the processed spectra and the purpose of baseline removal. In recent literature mentioned above, the underlying criterion is often to make the processed spectra as "flat" as possible. Also, the goal of ‘flatness’ requires knowledge of which spectral regions should not have SERS features, which is usually subjectively determined by the operator analyzing the spectra. While this criterion and hypothesis may be reasonable for identifying SERS peaks, they can introduce unphysical data treatment and subjective assumptions for real spectra in many other applications, such as spectral classification and quantification. This artificial removal of real information from targeted analytes can lead to inconsistency in future data analysis.

In previous discussions, we introduced two types of baselines: intrinsic and extrinsic baselines. The intrinsic baseline is directly associated with the target analytes and carries important information that should not be removed for spectral classification purposes. On the other hand, the extrinsic baseline, which includes contributions from SERS substrates, instruments, and background, should be removed as it is irrelevant to the targeted analytes and can pose problems

in data analysis. Additionally, in certain bio-detection scenarios, the targeted analytes may only be present in a background matrix, such as nasal swabs, saliva, or breath condensate, where the background molecules become part of the target analytes. Therefore, according to **Eq. 5**, I_{bk} and I_{medium} are indispensable in the final spectra analysis. In such cases, the variation in the spectra becomes more important than the flatness of the spectra.

Based on the above arguments, new criteria should be established for baseline removal. First, baseline removal should generally decrease the variation in spectra from measurement to measurement for the same sample and SERS substrate. Second, the removed baseline should have minimal spectral features. By removing the baseline, one should eliminate information that is common to all spectra, thereby enhancing the ability to differentiate between spectra. Third, after baseline removal, spectra from the same sample and SERS substrate should exhibit high correlation, while spectra from different samples or analytes should be more easily distinguishable.

8.5 Chemometric and machine learning analysis for SERS spectra

For most direct and indirect detections, since the specification of the detection is based on the fingerprint spectra of target analytes, the ability to distinguish one particular spectrum from a set of other spectra that can potential appear during the application, or to extract the spectral information from complex sample matrices, becomes critical. To achieve this objective, chemometric analysis and machine learning techniques emerges as potent tools, which can efficiently handle these spectra and uncover valuable insights for SERS detection or spectral analysis.[237-241]

Chemometric analysis, such as principal component analysis (PCA), partial least squares (PLS), and cluster analysis, is widely used for SERS spectra due to its ability to reduce data dimensionality

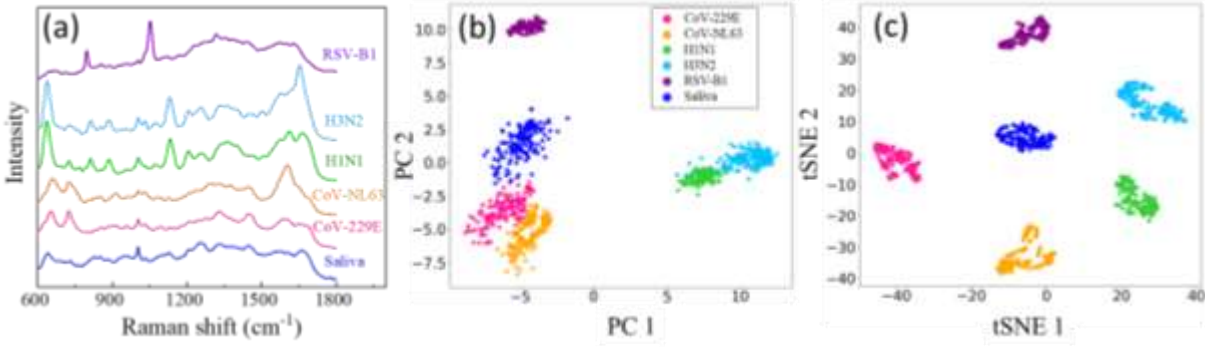

Fig. 47 (a) The average SERS spectra of saliva and 5 different viruses (RSV-B1, H3N2, H1N1, CoV-NL63, and CoV-229E) in saliva. (b) The corresponding PCA (PC2 versus PC1) and (c) tSNE plots.

and uncover hidden patterns. These techniques are particularly useful when dealing with large datasets or when the relationship between the spectra and analyte properties is not well understood. Chemometric methods can identify spectral features correlated with specific analytes, allowing for classification, quantification, and identification of target analytes. They are particularly effective when the spectra exhibit distinct and well-separated features. For examples, PCA and PLS methods have been widely used for AgNR-based detection and differentiation of viruses,[189, 191] bacteria,[128, 198, 207] microRNAs,[177-179] etc. For example, **Figure 47** shows the average SERS spectra of saliva and 5 viruses (RSV-B1, H3N2, H1N1, CoV-NL63, and CoV-229E) at 10^5 PFU/mL in saliva.[79] Although certain viruses like RSV-B1, H1N1, and CoV-NL63 exhibit distinct spectral features, due to internal variants within the same virus type, many display remarkably similar features (**Figure 47a**). Notably, spectra from H3N2 and H1N1, as well as CoV-NL63 and CoV229E, closely resemble each other. Distinguishing these subtle differences with the naked eye, particularly amidst the presence of multiple variants or viruses sharing similar structures, poses a considerable challenge. Nevertheless, employing chemometric methods provides an easy solution in resolving these distinctions. **Figure 47b** shows the corresponding PCA plot, revealing three primary clusters: saliva + CoV-NL63 + CoV-229E, H3N2 + H1N1, and RSV-B1. While some spectra from different viruses cluster together, many remain confined within their specific cluster boundaries. Utilizing an alternative chemometric approach, t-distributed stochastic neighbor embedding (tSNE) in **Figure 47c**, achieves a distinct separation of all virus clusters. However, when chemometric analysis confronts increasingly similar spectra, achieving clear distinctions becomes more difficult. This complexity is evident in **Figures 48a** & **b**, representing PCA and tSNE plots of spectra from the same five viruses in saliva but at different concentrations ranging from 195 to 10^5 PFU/mL. The high similarity in SERS spectra of the same virus at different concentrations leads to extensive intertwining of clusters in the PCA plot (**Figure 48a**). Although some separation is achieved in the tSNE plot (**Figure 48b**), many clusters remain entangled, highlighting the challenges in distinguishing closely related spectra through chemometric analysis.

In the light of above challenges, supervised machine learning algorithms offer a better solution to analyze SERS spectra by automating the process of pattern recognition and decision-making. Supervised learning algorithms, such as support vector machines (SVM), random forests, or neural networks, can be trained on labeled spectral data to build predictive models for analyte identification or quantification. Machine learning techniques are good at handling complex and

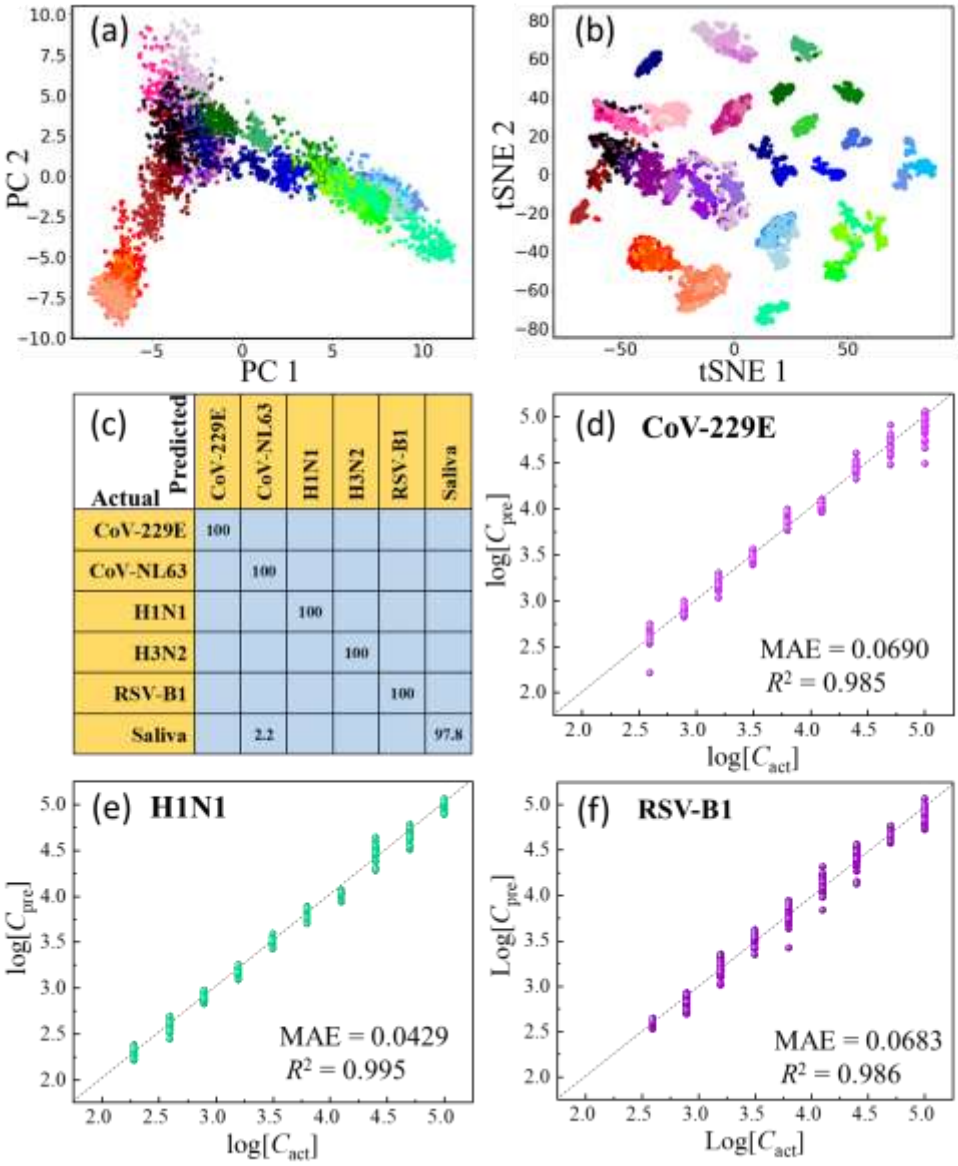

Fig. 48 The chemometric analysis of SERS spectra of 5 viruses in saliva with different concentrations: the (a) PCA and (b) tSNE plots. (c) The confusion matrix of the SVM model for saliva and 5 viruses with different concentrations in saliva. (d)-(f) The SVR regression results of CoV229E, H1N1, and RSV-B1. The x-axis is $\log_{10}C_{act}$ of testing spectra, and y-axis is $\log_{10}C_{pre}$. The dash line shows $\log_{10}C_{act} = \log_{10}C_{pre}$. (Adapted with permission from Ref. 79. Copyright 2022 Elsevier.)

nonlinear relationships within the data and can deal with overlapping spectral features. They can also incorporate additional features or metadata to enhance the predictive models. Recently Yang et al has employed SVM and support vector regression (SVR) to differentiate and quantify bacterial endotoxins[78] and respiratory viruses[79]. To address the challenges presented in **Figures 48a** & **b**, a two-step machine learning strategy is implemented to differentiate virus types and

quantify virus concentration: Initially, a SVM is utilized to recognize viral species based on the SERS spectra. Once identified, a regression model, specifically SVR, is applied to estimate the virus concentration. The resulting confusion matrix, as shown in **Figure 48c**, demonstrates an impressive overall classification accuracy of 99.6%. Notably, all five viruses achieve a perfect classification accuracy, while a mere 2.2% of saliva SERS spectra are misclassified as CoV-NL63. Quantitative results from SVR predictions are shown in **Figure 48b-f.** The predicted concentration C_{pre} aligns closely with the actual concentration C_{act}, with mean absolute errors (MAEs) ranging from 0.06 to 0.09 and R^2 from 0.995 to 0.974. These exceptional classification and quantification outcomes demonstrate the effectiveness of the machine learning method in analyzing complex SERS spectra. However, it is crucial to note that this analysis demands a sufficient amount of labeled training data, thorough hyperparameter optimization, and careful experimental design to mitigate issues related to overfitting or underfitting. Interpretability of the models can also be a challenge in some cases.

Deep learning, a subset of machine learning, involves the use of artificial neural networks with multiple layers to extract hierarchical representations from the input data. Deep learning has gained significant attention in various fields, including SERS, due to its ability to automatically learn complex features and patterns from raw spectral data. Convolutional neural networks (CNN) and recurrent neural networks (RNN) are commonly employed for SERS spectra analysis. Deep learning methods excel at capturing intricate relationships within the data and can handle large amounts of data without explicit feature engineering. They are well-suited for complex SERS spectra with overlapping or convoluted features. Yang et al has achieved SARS-CoV-2 detection from real nasal swap specimen using AgNR-based SERS and RNN method.[186] However, deep learning models often require large amounts of labeled training data and substantial computational resources for training. The interpretability of deep learning models can be challenging due to their black-box nature.

Therefore, based on the final targeted application, different statistical data analysis techniques can be used for SERS-based detections. Chemometric analysis is effective for reducing data dimensionality and uncovering patterns in SERS spectra, while machine learning and deep learning methods provide more sophisticated approaches for analyte identification and quantification. Chemometric analysis is suitable for datasets with distinct and well-separated spectral features, while machine learning and deep learning are better equipped to handle complex

and overlapping spectral patterns. The choice of the methods depends on the specific characteristics of the dataset, available labeled training data, computational resources, and the desired level of interpretability. Combining these techniques in a hybrid approach can often yield the most accurate and robust results for SERS spectra analysis.

9. Lessons Learned from AgNR SERS Substrates

From a practical point of view, if the SERS detection method could be commercialized, it must meet the following requirements:

1. **Sensitivity:** The SERS substrate should be highly sensitive to small changes in the analyte concentration, enabling the detection of analytes at low concentrations. The sensitivity of SERS-based sensing depends on many factors, including: 1) *Enhancement factor*: The SERS signal is dominated by the radiation of target analytes at hot-spot locations. The higher the EF, the more sensitive the SERS-based sensor will be. 2) *Substrate design*: The design of the SERS substrate can provide a high density of hot-spots that can interact with the target analytes. The substrate should also be optimized to provide appropriate wetting property and enhance analyte affinity, in addition to strong electromagnetic and/or chemical enhancement. 3) *Laser excitation wavelength*: The excitation wavelength should be chosen to match the absorption or resonance frequency of the SERS substrate or the target analyte to achieve maximum enhancement. 4) *Sample pretreatment and preparation*: Necessary sample pretreatment procedure such as filtration, separation, etc. and proper sample preparation method are required to enhance the SERS signals from target analytes and ensure the reliability of the measurements. 5) *Analyte concentration*: The higher the concentration of the target analyte, the stronger the signal will be, and the more sensitive the detection will be. 6) *Raman scattering cross-section of the analyte*: The Raman scattering cross-section of an analyte can vary depending on its chemical structure, vibrational modes, and other physical properties. The interaction between the hot-spots and target analytes can significantly influence the Raman scattering cross-section, leading to a stronger and more detectable Raman signal. 7) *The size of the analyte*: The traditional hot-spot location may not be able to accommodate large sized analyte. Therefore, for large sized analyte, the location of the hot-spots and the EF may be changed. 8) *Spectral data analysis*: The spectral data analysis should be optimized to remove noise and artifacts from the SERS spectra and to extract meaningful information from the data. The analysis should be performed using standardized methods to ensure reproducibility and accuracy. 9) *Environmental factors*: Environmental factors such as

temperature, pH, and ionic strength can affect the binding affinity and the conformation of the target analytes on the SERS substrate, which in turn affects the sensitivity of detection. Binding affinity refers to the strength of the interaction between the target molecule and the SERS substrate. Ideally, the target molecule should bind tightly to the SERS substrate to ensure that it remains in close proximity to the hot-spots and maximizes the enhancement of the Raman signal. The conformation of the target molecule on the SERS substrate refers to the specific way in which the analyte molecule is oriented and arranged on the surface of the substrate. The conformation can affect the accessibility of the molecule to the hot-spots and the overall enhancement of the Raman signal. For example, if the target molecule is oriented in a way that places it too far away from the hot-spots, the Raman signal may be weaker and the sensitivity may be lower (see **Section 8.2**). 10) *Interference and background signals*: Interference can arise from a variety of sources, including other molecules in the sample that may absorb or scatter light at the same wavenumber regions as the analyte. Background signals can also be a source of interference in SERS-based sensing. These signals can arise from a variety of sources, including fluorescence, impurities in the sample, and non-specific adsorption of other molecules onto the surface of the SERS substrate. These background signals can be especially problematic in complex biological samples, where the presence of a large number of other biomolecules can lead to significant background noise and make it difficult to detect the target analyte.

2. **Selectivity**: The SERS sensor should provide high selectivity for the analyte of interest, enabling the detection of specific molecules in complex mixture. SERS selectivity originates from the following: 1) Molecular fingerprints of the vibrational spectroscopy: SERS is based on the vibrational spectroscopy of molecules, which provides a unique "fingerprint" for each molecule based on the specific vibrational modes of its chemical bonds. This allows SERS to selectively detect and identify specific molecules based on their unique Raman spectra. 2) *AI-based techniques for achieving specificity or selectivity*: As the target system becomes more complex, it becomes more challenging to achieve selectivity and specificity using traditional SERS techniques. However, artificial intelligence (AI)-based techniques, such as machine learning and deep learning, can be applied to SERS spectral analysis to improve the specificity and selectivity of the technique. These techniques can be used to identify patterns and correlations in large SERS datasets and to classify samples based on their Raman spectra. 3) *Different detection strategies*: As discussed in **Section 8.1**, different detection strategies, other than direct detection, can be implemented to

improve the specificity. The adoption of different detection strategies is a compromise decision between the sensitivity and specificity.

3. **Reproducibility**: Reproducibility ensures that SERS sensors provide consistent results and is essential for quantitative analysis. It allows for reliable comparisons between different samples or experimental conditions and can be used to establish standardized protocols and facilitate interlaboratory comparisons. The reproducibility of SERS measurements depends on several factors, including the uniformity and reproducibility of SERS substrates, the chemical compatibility of the SERS substrate and target analyte or environment, the uniformity of sample preparation, the stability of the instrument, and other factors that may affect the measurement variability.

4. **Stability**: The SERS substrate/sensor should be stable and have a long lifetime under various experimental conditions and environments, including changes in buffer media and humidity, sometimes in temperature, pH, etc.

5. **Compatibility**: The SERS substrate should be compatible with a range of analytes, including both chemical and biological molecules, to enable its use in a range of applications, including environmental monitoring, food safety, medical diagnostics, drug discovery, etc.

6. **Cost-effectiveness**: The SERS substrate should be cost-effective, enabling its widespread use in both research and commercial applications.

7. **Scalability**: The SERS substrate should be scalable, allowing for the production of large quantities of substrates for high-throughput applications.

Therefore, to really make SERS sensor practical, one requires a standardization procedure. Standardization in SERS-based sensing refers to the process of establishing consistent and uniform practices for substrate and sample preparation, data acquisition, data analysis, and reporting in SERS experiments. This ensures that SERS measurements are reliable, consistent, and comparable between different research groups, laboratories, and applications. Standardization also promotes better communication and collaboration between researchers, leading to increased efficiency and progress in the field. Additionally, the use of machine learning and artificial intelligence approaches for SERS data analysis may provide new opportunities for automated and standardized SERS measurements, enabling faster and more efficient SERS-based sensing applications. In the future, standardization is likely to play an increasingly important role in SERS-based sensing.

However, there are several challenges associated with standardization in SERS-based sensing. One of the major challenges is the variability in SERS substrates and instrumentation used between different research groups and laboratories, which can impact the reproducibility of SERS measurements. Another challenge is the diversity of SERS applications, with different sample types, analytes, sample matrices, and experimental conditions requiring different protocols and approaches. This can make it challenging to develop a standardized protocol that is applicable to all SERS experiments. Based on the above comprehensive review on AgNR-based SERS, the following issues need to be addressed to develop standardized SERS sensing protocols.

9.1 The SERS enhancement mechanism could be complicated and dynamic.

The SERS enhancement plays a crucial role in determining the quality of the SERS sensor. However, practically the SERS enhancement of a specific SERS substrate is more complicated than just to simply identifying the mechanism as electromagnetic enhancement or chemical enhancement, or both. It not only depends on the detailed nanoscale morphology and surface chemical property of the SERS substrate, but several other factors, such as sample preparation conditions, surface wettability, the size of the target analyte, and others.

The effect of detailed morphology of the AgNR substrates on their enhancement has been discussed in **Sections 2** and **4**, and has been commonly considered in most SERS literature. However, the sample preparation induced bundling effect discussed in **Section 6.2** is unique to AgNRs or other thin film-based SERS substrates. Such a wetting/dewetting induced change can significantly alter the SERS EF, therefore dramatically affecting the sensitivity of the detection. Similar but slightly different effect has also been observed on nanoparticle based SERS substrates, whether NP aggregations induced by drying (wetting/dewetting) or salt can significantly increase SERS signals.[242, 243]

The other important factor is the size of the target analyte compared to the gaps between the AgNRs, which has been addressed in several subsections, such as **Sections 4** and **8.2**. Even for small sized analyte, if the binding affinity of the target analytes on the SERS substrate varies, the resulting EF could be different.

Therefore, in a SERS standardization process, the difference induced by these effects must be considered.

9.2 The detailed measurement configuration can alter the SERS signal strength.

The measurement configuration of the SERS refers to the optical setup and parameters used during the acquisition of SERS spectra, including the laser excitation wavelength, incident angle, polarization, and detection scheme. As discussed in **Section 3**, both the polarization and incident angle of the excitation laser could significantly change the measured SERS signal, similar to the effects of the wavelength and power of the excitation laser as examined in **Sections 6.4** and **6.5**. Factors such as the excitation wavelength and polarization can excite different plasmonic modes of the SERS substrate, leading to different enhancement of the Raman signals and optical response of the substrate. The measurement configuration can be tailored to selectively detect specific optical signals from the analyte-substrate system. By choosing the excitation wavelength that corresponds to the absorption or resonance of the target analyte, researchers can enhance the Raman scattering from the analyte of interest while minimizing the background signals. However, as shown in **Figure 29**, the underline mechanism on how different excitation wavelength changes the baseline and shape of the SERS spectra is still unknown.

Also, by modulating the polarization of the excitation laser, one can further eliminate the background florescence signal, as demonstrated in **Section 6.6.1**. In addition, by optimizing the incident angle and polarization, one can maximize the collection of Raman scattered photons while minimizing the background noise. This ensures that the weak Raman signals from the analyte are efficiently detected and distinguished from the noise, leading to improved SNR of SERS measurements. Therefore, by selecting the appropriate measurement configuration, one can optimize the enhancement factor, enhance the quality of the measured SERS spectrum, and improve the sensitivity and detection limit of the SERS sensor. Nevertheless, one must notice that the change of the optical measurement configuration could introduce different instrument response, vary the optical response of the substrate, alter the EF, affect the stability of the collected signals, thus ultimately modify the amplitude and shape of the obtained spectrum.

9.3. Scalable reproducible SERS substrate fabrication is crucial for commercialization.

Scalable fabrication of reproducible SERS substrates is a historical challenge in the SERS community, and the importance of the reproducibility of SERS substrates has been discussed above. Mass production of SERS substrates with consistent properties and high quality is essential for commercialization and for designing various devices to integrate SERS technology into real-world applications. OAD method is a physical vapor deposition method, and it is compatible with the standard microfabrication processing in semiconductor industry. **Section 7** unarguably

demonstrates the scalable fabrication capability of AgNR substrates *via* OAD, their reproducibility and uniformity, as well as multiple device designs. All these results show that the AgNR substrates have the potential to be commercial high performance SERS substrate.

9.4. Storage and cleaning of the SERS substrates directly impact the quality and accuracy of the SERS measurements.

All SERS substrates are susceptible to contamination when exposed in ambience, which can arise from various sources such as moisture, airborne particles, oils, fingerprints, or residual chemicals. Contamination can negatively affect the SERS measurements by introducing additional background signals, interfering with analyte adsorption, altering the wettability of the substrate, and adjusting other properties. Therefore, by storing the substrates in appropriate conditions, such as desiccated environments or sealed containers, one can preserve the inherent SERS activity and ensure consistent and reproducible measurements over time. Our method to store AgNR substrates in Argon filled pouch demonstrates a shelf-life of 7 years, which can lead to cost savings and ensure the availability of high-quality substrates for an extended period. This long shelf-life is very attractive for commercial applications.

Regardless of the storage methods, contamination is inevitable for SERS substrates and proper cleaning procedures must be implemented to remove contaminants and maintain high quality SERS measurement. For different SERS substrates, the cleaning procedure may be different. As for the AgNR substrates, we demonstrated two different methods as shown in **Section 5.5**: plasma cleaning and the chemical cleaning. Plasma cleaning can produce high quality substrates with very low background spectral features, but the instrument used is bulky and expensive. The chemical cleaning method is handy and easy to use, but it may introduce additional contamination. Clearly challenges remain to figure out a simple and reliable cleaning procedure for different SERS substrates. One possible solution is to design a compact and cost-effective plasma cleaning system, and the other is to develop a simple chemical cleaning procedure.

Notice that the above discussion is based on disposable SERS substrate, i.e., the substrate cannot be reused once finished one measurement. The design and production of reusable SERS substrates or SERS substrates for *in-situ* continuous monitoring is facing great challenges. Among them, one challenge is how to continuously clean or regenerate a fresh SERS substrate with steady performance. This will be discussed further in **Section 10**.

9.5 Sample preparation needs to be standardized.

As discussed above, the sample preparation method not only could alter the final SERS enhancement mechanism for particular SERS substrates (such as the AgNR substrates), but it can also introduce the non-uniform distribution of the analyte on the substrates, i.e., the CRE as discussed in **Section 6.1**. In addition, other sample preparation methods, such as thorough mixing, appropriate dilution, or standardization procedures, help achieve the homogeneity and reproducibility of the sample, ensuring the reliable and consistent SERS measurements. In a broad sense, sample preparation methods can involve techniques such as concentrating the analytes of interest, controlling the pH and ionic strength of the sample, and selecting appropriate solvents or extraction methods. By carefully tailoring the sample preparation, one can improve the adsorption and distribution of analyte molecules on the substrate surface, leading to stronger and more reproducible SERS signals. Furthermore, components in mixed samples can be separated during the wicking of the AgNR substrates, laying the foundation for UTLC device (see **Section 7.7**). For samples with complex matrices, by employing appropriate sample preparation techniques such as filtration, centrifugation, extraction, or purification methods, researchers can selectively remove or separate interfering substances, thereby reducing background interference and improving the specificity and sensitivity of the SERS analysis.

It should be noted that sample preparation methods need to be tailored to the specific properties of the analytes under investigation as well as the SERS substrates. Different analytes may require different sample preparation techniques depending on their physical or chemical properties. For example, volatile analytes may require techniques such as headspace sampling or solid-phase microextraction, while solid or particulate analytes may require grinding or dispersal methods. Understanding the nature of the analytes and selecting the appropriate sample preparation methods can ensure the stability, integrity, and accessibility of the analytes for effective SERS detection.

Thus, proper sample preparation methods can significantly enhance the SERS signal by optimizing the interaction between the target analytes and the SERS substrate, and greatly improve the reliability, accuracy, and comparability of SERS measurements between different samples and experimental conditions. It is a very important procedure to standardize the SERS measurement.

9.6 Understanding the SERS spectra from complex sample metrices cannot be neglected.

The SERS spectra from complex sample matrices are not only be interfered by the contents from their host media, including biological fluids, environmental substances, or complex mixtures, but

also may not contain any useful spectral information from the target analytes, possibly due to errors in measurement or strong interference background. Thus, it is very important to have a good understanding of the SERS spectra from complex sample matrices before trusting any classification or quantification results from chemometric analysis or machine learning. One key aspect of understanding SERS spectra from complex samples is the identification and characterization of target analytes within the sample matrix. By comparing the SERS spectra obtained from the sample matrix with reference spectra of known analytes, one can confirm the presence and determine the concentration of target analytes. This knowledge is crucial for various applications, where the detection and quantification of specific analytes are of paramount importance. If the spectra of the samples and their reference are very similar, at least two efforts should be made to ensure the presence of the information from the target analytes: From the spectra analysis point of view, if chemometrics or machine learning is used to differentiate those spectra, a parameter plot similar to feature importance which is used to differentiate the spectra shall be obtained and the main peaks/dips in the feature importance plot shall correspond to the main peaks of the target analytes. In addition, more experiments with different concentrations of analyte in the same sample matrix shall be conducted and the ability to differentiate and quantify the analyte as a function of concentration shall reflect the information changes due to the analytes. For example, in recent AgNR-based substrate to detect RNA of SARS-CoV-2 work, the SER spectra from both the SARS-CoV-2 positive and negative nasal swap specimens are very alike, yet the developed RNN model can achieve a very good differentiation accuracy.[186] According to the feature importance plot, the ability to differentiate positive and genitive specimens are mainly attributed to the peaks intrinsic to RNA, which is consistent with the principle of the detection strategy.

Furthermore, understanding the SERS spectra from complex sample matrices helps in distinguishing and mitigating the interference caused by coexisting substances. In complex matrices, interfering substances may exhibit overlapping spectral features with the target analytes, leading to challenges in accurate identification and quantification. By comprehensively studying the SERS spectra and the interaction between the analytes and matrix components, one can develop strategies to address interference effects. This may involve employing chemometric methods, such as multivariate analysis or machine learning algorithms, to differentiate the spectral contributions of analytes from those of interferents. Additionally, optimizing sample preparation techniques or

employing selective surface functionalization can help minimize the influence of interfering substances and improve the specificity and sensitivity of SERS detection.

Finally, understanding the SERS spectra from complex sample matrices enables researchers to uncover valuable information about the interaction between the analytes and the matrix components. The presence of complex matrices can affect the behavior of analyte molecules on the SERS substrate, leading to changes in the spectral features or intensities. By studying these spectral variations, researchers can gain insights into the mechanisms of adsorption, chemical interactions, and surface-enhanced effects occurring between the analytes and the substrate in the presence of complex matrices (see **Section 6.3.2**). This understanding is crucial for optimizing experimental conditions, designing effective sensing strategies, and developing robust analytical protocols that can account for the complexities introduced by the sample matrix.

9.7. Adopting an appropriate baseline removal method or other spectral pretreatment methods can improve the accuracy of the detection.

The issues regarding baseline removal have been addressed extensively in **Section 8.4**. Removing the baseline is essential to isolate the analyte-specific information and improve the accuracy of subsequent data analysis. As discussed in **Section 8.4**, a new and more reasonable baseline removal criteria shall be implemented in the future in order to obtain more consistent SERS analysis results. This is also a very important step to standardize SERS detection.

9.8 Selecting appropriate chemometric methods or machine learning algorithms can significantly improve the performance of the SERS sensor.

Section 8.5 discusses the need to use chemometric or machine learning methods for SERS spectral analysis. However, the choice of chemometric methods or machine learning algorithms for SERS spectrum analysis depends on the specific characteristics of the data, the research question or application, and the desired outcomes.

SERS spectra can exhibit significant variability due to various factors, such as different experimental conditions, sample matrices, analyte concentrations, and instrumental setups, see **Table 1**. These variations can affect the spectral patterns and relationships within the data. As a result, different data sets may require different strategies to handle their specific sources of variability. For example, one data set may require advanced noise reduction techniques, while another data set may require specific methods to deal with baseline drift or instrumental artifacts.

SERS spectra can follow different concentration dependent relationship, some may exhibit linear relationships, while others may have nonlinear or more intricate relationships, as presented **Section 6.7**. The choice of chemometric methods or machine learning algorithms should consider the underlying distribution of the data and its nonlinearities, if any. Certain algorithms are designed to handle linear relationships, while others are more suitable for nonlinear or non-parametric models.

SERS spectra can vary in terms of data size (number of samples) and dimensionality (number of variables or wavenumbers), especially when spectra are collected by different instruments. Some data sets may have a small number of samples but a high-dimensional feature space, while others may have a large number of samples with relatively low dimensionality. The selection of appropriate methods should consider the specific characteristics of the data in order to avoid overfitting (in the case of small data sets) or the curse of dimensionality (in the case of high-dimensional data sets).

Different research questions or applications may require different approaches to data analysis. For example, if the goal is to classify or identify different analytes or sample classes based on their spectral fingerprints (especially in diagnostic applications), certain classification algorithms (e.g., SVM, random forests) may be more appropriate. If the focus is on quantification or regression, other regression-based algorithms (e.g., partial least squares regression, neural networks) may be preferred. The specific objectives of the study or application drive the choice of suitable algorithms.

Up-to-now, it has been common practice to compare and benchmark different methods or algorithms using multiple data sets. This allows researchers to evaluate the strengths and limitations of various approaches and identify the best-performing methods for specific data sets or research questions.[78, 79, 244] The absence of a general one-for-all algorithm promotes diversity, innovation, and ongoing development in the field, as researchers continually strive to improve the performance and applicability of different methods. However, for the benefit of the SERS community, certain standards in spectral dimension, data size, sampling, etc. as well as spectra-pretreatment algorithms, shall be implemented to promote the application of this technique.

9.9 Establishing a spectra database is indispensable for practical SERS sensors.

Based on all discussions above, for real world SERS applications, the establishment of a comprehensive spectral database for SERS is of paramount importance for advancing the field and

realizing its full potential. Such a database can provide a standardized approach to data analysis and interpretation, leading to enhanced reliability, reproducibility, and comparability of results. A well-curated database would serve as a valuable resource for researchers, enabling them to identify and classify different analytes based on their characteristic spectral signatures. This knowledge can aid in the rapid identification and quantification of target molecules, discovering and understanding issues related to fundamentals of SERS, facilitating applications in various fields such as medical diagnostics, drug discovery, food safety, and environmental monitoring.

Moreover, a spectral database would provide a foundation for the development and validation of machine learning models and data-driven approaches for SERS analysis. By training algorithms on a comprehensive dataset, researchers can improve the accuracy and efficiency of analyte identification and classification. This can significantly enhance the speed and reliability of SERS-based detection methods, allowing for high-throughput screening and analysis.

In addition, a spectral database would enable researchers to investigate the underlying mechanisms and interactions between analytes and SERS substrates. By studying the spectral variations observed for different substrates and analyte-substrate combinations, researchers can gain insights into the factors influencing the SERS signal and optimize the design and fabrication of SERS substrates for improved performance.

Furthermore, a well-curated spectral database can serve as a reference for quality control and standardization in SERS measurements. Researchers can compare their experimental results with established spectra in the database to assess the quality and consistency of their measurements. This helps identify potential sources of error, such as substrate quality, sample preparation, or measurement conditions, ensuring reliable and reproducible SERS measurements across different laboratories.

However, there are two foreseeing challenges (among others) to establish such a generic SERS database, the effects of different SERS substrates and different Raman instruments:

1. Eliminating the differences between the spectra collected from different SERS substrates: SERS is highly dependent on the properties of the SERS substrates, which can lead to significant spectral variations even for the same analyte. These differences pose challenges in establishing a unified and standardized approach to SERS measurements and hinder the development of robust analytical methods. Therefore, the key is to find the fundamental relationships among different SERS substrates and correct or modify standard SERS spectra based on the specific relationship

for a specific substrate. Clearly this also requires standardizing the procedure of the spectra collection from different SERS substrates, ensuring consistent experimental conditions across different SERS measurements, including laser power, excitation wavelength, integration time, measurement configuration, to name a few. Similarly, a standardized spectra-pretreatment procedure, such as baseline removal, spectrum averaging and smoothening, normalization, needs to be implemented.

2. ***Eliminating the effect of different Raman instruments:*** One key factor to preventing the standardization of SERS is due to the variation in Raman instruments. [245-247] Different Raman instruments could vary in laser power, wavelength, focal spot size, spectral resolution, and detector sensitivity, etc. These instrumental differences can lead to variations in the observed SERS spectra, making it difficult to compare results obtained from different instruments or laboratories. **Figure 49** shows an example of the instrument effect. For the same analyte on the same AgNR substrate, the spectra measured from different instruments have different baseline shapes and relative peak intensities. One way to eliminate the effect of instruments is to use a high-end instrument as a standard and obtain the instrument response functions of other instruments by measuring and comparing some standard reference materials/SERS substrates.[246] Such a method is heavily dependent on the reliability of the instrument manufactured by different company as well as on how to choose the standard instrument and reference materials/SERS substrates. The other possible method is to use transfer learning from machine learning algorithms, where a model developed on one instrument can be transferred and used on a new instrument. [248]

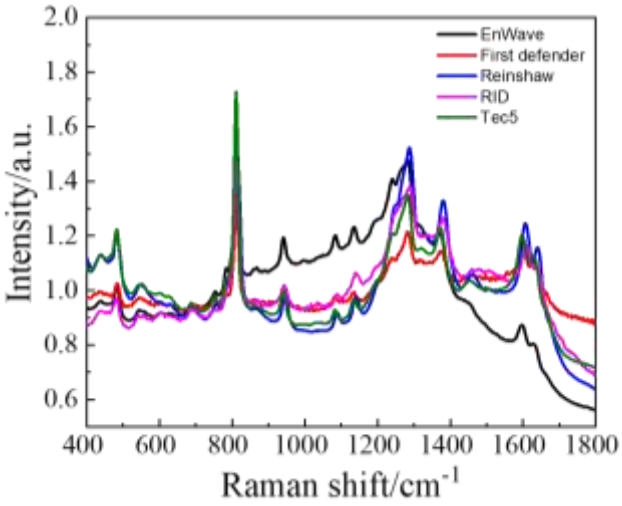

Fig. 49 The normalized SERS spectra of 2,5-Dihydroxybenzoic acid on a AgNR substrate using 5 different Raman instruments.

10. Conclusions and Future Perspectives

In a summary, we present a detail and comprehensive review on the AgNR SERS substrates fabricated by OAD method, and many practical issues for SERS measurements and detections, including SERS substrate optimization (morphology and structure designs), measurement configurations (wavelength, power, polarization, and incident angle of excitation laser), enhancement mechanism (intrinsic property induced by the structure and materials, extrinsic due to wetting/dewetting and analyte size), the manufacturing and storage (scalable fabrication, contamination, cleaning, and storage), device design (well array, flow cell, fiber probe, …, etc.) sample preparation (drop-cast and immersion), measurement issues (wavelength and power of excitation laser, buffer effect, etc.), spectral analysis (baseline removal, chemometric analysis and machine learning), as well as various applications, have been extensively addressed. These results show that even for a single type of SERS substrates, issues associated with SERS detection are multi-dimensional and complicated, which requires years of investigation and innovation.

Based on all the results, one can conclude that the AgNR substrate fabricated by OAD method is an excellent and versatile SERS substrate with the following advantages: (1) The fabrication method is readily accessible and compatible with conventional microfabrication process. The fabrication process is scalable; (2) the substrate is very uniform and have very low batch-to-batch variation under better quality control and practice; (3) the substrate has very high SERS EF, up to 10^9; (4) the substrate has a very long shelf life when stored properly, ~ 7 years; and (5) the substrate or the fabrication process is adaptable to make different devices. It has been used for many different applications as shown in **Table 1**. The AgNR substrate also has some distinct shortcomings, especially (1) It can be easily contaminated which requires a sophisticated cleaning technique (Ar^+ plasma clean); (2) it is reactive in some buffer and require protection coating; and (3) it cannot be used for SERS imaging applications.

In addition to the above pros and cons of AgNR substrates, there are still many issues and challenges which could be the future directions for these substrates. Below we outline a few:

1. ***Improving the quality of SERS measurement***: It is always important to improve the quality of the measured SERS spectra, which refers to two aspects, improving the SNR and the visibility of signals coming from the target analyte. To improve SNR, one can address it from three aspects, 1) SERS substrate optimization, i.e., choose an appropriate SERS substrate with high enhancement factors; 2) measurement configuration adjustment, i.e., select appropriate excitation wavelength

and power, as well as optical configuration for detection; and 3) appropriate spectral analysis method, such as spectral filtering or smoothening, signal averaging, baseline removing, statistical analysis, etc. To improve the visibility of signals from the target analyte, the most important strategy is to reduce background, i.e., to minimize or eliminate background interference sources, such as fluorescence from impurities or contaminants, complex medium matrices, etc. This can be achieved through proper sample preparation, purification, control of experimental conditions, and baseline removal. In addition, in certain applications where stability is important, appropriate surface coating can be applied.

2. ***An easy method to clean the AgNR substrates***: As demonstrated in **Sections 5.3** and **5.4**, the cleanliness of the substrate directly affects the quality and reliability of the SERS measurements. As discussed in **Section 9.4**, there are two possible solutions, one is to design a compact and cost-effective plasma cleaning system, and the other is to develop a simple chemical cleaning procedure.

3. ***In-situ real time measurement strategy for AgNR substrates***: SERS has not been used intensively in in-situ measurement though it has been demonstrated as a highly sensitive technique.[249] There are three major challenges: First, regenerating the SERS activity in-situ due to the potential loss or degradation of the substrate's plasmonic properties during the measurement process. Continuous exposure to the analyte solution and environment can lead to the accumulation of impurities or contaminants on the substrate surface, which may hinder the SERS activity. These impurities can include adsorbed molecules, ions, or residues from the analyte solution or the surrounding environment. Second, maintaining the stability of the AgNR substrate during in-situ real-time measurements. The stability issue arises from several factors: 1) The AgNR substrate is prone to oxidation and degradation over time, especially in the presence of reactive analytes or harsh experimental conditions, such as PBS shown in **Section 6.3.2**. The formation of oxide layers or structural changes in the AgNRs can significantly impact their plasmonic properties and, consequently, the SERS activity. 2) The AgNR substrate's stability can be affected by factors such as temperature fluctuations, pH variations, and exposure to reactive species or chemicals in the analyte solution. These factors can lead to changes in the substrate's surface morphology, oxidation, or even detachment of the AgNRs from the substrate surface. The instability of the substrate can result in inconsistent SERS signals and unreliable measurements. As discussed in **Section 6.3**, the stability issues of AgNR substrates can be addressed by coating an ultra-thin oxide layer on the

surfaces. Finally, adapting an appropriate measurement configuration to eliminate other possible time-dependent variations during measurement. As discussed in **Section 6.5**, by shining an excitation laser on one location of a SERS substrate, a time-dependent SERS signal variation can be observed due to either photo-thermal degradation or ablation of the analytes on the substrate. Such an additional time-dependent effect in measurement should be eliminated in in-situ measurement in order to reveal the true dynamic process under investigation. Thus, the measurement conditions such as excitation laser power, wavelength, measurement integration time, as well as measurement configuration such as rastering measurement, shall all be carefully considered.

4. ***Expanding the applications***: there are many potential applications for SERS, including biomedical diagnostics, environmental monitoring, food safety and quality control, forensic analysis, pharmaceutical industry, energy and catalysis, security, and defense. Different applications imply different target analytes, different detection environments, and different instrument requirements. Therefore, the AgNR-based SERS detection shall be amendable to those requirements. Most importantly, the application of AgNR-based SERS detection shall pay attention to the following issues: (1) *Detection strategy*: The detection strategy employed for different applications can vary significantly. For example, some applications may require direct detection of analytes on the substrate surface, while others may involve sandwich assays or capture-based detection. Ensure that the SERS substrate is compatible with the chosen detection strategy and can provide the necessary sensitivity and specificity. (2) *Analyte compatibility*: Different analytes may exhibit different affinities and interactions with the SERS substrate. It is important to assess the compatibility of the analytes with the substrate surface to ensure effective adsorption and signal enhancement. The substrate should be selected or modified to accommodate a wide range of analytes, their chemical properties or detection strategies. (3) *Surface modification and functionalization*: The ability to modify the SERS substrate surface is valuable for tailoring its properties to different applications. Consider using surface functionalization techniques to enhance selectivity, improve analyte binding, or introduce specific molecular recognition elements for target analytes. (4) *Substrate sensitivity and enhancement*: The sensitivity and enhancement capabilities of the SERS substrate should be evaluated in the context of the target analytes. Some substrates may be more suitable for certain types of analytes (e.g., specific functional groups or molecular structures). Consider the substrate's ability to generate strong and reproducible signals

for a diverse range of analytes. (5) *Device compatibility*: Consider the specific device requirements for each application, the SERS substrate should be adaptable to different device configurations, such as microfluidic systems, fiber sensors, electrochemical sensors, portable sensors, or integrated lab-on-a-chip platforms. Compatibility with the device's optical setup and excitation wavelength is also crucial for achieving optimal signal detection. (6) *Reproducibility and stability*: Consistency and reproducibility are key factors to implement SERS-based detection strategy. The modified AgNR substrate should exhibit high reproducibility in terms of signal intensity and spectral features. Additionally, stability is important to ensure the substrate's performance is maintained over time and under various experimental conditions. (7) *Validation and calibration*: It is crucial to validate the performance of the SERS detection strategy with relevant analytes and compare the results with established standards or reference measurements. Calibration using known analytes or internal controls can help ensure accurate and quantitative analysis across different applications.

5. ***Establishing a reliable SERS database***: As discussed in **Section 9.9**, it is crucial to establish a reliable SERS database for various applications. To do so, many challenges need to be targeted, especially three: standardization, community collaboration, and overcoming various hurdles. (1) *Establishing certain standardization procedures* in SERS measurements to ensure consistency and reproducibility as well as the potential for quantitative analysis. The standardized protocols could include substrate fabrication, sample preparation, experimental conditions, and instrument calibration, to just name a few. (2) *Inviting a broad community participation*: To invite researchers in SERS community to contribute their validated spectra to the database, increasing its diversity and coverage. By pooling together data from various sources, the database becomes more comprehensive and representative of different analytes, substrates, and experimental conditions. They can also verify the accuracy and reproducibility of spectra contributed by others, improving the overall reliability of the database. Peer feedback and discussions can lead to refinement and improvement of analytical methods and data interpretation. In addition, such a collaboration fosters the exchange of ideas, knowledge, and expertise. This can spur the development of new applications for SERS detection and drive innovation in the field. Collaborative efforts also facilitate the identification of emerging trends, challenges, and areas requiring further investigation. (3) *Hurdles and variations need to overcome*: As discussed in **Section 9.9**, there are many hurdles need to address to establish a reliable SERS database, especially the variations in SERS substrates and Raman instruments. Detailed investigations to understand the fundamental physical and

chemical links in the variations of SERS spectra from different substrates need to be carried out, while for instrument effect, the comparison of measurements from standard instrument and an appropriate statistic analysis method can be implemented. In a summary, overcoming these hurdles requires collaborative efforts among researchers, industry stakeholders, and standardization bodies. It involves establishing guidelines, sharing best practices, conducting inter-laboratory studies, and continuously refining protocols to address the challenges associated with variations in substrates, instruments, and environments. Through collective efforts, the SERS community can work towards establishing a reliable and comprehensive SERS database that serves as a valuable resource for researchers and analysts in the field.

Acknowledgement: The authors are supported by Qatar National Research Fund Grant number NPRP12S-0224-190144 and USDA NIFA Grant number 2023-67015-39237. The authors would like to thank Profs. Chunyuan Song and Caiqing Han for sharing some spectral data for excitation wavelength-dependent measurements and nitric acid cleaning. We also used ChatGPT to correct writing and grammar mistakes.

References:

1. E. C. Le Ru and P. G. Etchegoin, *Principles of Surface-Enhanced Raman Spectroscopy and Related Plasmonic Effects*, Elsevier, 2009.
2. Y. Wang, *Principles and Clinical Diagnostic Applications of Surface-Enhanced Raman Spectroscopy*, Elsevier, 2022.
3. E. C. Le Ru and P. G. Etchegoin, *Annual Review of Physical Chemistry*, 2012, **63**, 65-87.
4. Y. Qiu, C. Kuang, X. Liu and L. Tang, *Sensors (Basel)*, 2022, **22**.
5. A. Otto, *Journal of Raman Spectroscopy*, 1991, **22**, 743-752.
6. Z.-Q. Tian, B. Ren and D.-Y. Wu, *The Journal of Physical Chemistry B*, 2002, **106**, 9463-9483.
7. X. M. Lin, Y. Cui, Y. H. Xu, B. Ren and Z. Q. Tian, *Anal Bioanal Chem*, 2009, **394**, 1729-1745.
8. B. Sharma, R. R. Frontiera, A.-I. Henry, E. Ringe and R. P. Van Duyne, *Materials Today*, 2012, **15**, 16-25.
9. C. Li, Y. Huang, X. Li, Y. Zhang, Q. Chen, Z. Ye, Z. Alqarni, S. E. J. Bell and Y. Xu, *Journal of Materials Chemistry C*, 2021, **9**, 11517-11552.
10. K.-Q. Lin, J. Yi, J.-H. Zhong, S. Hu, B.-J. Liu, J.-Y. Liu, C. Zong, Z.-C. Lei, X. Wang, J. Aizpurua, R. Esteban and B. Ren, *Nature Communications*, 2017, **8**, 14891.
11. S. B. Chaney, S. Shanmukh, R. A. Dluhy and Y. P. Zhao, *Applied Physics Letters*, 2005, **87**, 031908.
12. J. L. Abell, J. D. Driskell, R. A. Tripp and Y. Zhaod, in *Functional Nanoparticles for Bioanalysis, Nanomedicine, and Bioelectronic Devices, Vol 2*, eds. M. Hepel and C. J. Zhong, 2012, vol. 1113, pp. 235-272.
13. X. M. Wu, J. Chen, B. Park, Y. W. Huang and Y. P. Zhao, in *Advances in Applied Nanotechnology for Agriculture*, eds. B. Park and M. Appell, 2013, vol. 1143, pp. 85-108.
14. S. Kumar, S. K. Gahlaut and J. P. Singh, *Applied Surface Science Advances*, 2022, **12**, 100322.
15. M. Meier, A. Wokaun and T. Vo-Dinh, *The Journal of Physical Chemistry*, 1985, **89**, 1843-1846.
16. T. Vo-Dinh, M. Meier and A. Wokaun, *Analytica Chimica Acta*, 1986, **181**, 139-148.
17. J. L. Martinez, Y. Gao and T. Lopezrios, *Physical Review B*, 1986, **33**, 5917-5919.
18. J. L. Martinez, Y. Gao, T. Lopezrios and A. Wirgin, *Physical Review B*, 1987, **35**, 9481-9488.
19. E. A. Wachter, A. K. Moore and J. W. Haas, *Vibrational Spectroscopy*, 1992, **3**, 73-78.
20. J. D. Driskell, S. Shanmukh, Y. Liu, S. B. Chaney, X. J. Tang, Y. P. Zhao and R. A. Dluhy, *Journal of Physical Chemistry C*, 2008, **112**, 895-901.
21. M. M. Hawkeye, M. T. Taschuk and M. J. Brett, *Glancing Angle Deposition of Thin Films - Engineering the Nanoscale*, John Wiley & Sons, Ltd, West Sussex, United Kingdom, 2014.
22. Y. J. Liu, H. Y. Chu and Y. P. Zhao, *Journal of Physical Chemistry C*, 2010, **114**, 8176-8183.
23. Q. Zhou, Z. C. Li, Y. Yang and Z. J. Zhang, *Journal of Physics D-Applied Physics*, 2008, **41**.
24. P. Shah, D. Q. Ju, X. X. Niu and A. M. Sarangan, *Journal of Sensors*, 2013, **2013**.
25. M. K. Oh, Y. S. Shin, C. L. Lee, R. De, H. Kang, N. E. Yu, B. H. Kim, J. H. Kim and J. K. Yang, *Nanoscale Research Letters*, 2015, **10**.
26. J. P. Singh, T. E. Lanier, H. Zhu, W. M. Dennis, R. A. Tripp and Y. P. Zhao, *Journal of Physical Chemistry C*, 2012, **116**, 20550-20557.
27. Q. Zhou, Y. J. Liu, Y. P. He, Z. J. Zhang and Y. P. Zhao, *Applied Physics Letters*, 2010, **97**.
28. Y. J. Liu and Y. P. Zhao, *Physical Review B*, 2008, **78**.
29. Y. J. Liu, Z. Y. Zhang, R. A. Dluhy and Y. P. Zhao, *Journal of Raman Spectroscopy*, 2010, **41**, 1112-1118.
30. X. Zhang, Q. Zhou, W. P. Wang, L. Shen, Z. C. Li and Z. J. Zhang, *Materials Research Bulletin*, 2012, **47**, 921-924.
31. M. Keating, S. Song, G. Wei, D. Graham, Y. Chen and F. Placido, *Journal of Physical Chemistry C*, 2014, **118**, 4878-4884.

32. Q. Zhou, Y. P. He, J. Abell, Z. J. Zhang and Y. P. Zhao, *Journal of Physical Chemistry C*, 2011, **115**, 14131-14140.
33. J. Li, Y. Fan, X. Xue, L. Ma, S. Zou, Z. Fei, Z. Xie and Z. Zhang, *Physical Chemistry Chemical Physics*, 2018, **20**, 25623-25628.
34. Y. Song, Q. Wang, Y. Luo, W. Cao, Z. Cao, C. Yan, A. Lu and C. Han, *Opt. Express*, 2021, **29**, 13968-13977.
35. Q. Zhou, X. Zhang, Y. Huang, Z. C. Li, Y. P. Zhao and Z. J. Zhang, *Applied Physics Letters*, 2012, **100**.
36. Y. J. Jen, W. C. Liu, C. Y. Jheng, J. W. Huang and Y. T. Chang, *Journal of Nanophotonics*, 2016, **10**.
37. Q. Zhou, Y. P. He, J. Abell, Z. J. Zhang and Y. Zhao, *Chemical Communications*, 2011, **47**, 4466-4468.
38. Y. J. Jen, S. Chan, J. W. Huang, C. Y. Jheng and W. C. Liu, *Nanoscale Research Letters*, 2015, **10**.
39. Y. J. Jen, J. W. Huang, W. C. Liu, S. Chan and C. H. Tseng, *Optical Materials Express*, 2016, **6**, 697-704.
40. Y. P. Zhao, S. B. Chaney, S. Shanmukh and R. A. Dluhy, *Journal of Physical Chemistry B*, 2006, **110**, 3153-3157.
41. M. Šubr, M. Petr, O. Kylián, J. Štěpánek, M. Veis and M. Procházka, *Scientific Reports*, 2017, **7**, 4293.
42. Y. J. Liu, J. G. Fan, Y. P. Zhao, S. Shanmukh and R. A. Dluhy, *Applied Physics Letters*, 2006, **89**.
43. Y. P. Zhao, S. B. Chaney and Z. Y. Zhang, *Journal of Applied Physics*, 2006, **100**.
44. C. Y. Lin, Y. H. Wang, J. Y. Huang, Y. J. Liu and Y. P. Zhao, *Journal of Physics-Condensed Matter*, 2010, **22**.
45. B. L. Ge, S. Larson, H. T. Tu, Y. P. Zhao and Y. Y. Fei, *Nanotechnology*, 2020, **31**.
46. S. A. Maier, *PLASMONICS: FUNDAMENTALS AND APPLICATIONS*, Springer, 2007.
47. J. L. Abell, J. D. Driskell and Y. P. Zhao, *Chemical Communications*, 2014, **50**, 106-108.
48. Y. J. Liu, Z. Y. Zhang, Q. Zhao, R. A. Dluhy and Y. P. Zhao, *Journal of Physical Chemistry C*, 2009, **113**, 9664-9669.
49. Z. Y. Zhang, Y. J. Liu, Q. Zhao and Y. P. Zhao, *Applied Physics Letters*, 2009, **94**.
50. G. Wei, J. Wang and Y. Chen, *Beilstein Journal of Nanotechnology*, 2015, **6**, 686-696.
51. N. E. Marotta and L. A. Bottomley, *Applied Spectroscopy*, 2013, **67**, 614-619.
52. R. G. Greenler, *Surface Science*, 1977, **69**, 647-652.
53. P. Negri, N. E. Marotta, L. A. Bottomley and R. A. Dluhy, *Applied Spectroscopy*, 2011, **65**, 66-74.
54. N. Nuntawong, P. Eiamchai, B. Wong-ek, M. Horprathum, K. Limwichean, V. Patthanasettakul and P. Chindaudom, *Vacuum*, 2013, **88**, 23-27.
55. M. Subr, M. Petr, V. Peksa, O. Kylian, J. Hanus and M. Prochazka, *Journal of Nanomaterials*, 2015, **2015**.
56. L. Bachenheimer, R. Scherzer, P. Elliott, S. Stagon, L. Gasparov and H. C. Huang, *Scientific Reports*, 2017, **7**.
57. J. Plou, M. Charconnet, I. García, J. Calvo and L. M. Liz-Marzán, *ACS Nano*, 2021, **15**, 8984-8995.
58. R. De, Y.-S. Shin, C.-L. Lee and M.-K. Oh, *Applied Spectroscopy*, 2016, **70**, 1137-1149.
59. S. Limwichean, H. Nakajima, T. Lertvanithphol, K. Seawsakul, C. Chananonnawathorn, R. Botta, P. Eiamchai, V. Patthanasettakul, P. Chindaudom, A. Klamchuen, N. Nuntawong, P. Songsiriritthigul and M. Horprathum, *Vacuum*, 2022, **196**.
60. C. E. Taylor, S. D. Garvey and J. E. Pemberton, *Analytical Chemistry*, 1996, **68**, 2401-2408.
61. A. Matikainen, T. Nuutinen, T. Itkonen, S. Heinilehto, J. Puustinen, J. Hiltunen, J. Lappalainen, P. Karioja and P. Vahimaa, *Scientific Reports*, 2016, **6**, 37192.
62. J. Cheng, X. O. Su, Y. Yao, C. Q. Han, S. Wang and Y. P. Zhao, *Plos One*, 2016, **11**.
63. J.-C. Valmalette, Z. Tan, H. Abe and S. Ohara, *Scientific reports*, 2014, **4**, 5238.

64. P. J. Yunker, T. Still, M. A. Lohr and A. G. Yodh, *Nature*, 2011, **476**, 308-311.
65. D. Mampallil and H. B. Eral, *Advances in Colloid and Interface Science*, 2018, **252**, 38-54.
66. J. G. Fan, D. Dyer, G. Zhang and Y. P. Zhao, *Nano Letters*, 2004, **4**, 2133-2138.
67. B. Roman and J. Bico, *Journal of Physics: Condensed Matter*, 2010, **22**, 493101.
68. D. Chandra and S. Yang, *Langmuir*, 2009, **25**, 10430-10434.
69. Y. P. Zhao and J. G. Fan, *Applied Physics Letters*, 2006, **88**, 103123.
70. J. G. Fan and Y. P. Zhao, *Langmuir*, 2008, **24**, 14172-14175.
71. M. Hu, F. S. Ou, W. Wu, I. Naumov, X. Li, A. M. Bratkovsky, R. S. Williams and Z. Li, *Journal of the American Chemical Society*, 2010, **132**, 12820-12822.
72. M. S. Schmidt, J. Hübner and A. Boisen, *Advanced Materials*, 2012, **24**, OP11-OP18.
73. S. Stewart and P. M. Fredericks, *Spectrochimica Acta Part A: Molecular and Biomolecular Spectroscopy*, 1999, **55**, 1641-1660.
74. J. S. Suh and M. Moskovits, *Journal of the American Chemical Society*, 1986, **108**, 4711-4718.
75. T. Cai, H. Gu, X. Yuan and F. Liu, *Journal of Physics: Conference Series*, 2011, **277**, 012010.
76. A. Kokaislová and P. Matějka, *Anal Bioanal Chem*, 2012, **403**, 985-993.
77. C. Song, J. L. Abell, Y. He, S. Hunyadi Murph, Y. Cui and Y. Zhao, *Journal of Materials Chemistry*, 2012, **22**, 1150-1159.
78. Y. J. Yang, B. B. Xu, J. Haverstick, N. Ibtehaz, A. Muszynski, X. Y. Chen, M. E. H. Chowdhury, S. M. Zughaier and Y. P. Zhao, *Nanoscale*, 2022, **14**, 8806-8817.
79. Y. J. Yang, B. B. Xu, J. Murray, J. Haverstick, X. Y. Chen, R. A. Tripp and Y. P. Zhao, *Biosensors & Bioelectronics*, 2022, **217**.
80. L. W. Ma, Y. Huang, M. J. Hou, Z. Xie and Z. J. Zhang, *Scientific Reports*, 2015, **5**.
81. L. W. Ma, Y. Huang, M. J. Hou, Z. Xie and Z. J. Zhang, *Scientific Reports*, 2015, **5**.
82. X. Zhang, J. Zhao, A. V. Whitney, J. W. Elam and R. P. Van Duyne, *Journal of the American Chemical Society*, 2006, **128**, 10304-10309.
83. J. F. John, S. Mahurin, S. Dai and M. J. Sepaniak, *Journal of Raman Spectroscopy: An International Journal for Original Work in all Aspects of Raman Spectroscopy, Including Higher Order Processes, and also Brillouin and Rayleigh Scattering*, 2010, **41**, 4-11.
84. B. N. Li, T. R. Wang, Q. Q. Su, X. Z. Wu and P. T. Dong, *Sensors*, 2019, **19**.
85. C. Y. Song, J. L. Abell, Y. P. He, S. H. Murph, Y. P. Cui and Y. P. Zhao, *Journal of Materials Chemistry*, 2012, **22**, 1150-1159.
86. J. L. Abell, J. M. Garren, J. D. Driskell, R. A. Tripp and Y. P. Zhao, *Journal of the American Chemical Society*, 2012, **134**, 12889-12892.
87. K. A. Willets and R. P. Van Duyne, *Annu Rev Phys Chem*, 2007, **58**, 267-297.
88. N. G. Greeneltch, M. G. Blaber, G. C. Schatz and R. P. Van Duyne, *The Journal of Physical Chemistry C*, 2013, **117**, 2554-2558.
89. T. Tan, C. Tian, Z. Ren, J. Yang, Y. Chen, L. Sun, Z. Li, A. Wu, J. Yin and H. Fu, *Physical Chemistry Chemical Physics*, 2013, **15**, 21034-21042.
90. M. A. De Jesus, K. S. Giesfeldt and M. J. Sepaniak, *Journal of Raman Spectroscopy*, 2004, **35**, 895-904.
91. B. S. Yeo, T. Schmid, W. H. Zhang and R. Zenobi, *Applied Spectroscopy*, 2008, **62**, 708-713.
92. M. A. De Jesus, K. S. Giesfeldt and M. J. Sepaniak, *Applied Spectroscopy*, 2003, **57**, 428-438.
93. J. L. Abell, J. M. Garren and Y. P. Zhao, *Applied Spectroscopy*, 2011, **65**, 734-740.
94. S. Liu, Z. Hou, X. Bao, X. Wang, H. Zhang, T. Li, F. Pang, Z. Chen, T. Wang and N. Chen, *Journal of Raman Spectroscopy*, 2020, **51**, 1278-1285.
95. P. Strobbia, T. Sadler, R. A. Odion and T. Vo-Dinh, *Analytical Chemistry*, 2019, **91**, 3319-3326.
96. S. Nath, PhD, Carnegie Mellon University, 2005.
97. G. Dyankov, M. Zekriti and M. Bousmina, *Appl. Opt.*, 2012, **51**, 2451-2456.

98. J. Guo, P. D. Keathley and J. T. Hastings, *Opt. Lett.*, 2008, **33**, 512-514.
99. M. Potara, A.-M. Gabudean and S. Astilean, *Journal of Materials Chemistry*, 2011, **21**, 3625-3633.
100. C. Song, X. Jiang, Y. Yang, J. Zhang, S. Larson, Y. Zhao and L. Wang, *ACS Applied Materials & Interfaces*, 2020, **12**, 31242-31254.
101. C. Q. Han, Y. Yao, W. Wang, L. L. Qu, L. Bradley, S. L. Sun and Y. P. Zhao, *Sensors and Actuators B-Chemical*, 2017, **251**, 272-279.
102. X. M. Wu, S. M. Gao, J. S. Wang, H. Y. Wang, Y. W. Huang and Y. P. Zhao, *Analyst*, 2012, **137**, 4226-4234.
103. C. Y. Song, B. Y. Yang, Y. Zhu, Y. J. Yang and L. H. Wang, *Biosensors & Bioelectronics*, 2017, **87**, 59-65.
104. K. Tian, W. Wang, X. Wang, S. Chen, J. Zhao, F. Tang, X. Nie and C. Han, *Optical Engineering*, 2019, **58**, 084109.
105. C. Q. Han, J. Chen, X. M. Wu, Y. W. Huang and Y. P. Zhao, *Talanta*, 2014, **128**, 293-298.
106. X. B. Du, H. Y. Chu, Y. W. Huang and Y. P. Zhao, *Applied Spectroscopy*, 2010, **64**, 781-785.
107. A. W. Adamson and A. P. Gast, *Physical Chemistry of Surfaces*, Wiley, 6th edn., 1997.
108. J. P. Singh, H. Y. Chu, J. Abell, R. A. Tripp and Y. P. Zhao, *Nanoscale*, 2012, **4**, 3410-3414.
109. L. Bradley, G. Larsen and Y. P. Zhao, *Journal of Physical Chemistry C*, 2016, **120**, 14969-14976.
110. S. Kumar, P. Goel and J. P. Singh, *Sensors and Actuators B: Chemical*, 2017, **241**, 577-583.
111. J. Jiang, S. Zou, L. Ma, S. Wang, J. Liao and Z. Zhang, *ACS Appl Mater Interfaces*, 2018, **10**, 9129-9135.
112. J. L. Abell, J. D. Driskell, R. A. Dluhy, R. A. Tripp and Y. P. Zhao, *Biosens. Bioelectron.*, 2009, **24**, 3663-3670.
113. J. G. Fan and Y. P. Zhao, *Journal of Vacuum Science & Technology B: Microelectronics and Nanometer Structures Processing, Measurement, and Phenomena*, 2005, **23**, 947-953.
114. Y. Zhu, R. A. Dluhy and Y.-P. Zhao, *Sensors & Actuators B*, 2011, **157**, 42-50.
115. C. F. Edman, D. E. Raymond, D. J. Wu, E. Tu, R. G. Sosnowski, W. F. Butler, M. Nerenberg and M. J. Heller, *Nucleic Acids Res*, 1997, **25**, 4907-4914.
116. M. J. Heller, A. H. Forster and E. Tu, *ELECTROPHORESIS*, 2000, **21**, 157-164.
117. R. Cabeça, M. Rodrigues, D. M. Prazeres, V. Chu and J. P. Conde, *Nanotechnology*, 2009, **20**, 015503.
118. H. Zhou and J. Kneipp, *Analytical Chemistry*, 2023, **95**, 3363-3370.
119. J. L. Abell, PhD, University of Georgia, 2012.
120. P. Delahay, M. Pourbaix and P. V. Rysselberghe, *Journal of The Electrochemical Society*, 1951, **98**, 65.
121. M. A. M. Ibrahim, H. H. Hassan, S. S. Abd El Rehim and M. A. Amin, *Journal of Solid State Electrochemistry*, 1999, **3**, 380-386.
122. X. J. Tang, G. Zhang and Y. P. Zhao, *Nanotechnology*, 2006, **17**, 4439-4444.
123. M. Santiago and S. Strobel, *Methods Enzymol*, 2013, **533**, 303-324.
124. J. Abell, J. Lee, Q. Zhao, H. Szu and Y. Zhao, *Analyst* 2012, **137**, 73-76.
125. J. Chen, J. Abell, Y. W. Huang and Y. P. Zhao, *Lab on a Chip*, 2012, **12**, 3096-3102.
126. J. Chen, Y. W. Huang and Y. P. Zhao, *Journal of Materials Chemistry B*, 2015, **3**, 1898-1906.
127. C. Y. Song, J. D. Driskell, R. A. Tripp, Y. P. Cui and Y. P. Zhao, Baltimore, MD, 2012.
128. X. M. Wu, C. Xu, R. A. Tripp, Y. W. Huang and Y. P. Zhao, *Analyst*, 2013, **138**, 3005-3012.
129. P. Negri and R. A. Dluhy, *J Biophotonics*, 2013, **6**, 20-35.
130. X. Wu, J. Chen, B. Park, Y.-W. Huang and Y. Zhao, in *Advances in Applied Nanotechnology for Agriculture*, American Chemical Society, 2013, vol. 1143, ch. 5, pp. 85-108.
131. P. Shah, D. Ju, X. Niu and A. M. Sarangan, *Journal of Sensors*, 2013, **2013**, 823041.

132. M. K. Oh, R. De and S. Y. Yim, *Journal of Raman Spectroscopy*, 2018, **49**, 800-809.
133. L. Ma, H. Wu, Y. Huang, S. Zou, J. Li and Z. Zhang, *ACS Appl Mater Interfaces*, 2016, **8**, 27162-27168.
134. S. K. Gahlaut, K. Yadav, C. Sharan and J. P. Singh, *Analytical Chemistry*, 2017, **89**, 13582-13588.
135. M.-K. Oh, R. De and S.-Y. Yim, *Journal of Raman Spectroscopy*, 2018, **49**, 800-809.
136. C. L. Leverette, E. Villa-Aleman, S. Jokela, Z. Y. Zhang, Y. J. Liu, Y. P. Zhao and S. A. Smith, *Vibrational Spectroscopy*, 2009, **50**, 143-151.
137. J. Jiang, L. Ma, J. Chen, P. Zhang, H. Wu, Z. Zhang, S. Wang, W. Yun, Y. Li, J. Jia and J. Liao, *Microchimica Acta*, 2017, **184**, 2775-2782.
138. S. Wang, S. Zou, S. Yang, H. Wu, J. Jia, Y. Li, Z. Zhang, J. Jiang, M. Chu and X. Wang, *Sensors and Actuators B: Chemical*, 2018, **265**, 539-546.
139. Y. Yao, W. Wang, K. Z. Tian, W. M. Ingram, J. Cheng, L. L. Qu, H. T. Li and C. Q. Han, *Spectrochimica Acta Part a-Molecular and Biomolecular Spectroscopy*, 2018, **195**, 165-171.
140. X. K. Duan, Y. Yao, J. W. Li, W. Wang, Q. Zou, L. L. Qu, H. T. Li and C. Q. Han, *Optical Engineering*, 2018, **57**.
141. Z. Liu, Q. Zhang, X. Zhong and C. Han, *Physical Chemistry Chemical Physics*, 2022, **24**, 26413-26420.
142. Q. Zhang, Z. Liu, L. Duan, Z. Cao, B. Wu, L. Qu and C. Han, *Applied Surface Science*, 2023, **611**, 155577.
143. J. Chen, Y. W. Huang and Y. P. Zhao, *Journal of Raman Spectroscopy*, 2015, **46**, 64-69.
144. Q. Zhang, Z. Liu, H. Zhang, C. Han, Y. Wu, C. Yan, Y. Liu, B. Wu, G. Yang and P. Duan, *Analyst*, 2023, **148**, 814-822.
145. K. Tian, W. Wang, Y. Yao, X. Nie, A. Lu, Y. Wu and C. Han, *Journal of Raman Spectroscopy*, 2018, **49**, 472-481.
146. Q. Zhou, Y. Yang, J. Ni, Z. Li and Z. Zhang, *Nano Research*, 2010, **3**, 423-428.
147. Q. Zhou, Y. Yang, J. Ni, Z. C. Li and Z. J. Zhang, *Physica E-Low-Dimensional Systems & Nanostructures*, 2010, **42**, 1717-1720.
148. X. Zhang, Q. Zhou, Y. Huang, Z. Li and Z. Zhang, *Journal*, 2011, **11**, 11510-11515.
149. Q. Zhou, X. Zhang, Y. Huang, Z. Li and Z. Zhang, *Sensors (Basel)*, 2011, **11**, 10851-10858.
150. S. Zou, M. Hou, J. Li, L. Ma and Z. Zhang, *Scientific Reports*, 2017, **7**, 6186.
151. S. Zou, L. Ma, J. Li, Z. Xie, D. Zhao, Y. Ling and Z. Zhang, *Talanta*, 2018, **186**, 452-458.
152. X. Fang, Y. Song, Y. Huang, G. Yang, C. Han, H. Li and L. Qu, *Analyst*, 2020, **145**, 7421-7428.
153. J. Li, W. Wang, C. Xie, Q. Jia, C. Yan, Y. Yao, Z. Fang, L. Duan, J. Cheng, L. Qu and C. Han, *Journal of Materials Science*, 2020, **55**, 7029-7038.
154. Q. Wang, J. W. Li, Y. H. Song, L. F. Duan, C. C. Yan, L. L. Qu, Y. Wu and C. Q. Han, *Journal of Hazardous Materials*, 2022, **426**.
155. W. Cao, Y. Luo, J. Li, A. Qian, Q. Wang, X. Wang, L. Duan, Y. Wu and C. Han, *Results in Chemistry*, 2021, **3**.
156. W. Zhang, J. Cheng, J. Li, Y. Yao, C. Yan and C. Han, 2018.
157. C.-q. Han, Y. Yao, W. Wang, L.-q. Tao, W.-x. Zhang, W. M. Ingram, K.-z. Tian, Y. Liu, A.-x. Lu, Y. Wu, C.-c. Yan, L.-L. Qu and H.-t. Li, *Chinese Journal of Chemical Physics*, 2018, **31**, 152-158.
158. J. Jiang, S. Zou, Y. Li, F. Zhao, J. Chen, S. Wang, H. Wu, J. Xu, M. Chu, J. Liao and Z. Zhang, *Microchimica Acta*, 2019, **186**, 603.
159. Y. Luo, Q. Zhang, Q. Wang, Z. L. Liu, L. F. Duan, W. X. Cao, Z. J. Cao and C. Q. Han, *Microchimica Acta*, 2022, **189**.
160. W. Qin, L. Jingwen, S. Yuhang, L. Ying, L. Aixia, H. Caiqin, W. Ying and D. Peitong, *Optical Engineering*, 2020, **59**, 057106.

161. L.-L. Qu, Q. Jia, C. Liu, W. Wang, L. Duan, G. Yang, C.-Q. Han and H. Li, *Journal of Chromatography A*, 2018, **1579**, 115-120.
162. L.-L. Qu, Z.-Q. Geng, W. Wang, K.-C. Yang, W.-P. Wang, C.-Q. Han, G.-H. Yang, R. Vajtai, D.-W. Li and P. M. Ajayan, *Journal of Hazardous Materials*, 2019, **379**, 120823.
163. X. C. Sun, S. Stagon, H. C. Huang, J. Chen and Y. Lei, *Rsc Advances*, 2014, **4**, 23382-23388.
164. X. M. Wu, J. Chen, X. B. Li, Y. P. Zhao and S. M. Zughaier, *Nanomedicine-Nanotechnology Biology and Medicine*, 2014, **10**, 1863-1870.
165. S. K. Srivastava, A. Shalabney, I. Khalaila, C. Grüner, B. Rauschenbach and I. Abdulhalim, *Small*, 2014, **10**, 3579-3587.
166. X. M. Wu, Y. P. Zhao and S. M. Zughaier, *Biosensors-Basel*, 2021, **11**.
167. Z.-Q. Geng, D. Xu, Y. Song, W.-P. Wang, Y.-P. Li, C.-Q. Han, G.-H. Yang, L.-L. Qu and P. M. Ajayan, *Sensors and Actuators B: Chemical*, 2021, **334**, 129634.
168. O. E. Rivera-Betancourt, R. Karls, B. Grosse-Siestrup, S. Helms, F. Quinn and R. A. Dluhy, *Analyst*, 2013, **138**, 6774-6785.
169. K. Tian, W. Wang, X. Wang, S. Chen, J. Zhao, F. Tang, X. Nie and C. Han, *Optical Engineering*, 2019, **58**, 084109-084109.
170. C. Y. Song, J. Chen, Y. P. Zhao and L. H. Wang, *Journal of Materials Chemistry B*, 2014, **2**, 7488-7494.
171. T. Wang, P. Dong, C. Zhu, P. Sha, W. Gao, Y. Wu and X. Wu, *Sensors and Actuators B: Chemical*, 2021, **346**, 130467.
172. X. Meshik, X. Wu, Y. Zhao, J. Schwartz, M. Dutta and M. Stroscio, *Journal of Raman Spectroscopy*, 2015, **46**, 194-196.
173. K.-z. Tian, C.-c. Cao, X.-m. Nie, W. Wang and C.-q. Han, *Chinese Journal of Chemical Physics*, 2019, **32**, 603-610.
174. P. Negri, A. Kage, A. Nitsche, D. Naumann and R. A. Dluhy, *Chemical Communications*, 2011, **47**, 8635-8637.
175. P. Negri, G. Chen, A. Kage, A. Nitsche, D. Naumann, B. Xu and R. A. Dluhy, *Analytical Chemistry*, 2012, **84**, 5501-5508.
176. S. K. Gahlaut, D. Savargaonkar, C. Sharan, S. Yadav, P. Mishra and J. P. Singh, *Analytical Chemistry*, 2020, **92**, 2527-2534.
177. J. D. Driskell, A. G. Seto, L. P. Jones, S. Jokela, R. A. Dluhy, Y. P. Zhao and R. A. Tripp, *Biosensors & Bioelectronics*, 2008, **24**, 917-922.
178. J. D. Driskell, O. M. Primera-Pedrozo, R. A. Dluhy, Y. P. Zhao and R. A. Tripp, *Applied Spectroscopy*, 2009, **63**, 1107-1114.
179. J. D. Driskell and R. A. Tripp, *Chemical Communications*, 2010, **46**, 3298-3300.
180. K. L. Brenneman, J. Abell, X. Meshik, K. Xu, Y. P. Zhao, M. Dutta and M. A. Stroscio, Campus Univ Michigan, Ann Arbor, MI, 2012.
181. N. E. Marotta, K. R. Beavers and L. A. Bottomley, *Analytical Chemistry*, 2013, **85**, 1440-1446.
182. P. Negri and R. A. Dluhy, *Analyst*, 2013, **138**, 4877-4884.
183. C. Y. Song, Y. J. Yang, B. Y. Yang, Y. Z. Sun, Y. P. Zhao and L. H. Wang, *Nanoscale*, 2016, **8**, 17365-17373.
184. J. Zhang, Y. Yang, X. Jiang, C. Dong, C. Song, C. Han and L. Wang, *Biosensors and Bioelectronics*, 2019, **141**, 111402.
185. Y. J. Yang, C. Y. Song, J. J. Zhang, J. Chao, H. M. Luong, Y. P. Zhao and L. H. Wang, *Nanoscale*, 2022, **14**, 4538-4547.
186. Y. Yang, H. Li, L. Jones, J. Murray, J. Haverstick, H. K. Naikare, Y.-Y. C. Mosley, R. A. Tripp, B. Ai and Y. Zhao, *ACS Sensors*, 2023, **8**, 297-307.

187. J. Li, Y. Yuan, H. Gan, C. Dong, B. Cao, J.-l. Ni, X. Li, W. Gu, C. Song and L. Wang, *ACS Applied Materials & Interfaces*, 2022, **14**, 32869-32879.
188. J. J. Zhang, C. Y. Song, Y. F. Zhu, H. Y. Gan, X. Y. Fang, Q. Peng, J. R. Xiong, C. Dong, C. Q. Han and L. H. Wang, *Biosensors & Bioelectronics*, 2023, **219**.
189. S. Shanmukh, L. Jones, J. Driskell, Y. P. Zhao, R. Dluhy and R. A. Tripp, *Nano Letters*, 2006, **6**, 2630-2636.
190. R. A. Tripp, R. A. Dluhy and Y. P. Zhao, *Nano Today*, 2008, **3**, 31-37.
191. S. Shanmukh, L. Jones, Y. P. Zhao, J. D. Driskell, R. A. Tripp and R. A. Dluhy, *Analytical and Bioanalytical Chemistry*, 2008, **390**, 1551-1555.
192. J. D. Driskell, S. Shanmukh, Y. J. Liu, S. Hennigan, L. Jones, Y. P. Zhao, R. A. Dluhy, D. C. Krause and R. A. Tripp, *Ieee Sensors Journal*, 2008, **8**, 863-870.
193. V. Hoang, R. A. Tripp, P. Rota and R. A. Dluhy, *Analyst*, 2010, **135**, 3103-3109.
194. J. D. Driskell, Y. Zhu, C. D. Kirkwood, Y. P. Zhao, R. A. Dluhy and R. A. Tripp, *Plos One*, 2010, **5**.
195. J. D. Driskell, J. L. Abell, R. A. Dluhy, Y. P. Zhao and R. A. Tripp, Orlando, FL, 2010.
196. P. Negri, J. Y. Choi, C. Jones, S. M. Tompkins, R. A. Tripp and R. A. Dluhy, *Analytical Chemistry*, 2014, **86**, 6911-6917.
197. S. Yadav, S. Senapati, D. Desai, S. Gahlaut, S. Kulkarni and J. P. Singh, *Colloids and Surfaces B: Biointerfaces*, 2021, **198**, 111477.
198. H. Y. Chu, Y. W. Huang and Y. P. Zhao, *Applied Spectroscopy*, 2008, **62**, 922-931.
199. S. L. Hennigan, J. D. Driskell, R. A. Dluhy, Y. P. Zhao, R. A. Tripp, K. B. Waites and D. C. Krause, *Plos One*, 2010, **5**.
200. S. L. Hennigan, J. D. Driskell, N. Ferguson-Noel, R. A. Dluhy, Y. P. Zhao, R. A. Tripp and D. C. Krause, *Applied and Environmental Microbiology*, 2012, **78**, 1930-1935.
201. K. C. Henderson, E. S. Sheppard, O. E. Rivera-Betancourt, J. Y. Choi, R. A. Dluhy, K. A. Thurman, J. M. Winchell and D. C. Krause, *Analyst*, 2014, **139**, 6426-6434.
202. K. C. Henderson, A. J. Benitez, A. E. Ratliff, D. M. Crabb, E. S. Sheppard, J. M. Winchell, R. A. Dluhy, K. B. Waites, T. P. Atkinson and D. C. Krause, *Plos One*, 2015, **10**.
203. X. M. Wu, C. Q. Han, J. Chen, Y. W. Huang and Y. P. Zhao, *Jom*, 2016, **68**, 1156-1162.
204. J. Chen, X. M. Wu, Y. W. Huang and Y. P. Zhao, *Sensors and Actuators B-Chemical*, 2014, **191**, 485-490.
205. S. Kumar, D. K. Lodhi, P. Goel, Neeti, P. Mishra and J. P. Singh, *Chemical Communications*, 2015, **51**, 12411-12414.
206. S. K. Srivastava, H. B. Hamo, A. Kushmaro, R. S. Marks, C. Grüner, B. Rauschenbach and I. Abdulhalim, *Analyst*, 2015, **140**, 3201-3209.
207. X. M. Wu, Y. W. Huang, B. Park, R. A. Tripp and Y. P. Zhao, *Talanta*, 2015, **139**, 96-103.
208. C. N. Kotanen, L. Martinez, R. Alvarez and J. W. Simecek, *Sensing and Bio-Sensing Research*, 2016, **8**, 20-26.
209. J. Chen, B. Park, Y. W. Huang, Y. P. Zhao and Y. Kwon, *Journal of Food Measurement and Characterization*, 2017, **11**, 1773-1779.
210. F. N. Chen, B. R. Flaherty, C. E. Cohen, D. S. Peterson and Y. P. Zhao, *Nanomedicine-Nanotechnology Biology and Medicine*, 2016, **12**, 1445-1451.
211. J. Li, C. Wang, Y. Yao, Y. Zhu, C. Yan, Q. Zhuge, L. Qu and C. Han, *Talanta*, 2020, **216**, 120983.
212. S. S. Masango, R. A. Hackler, N. Large, A.-I. Henry, M. O. McAnally, G. C. Schatz, P. C. Stair and R. P. Van Duyne, *Nano Letters*, 2016, **16**, 4251-4259.
213. J. G. Fan, X. J. Tang and Y. P. Zhao, *Nanotechnology*, 2004, **15**, 501.
214. R. A. Wallace, J. J. Charlton, T. B. Kirchner, N. V. Lavrik, P. G. Datskos and M. J. Sepaniak, *Analytical Chemistry*, 2014, **86**, 11819-11825.

215. S. Chen, X. Lin, C. Yuen, S. Padmanabhan, R. W. Beuerman and Q. Liu, *Opt. Express*, 2014, **22**, 12102-12114.
216. X.-g. Fan, Y. Zeng, Y.-L. Zhi, T. Nie, Y.-j. Xu and X. Wang, *Journal of Raman Spectroscopy*, 2021, **52**, 890-900.
217. R. L. McCreery, in *Raman Spectroscopy for Chemical Analysis*, John Wiley & Sons, Inc., 2000, DOI: https://doi.org/10.1002/0471721646.ch4, ch. 4, pp. 49-71.
218. H. G. Schulze, M. M. L. Yu, C. J. Addison, M. W. Blades and R. F. B. Turner, *Applied Spectroscopy*, 2006, **60**, 820-825.
219. S. J. Barton, T. E. Ward and Bryan M. Hennelly, *Analytical Methods*, 2018, **10**, 3759-3769.
220. Y. Zhao, G. Che and X. Zhao, *Vibrational Spectroscopy*, 2022, **123**, 103441.
221. I. Loc, I. Kecoglu, M. B. Unlu and U. Parlatan, *Journal of Raman Spectroscopy*, 2022, **53**, 1445-1452.
222. J. Langer, D. Jimenez de Aberasturi, J. Aizpurua, R. A. Alvarez-Puebla, B. Auguié, J. J. Baumberg, G. C. Bazan, S. E. J. Bell, A. Boisen, A. G. Brolo, J. Choo, D. Cialla-May, V. Deckert, L. Fabris, K. Faulds, F. J. García de Abajo, R. Goodacre, D. Graham, A. J. Haes, C. L. Haynes, C. Huck, T. Itoh, M. Käll, J. Kneipp, N. A. Kotov, H. Kuang, E. C. Le Ru, H. K. Lee, J.-F. Li, X. Y. Ling, S. A. Maier, T. Mayerhöfer, M. Moskovits, K. Murakoshi, J.-M. Nam, S. Nie, Y. Ozaki, I. Pastoriza-Santos, J. Perez-Juste, J. Popp, A. Pucci, S. Reich, B. Ren, G. C. Schatz, T. Shegai, S. Schlücker, L.-L. Tay, K. G. Thomas, Z.-Q. Tian, R. P. Van Duyne, T. Vo-Dinh, Y. Wang, K. A. Willets, C. Xu, H. Xu, Y. Xu, Y. S. Yamamoto, B. Zhao and L. M. Liz-Marzán, *ACS Nano*, 2020, **14**, 28-117.
223. F. Lussier, V. Thibault, B. Charron, G. Q. Wallace and J.-F. Masson, *TrAC Trends in Analytical Chemistry*, 2020, **124**.
224. N. M. Ralbovsky and I. K. Lednev, *Chem Soc Rev*, 2020, **49**, 7428-7453.
225. J. Acquarelli, T. van Laarhoven, J. Gerretzen, T. N. Tran, L. M. C. Buydens and E. Marchiori, *Analytica Chimica Acta*, 2017, **954**, 22-31.
226. C. A. Lieber and A. Mahadevan-Jansen, *Applied Spectroscopy*, 2003, **57**, 1363-1367.
227. S. Mahajan, R. M. Cole, J. D. Speed, S. H. Pelfrey, A. E. Russell, P. N. Bartlett, S. M. Barnett and J. J. Baumberg, *The Journal of Physical Chemistry C*, 2010, **114**, 7242-7250.
228. C. Farcau and S. Astilean, *Chemical Communications*, 2011, **47**, 3861-3863.
229. S. Wu, O. H.-C. Cheng, B. Zhao, N. Hogan, A.-T. Lee, D. H. Son and M. T. Sheldon, *arXiv: Applied Physics*, 2020.
230. R. P. Vanduyne, D. L. Jeanmaire and D. F. Shriver, *Analytical Chemistry*, 1974, **46**, 213-222.
231. P. A. Mosierboss, S. H. Lieberman and R. Newbery, *Applied Spectroscopy*, 1995, **49**, 630-638.
232. J. Zhao, M. M. Carrabba and F. S. Allen, *Applied Spectroscopy*, 2002, **56**, 834-845.
233. J. B. Cooper, S. Marshall, R. Jones, M. Abdelkader and K. L. Wise, *Appl. Opt.*, 2014, **53**, 3333-3340.
234. L. E. Masson, C. M. O'Brien, I. J. Pence, J. L. Herington, J. Reese, T. G. van Leeuwen and A. Mahadevan-Jansen, *Analyst*, 2018, **143**, 6049-6060.
235. J. Zhao, H. Lui, D. I. McLean and H. Zeng, *Appl Spectrosc*, 2007, **61**, 1225-1232.
236. Z. M. Zhang, S. Chen and Y. Z. Liang, *Analyst*, 2010, **135**, 1138-1146.
237. D. P. dos Santos, M. M. Sena, M. R. Almeida, I. O. Mazali, A. C. Olivieri and J. E. L. Villa, *Analytical and Bioanalytical Chemistry*, 2023, DOI: 10.1007/s00216-023-04620-y.
238. F. Cui, Y. Yue, Y. Zhang, Z. Zhang and H. S. Zhou, *ACS Sensors*, 2020, **5**, 3346-3364.
239. R. Beeram, K. R. Vepa and V. R. Soma, *Journal*, 2023, **13**.
240. F. Lussier, V. Thibault, B. Charron, G. Q. Wallace and J.-F. Masson, *TrAC Trends in Analytical Chemistry*, 2020, **124**, 115796.
241. H. Zhou, L. Xu, Z. Ren, J. Zhu and C. Lee, *Nanoscale Advances*, 2023, **5**, 538-570.

242. L. Sun, Y. Song, L. Wang, C. Guo, Y. Sun, Z. Liu and Z. Li, *The Journal of Physical Chemistry C*, 2008, **112**, 1415-1422.
243. A. Shiohara, Y. Wang and L. M. Liz-Marzán, *Journal of Photochemistry and Photobiology C: Photochemistry Reviews*, 2014, **21**, 2-25.
244. L. Liu, T. Zhang, Z. Wu, F. Zhang, Y. Wang, X. Wang, Z. Zhang, C. Li, X. Lv, D. Chen, S. Jiao, J. Wu and Y. Li, *Analytical Chemistry*, 2023, **95**, 4050-4058.
245. J. D. Rodriguez, B. J. Westenberger, L. F. Buhse and J. F. Kauffman, *Analyst*, 2011, **136**, 4232-4240.
246. J. C. Weatherall, J. Barber, C. S. Brauer, T. J. Johnson, Y.-F. Su, C. D. Ball, B. T. Smith, R. Cox, R. Steinke, P. McDaniel and L. Wasserzug, *Applied Spectroscopy*, 2013, **67**, 149-157.
247. J. J. Workman, Jr., *Appl Spectrosc*, 2018, **72**, 340-365.
248. P. Mishra and D. Passos, *Infrared Physics & Technology*, 2021, **117**, 103863.
249. B.-Y. Wen, Q.-Q. Chen, P. M. Radjenovic, J.-C. Dong, Z.-Q. Tian and J.-F. Li, *Annual Review of Physical Chemistry*, 2021, **72**, 331-351.